Droplet-on-hydrogel bilayer based assay for functional study of membrane proteins



Zuzana Cocuľová

Linacre College

Department of Physics

University of Oxford

A thesis submitted for the degree of *Doctor of Philosophy*

Michaelmas 2022

Droplet-on-hydrogel bilayer based assay for functional study of membrane proteins

Zuzana Cocuľová

Linacre College

A thesis submitted for the degree of *Doctor of Philosophy*

at the University of Oxford, Michaelmas 2022

Abstract

Functional study of membrane proteins, especially when a transmembrane potential is required for protein function, is notoriously difficult. In this thesis, I introduce an experimental assay that adapts the droplet-on-hydrogel technique for a high-resolution functional study of membrane proteins with independent control of the electrical and chemical transmembrane potential.

This experimental assay is the next step toward studying a membrane protein of interest embedded into an energised lipid bilayer. The bilayer is formed between a 200 nl water droplet and a supporting layer of hydrogel, granting a stable, functional, and accessible lipid bilayer. Delivery of proteins, labels, substrates, or ions to the droplet above the bilayer is achieved through a low-cost custom-built electronically controlled perfusion system. Experiments presented in this work show a stable perfusion with 26.68 ± 2.5 nl steps.

The main motivation for creating this experimental assay is a desire to observe the ATP synthase F_1F_o in conditions mimicking the protein's natural environment. This complex of two molecular motors - membrane-embedded F_o and water-soluble F_1 - catalyses the synthesis of ATP molecules, the basic energy units of life. Using

site-directed mutagenesis, I modified TA2.A1 F_1F_o in two places, to be able to label the protein with a gold nanorod and anchor it to the agarose-streptavidin gel for a high-resolution functional study experiment. The assay may allow us to study the activation potential of the protein at different conditions, as well as to observe high-resolution single-molecule rotation steps of F_1F_o at the time scale of a few microseconds.

Acknowledgement

I would like to thank Professor Richard Berry for the chance to work on this exciting project and for his guidance through exploring all sorts of methods and topics.

This project was supported by funding from the Engineering and Physical Sciences Research Council (EPSRC) and the Medical Research Council (MRC), grant number EP/L016044/1. I would also like to acknowledge F. Hoffmann-La Roche for supporting my project financially, and to thank Dr Bryn Roberts for establishing this collaboration, and my previous and current co-supervisors Dr Jeffrey Hermes, Dr Armin Ruf, Dr Sylwia Huber, and Dr Arne Rufer for interesting discussions about the project.

I am very grateful to all the people who helped me with this project, especially Dr Matt Cornall, who taught me protein expression and purification; Dr Hafez El Sayyed for his frequent support in the wet lab, and, together with Dr Abhishek Mazumder and Dr Gokce Su Pulcu, for their help with mutagenesis; Dr Alessandro Alcinesio for contributing with his impressive CNC machining skills, and for all the valuable advice; Dr Ravinash Krishna Kumar for his help with spin coating; Dr Alex Cloake for all the brainstorming, and, together with Dr Linus Conrad and Dr Ehsan Nematian, for their help with micropipettes; Dr Stelios Chatzimichail for his friendly and proficient help with 3D printing; Dr Jia Khoo and Dr Helen Miller for their help with fluorescent microscopy; Dr Oliver Pambos for his advice on perfusion system; and Dr Martin Rieu, Dr Raquel Martinez Gonzalez, Dr Martin Chudjak,

Dr Matúš Balogh, and Mr. Ladislav Bačo for discussions about everyday scientific questions.

This thesis was written with the kind support of Dr Martin Chudjak, Dr Martin Rieu, Dr Raquel Martinez Gonzalez, Dr Matt Cornall, Dr Hafez El Sayeed, Mr. Alex Lawrenson, Dr Vihanga Munasinghe, and Mr. Dilhan Manawadu, who provided suggestions on the text, and my writing buddies Ms. Virginia Casablancas Antras, Dr Vihanga Munasinghe, Mr. Dilhan Manawadu, and my sister Lenka; and, importantly, with support from my boyfriend Martin.

Thank you.

Covid impact statement

The closure of the University buildings for over 15 weeks happened in the stage of my project when I had finished all the planning and preparations for building the experimental apparatus, which then required adjustments and troubleshooting, so it was not possible to carry on that work from home.

After this period, restricted access to the laboratories was possible for approximately one year. The restrictions prevented me from accessing our collaborator's facilities (which I was routinely using before the pandemic) and some of our research facilities. I also had minimal contact with my colleagues and almost no in-person supervision, which was especially limiting during this stage of the project. This resulted in much slower progress than expected in normal conditions.

When the facilities reopened normally, my work was further disrupted by a delay in manufacturing the metal platform which fits the perfusion system on the microscope. The original deadline for delivery, which was set for the middle of June 2021, was repeatedly postponed, and the platform was finalized in May 2022. Only then I was able to start the experiments I designed before the pandemic. Proteins and other samples prepared before the pandemic were no longer usable, so I needed to prepare them again.

Overall, my work was severely disrupted for approximately 2 years.

Contents

Abbreviations

1 Introduction **1**

1.1 Adenosine triphosphate (ATP) 1

1.2 ATP synthase F_1F_o 3

1.2.1 *E. coli* and TA2.A1 F_1F_o: differences 6

1.2.2 ATP synthase research 7

1.2.3 Open questions 11

1.3 Model lipid membranes 13

1.3.1 Liposomes 13

1.3.2 Supported planar membranes 14

1.3.3 Unsuported planar membranes 15

1.4 Foundations of the assay 17

1.4.1 Droplet-on-hydrogel bilayer 17

1.4.2 Charged membrane fusion 18

1.4.3 Gold nanorods 18

2 Preparation of proteins for functional study of F_1F_o **21**

2.1 Protein preparation 21

2.1.1 *E. coli* F_1F_o 22

2.1.2 TA2.A1 F_1F_o 22

2.1.3 Protein concentration assays 23

2.1.4 Polyacrylamide gel electrophoresis (PAGE) 24

2.1.5 F_1F_o activity assays: overview 25
2.1.6 Phenol red activity assay 28
2.2 Protein labelling: Site-directed mutagenesis 29
2.2.1 Site-directed mutagenesis 31
2.2.2 Calcium competent cells 35
2.2.3 DNA extraction and sequencing 35
2.3 Agarose-streptavidin 35
2.3.1 Calculation of fraction of modified agarose 36
2.3.2 Preparing agarose-streptavidin 37
2.3.3 Control experiments 38
2.4 Conclusion 41

3 Development of protocol for lipid bilayer formation 43
3.1 Droplet-on-hydrogel bilayer formation 44
3.2 Optimising conditions of bilayer formation 45
3.2.1 Lipid composition 45
3.2.2 Lipid concentration and duration of monolayer formation . . 46
3.2.3 Oil composition 47
3.2.4 Image of bilayer 48
3.3 Charged membrane fusion 49
3.3.1 Control fusion experiment: the design 49
3.3.2 Liposomes with two fluorescent labels 52
3.3.3 Two colour fluorescent microscope setup 53
3.4 Conclusion 55

4 Design, building and testing of the perfusion system 57
4.1 Mechanical support for droplet-on-hydrogel bilayer 58
4.1.1 Chip 60
4.1.2 Chip adapter 63
4.1.3 Platform 64

4.1.4 Stages, holders, and NanoCubes 64
4.1.5 Rod 66
4.1.6 Syringe holder 67
4.1.7 Electrode holder 68
4.2 Top view microscope 69
4.3 Microfluidic control 70
4.3.1 Pipettes 71
4.3.2 Actuators 76
4.3.3 Perfusion 83
4.3.4 Qualitative experiments 83
4.3.5 Quantitative experiments 84
4.4 Conclusion 88

5 Conclusion and future directions **91**
5.1 Future directions 93
5.1.1 Next steps 93
5.1.2 Ideas for future experiments 95

6 Methods **97**
6.1 Expression and purification of *E.coli* F_1F_o 97
6.2 Expression and purification of TA2.A1 F_1F_o 100
6.3 Protein concentration assay 102
6.4 Protein gel 103
6.5 Phenol red activity assay 105
6.6 Site-directed mutagenesis 105
6.7 Preparation of calcium competent cells 108
6.8 Preparation of agarose-streptavidin 110
6.9 Agarose-streptavidin control experiment 111
6.10 Cleaning of glass vials 113
6.11 Cleaning of cover slips 114

6.12 Preparation of lipid mixture 114
6.13 Spin-coating 115
6.14 Assembling the chip 115
6.15 Preparing the droplets 116
6.16 Preparation of liposomes with two fluorescent labels 117

A Appendix **119**

A.1 DNA sequence of the TA2.A1 F_1F_o operon inserted into PET3a 120

Abbreviations

2D ... two Dimensional

3D ... three Dimensional

A/a ... adenine

ADP ... Adenosine DiPhosphate

ATP ... Adenosine TriPhosphate

AU ... Arbitrary Units

BCA ... BiCinchoninic Acid

BME ... 2-MercaptoEthanol

BNC ... Bayonet Neill-Concelman

BSA ... Bovine Serum Albumin

C/c ... cytosine

CDI ... CarbonylDiImidazole

CNC ... Computer Numerical Control

cryo-EM ... cryogenic Electron Microscopy

DC ... Direct Current

DMSO ...DiMethyl SulfOxide

DNA ... DeoxyriboNucleic Acid

DOPC ... 1,2-DiOleoyl-sn-glycero-3-PhosphoCholine

DPhPC ... 1,2-DiPhytanoyl- sn-glycero-3-PhosphoCholine

E.coli ... Escherichia coli

E-PC ... 1,2-dioleoyl-sn-glycero-3-EthylPhosphoCholine

FRET ... Förster Resonance Energy Transfer

G/g ... guanine

HCl ... HydroChloric Acid

IPTG ... IsoPropyl β-D-1-ThioGalactopyranoside

kbp ... kilo (1,000) base pairs

LB ... Lysogeny Broth

LDAO ... LaurylDimethylAmine Oxide

NADH ... Nicotinamide Adenine Dinucleotide (NAD) + Hydrogen (H)

Ni-NTA ... Nickel - NiTriloacetic Acid

PA ... Phosphatidic Acid

PA 12 ... PolyAmide 12

PAGE ... PolyAcrylamide Gel Electrophoresis

PDB ID ... Protein Data Bank IDentification

PC ... PhosphatidylCholine

PCR ... Polymerase Chain Reaction

PMDC ... Permanent Magnet Direct Current

PMMA ... PolyMethyl MethAcrylate

$POPA^-$ ... 1-PalmitOyl-2- oleoyl-sn-glycero-3-PhosphAte

rpm ... revolutions per minute

SDS ... Sodium Dodecyl Sulphate

SLS ... Selective Laser Sintering

T/t ... thymine

TIFF ... Tag Image File Format

Chapter 1

Introduction

1.1 Adenosine triphosphate (ATP)

Adenosine triphosphate (ATP) is widely known as a universal energy currency. It fuels a wide range of core biological processes, including some metabolic reactions, active transport of substances across membranes, chemical synthesis, nerve impulse propagation, muscle contraction, and cell motility.

The ATP molecule is composed of a nucleotide base adenine, a sugar molecule ribose, and a chain of three phosphate groups (Figure 1.1). The phosphate groups are connected via phosphate bonds, which can be broken through the addition of a water molecule in a process called hydrolysis. Although breaking of any chemical bond (even the high-energy phosphate bond holding two negatively charged phosphate groups together) requires energy, the change of the free energy of the system upon hydrolysis of one phosphate bond of the ATP molecule under standard conditions is - 30.5 kJ/mol (the minus sign represents energy release). This means that the energy of all the bonds formed after hydrolysis is lower than the energy of the bonds broken during hydrolysis.

This makes phosphate bonds useful for energy transfers within living cells. Upon hydrolysis of the terminal phosphate bond of the ATP molecule, resulting adenosine

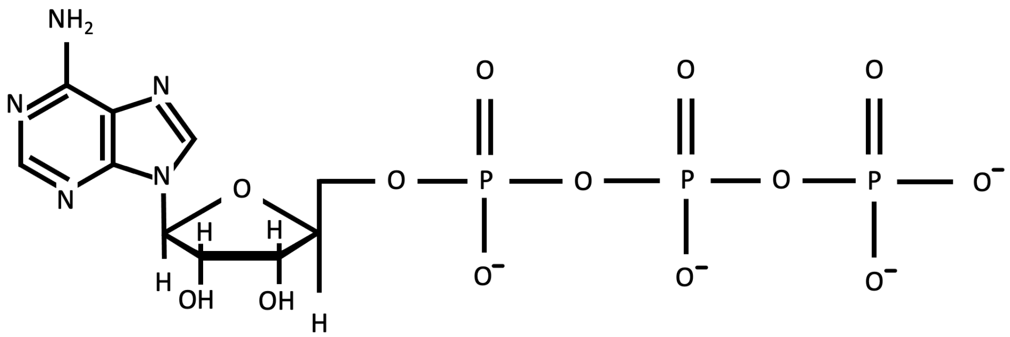


Figure 1.1: Molecular structure of ATP. The ATP molecule is composed of a nucleotide base adenine, a sugar molecule ribose, and a chain of three phosphate groups.

diphosphate (ADP) can be reused, together with inorganic phosphate, to synthesize another ATP molecule. There are various ways how are ATP molecules synthesized in living systems, the first one being vastly prevalent:

- by using the energy of oxygen reduction in a process during respiration called oxidative phosphorylation
- by using the energy of photons in a process during photosynthesis called photophosphorylation
- by using the reduction of sulphate, nitrate, sulfur, or fumarate during anaerobic respiration
- by using a substrate in a process during fermentation called substrate-level phosphorylation
- by using the high-energy phosphate supply phosphocreatine in a process called transphosphorylation

During cellular respiration, both aerobic and anaerobic, chemical compounds are used to build an electrochemical (proton) gradient across a membrane. Protons move along the proton gradient through ATP synthase, and their potential energy is used for catalysing ATP synthesis. ATP synthase is therefore present in almost every living organism, with the exception of some amitochondrial protists, such as

human parasites *Entamoeba histolytica*, *Giardia intestinalis* or *Cryptosporidium parvum*, and microsporidians [Tachezy and Smid, 2007]. They adapted to hypoxic environment or intracellular parasitism by gradually transforming their mitochondria into the reduced forms called mitosomes. In some cases, we can see alternations in the function and structure of mitochondria only during some stages of a life cycle of a parasite, for example in the case of *Trypanosoma*, employing substrate-level phosphorylation only in excess of glucose in mammalian host's bloodstream.

Apart from very few organisms, ATP synthase is an essential building block of living systems, and it is believed to be pre-dating the last universal common ancestor [Matzke et al., 2021]. However, it is not just the biological significance, but also the structural complexity, which makes it a fascinating subject of research.

1.2 ATP synthase F_1F_o

From the ATP synthase family, I will focus on F_1F_o, an F-type ATP synthase, with the first part of the name derived from "Fraction 1", and the second part from being a binding fraction for antibiotic oligomycin, which inhibits its function.

F_1F_o is an approximately 20 nm tall and 10 nm wide molecule with a molecular weight of approximately 550 kDa. Its function can be described as an operation of two molecular motors connected by one central stalk and one peripheral stalk.

Figure 1.2 a) shows a structural model of *E. coli* F_1F_o, its position in the lipid membrane, and the orientation of the transmembrane proton gradient during an ATP synthesis. Individual subunits are presented in different colours:

- **β_3 subunit** - contains the ATP catalytic binding site located near the interface where β_3 and α_3 meets

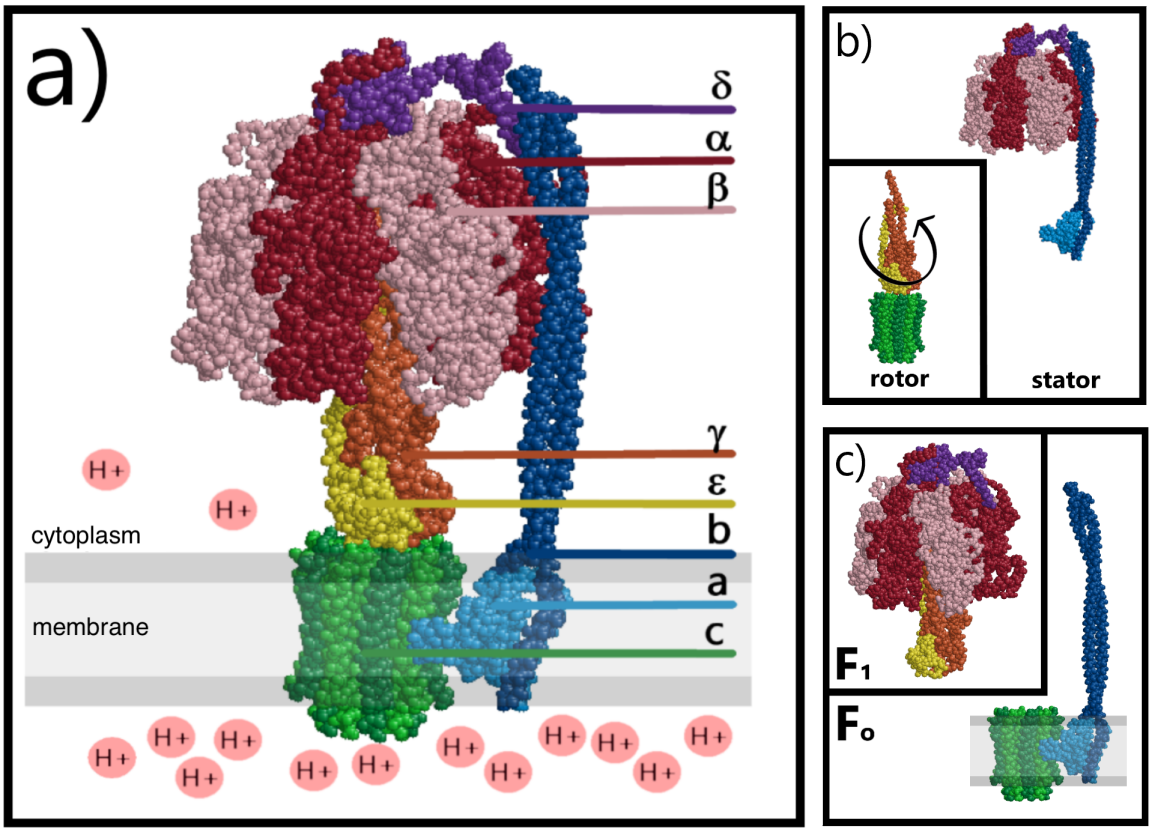


Figure 1.2: A structural model of *E. coli* ATP synthase, PDB ID 5T4O [Sobti et al., 2016], edited using RasMol software. a) The structure of the protein - individual subunits shown in different colours. The position of the lipid membrane is shown in grey. The difference in proton concentration through the membrane creates an electrochemical transmembrane potential. b) The F_1F_o molecule consists of a rotor and a stator. The direction of rotation during the ATP synthesis is shown by the black arrow. c) Two parts of F_1F_o: the water-soluble F_1 and the membrane protein F_o with a water-soluble part, subunit b.

- **α_3 subunit** - its structure is very similar to the structure of the β_3 subunit, but its binding site is non-catalytic. Specifically, it was shown in a crystallographic study of bovine heart mitochondrial F_1F_o, [Abrahams et al., 1994], that β-Glu-188 has been replaced by α-Gln-208, resulting in an inability to bind to the water molecule that in β_3 subunit reacts with the γ-phosphate of the ATP.

- **δ subunit** - located at the top of the hexametric structure, it is necessary for the F_1 binding to the F_o [Sternweis, 1978]

- **γ subunit** - a part of the main stalk, penetrating the hexametric head structure

- **ϵ subunit** - the second part of the asymmetric central stalk, which binds with

the c-ring

- c_{10} **subunit** - c subunit monomers create a c-ring, which varies in size from 8 to 17 in different species [Nirody et al., 2020]. Each c subunit contains one proton binding side and translocates one proton per revolution.

- **a subunit** - mediates proton translocation across the membrane

- b_2 **subunit** - occurs in the form of homo-dimer and forms a peripheral stalk. Due to the symmetry mismatch between the head with the 6-fold symmetry and the c-ring with the 10-fold symmetry, it may play a role of an elastic spring, temporarily storing some of the energy for the catalysis of ATP synthase.

Energy conversion by F_1F_o

Figure 1.2 c) shows *E. coli* F_1F_o divided into the two molecular motors F_1 and F_o. The two connect via the central and the peripheral stalk. However, when not connected, the two molecular motors can work independently.

F_o works as a passive proton channel, transporting the protons through the membrane in the direction of the proton motive force. This process can be described as a conversion of the electrochemical potential energy of the protons into the rotational energy of the rotor of F_o. The role of the rotor takes the c-ring, and the a and the b_2 subunits work as a stator.

F_1, when free, hydrolyses ATP molecules in the solution. In chemical equilibrium, almost all the ATP would eventually hydrolyse to ADP and phosphate. A system with a higher ATP : ADP ratio is kept away from equilibrium through Gibbs free energy. Therefore, we can conclude that F_1 is converting Gibbs free energy of the system into the rotational energy of the rotor of F_1 by hydrolysing ATP. In this case, the hexametric head structure, together with the δ subunit, play a role of a stator, and the γ and the β subunits work as a rotor. (Conveniently, in the case of a free

motor in solution, the rotor and the stator rotate relative to each other, and we can choose a more convenient coordinate system.)

Mechanical coupling of the rotors of F_1 and F_o causes a transfer of the rotational energy of the rotor of F_o to the rotor of F_1, reversing the direction of rotation of the rotor of F_1, and this rotational energy is used for catalysing the synthesis of ATP.

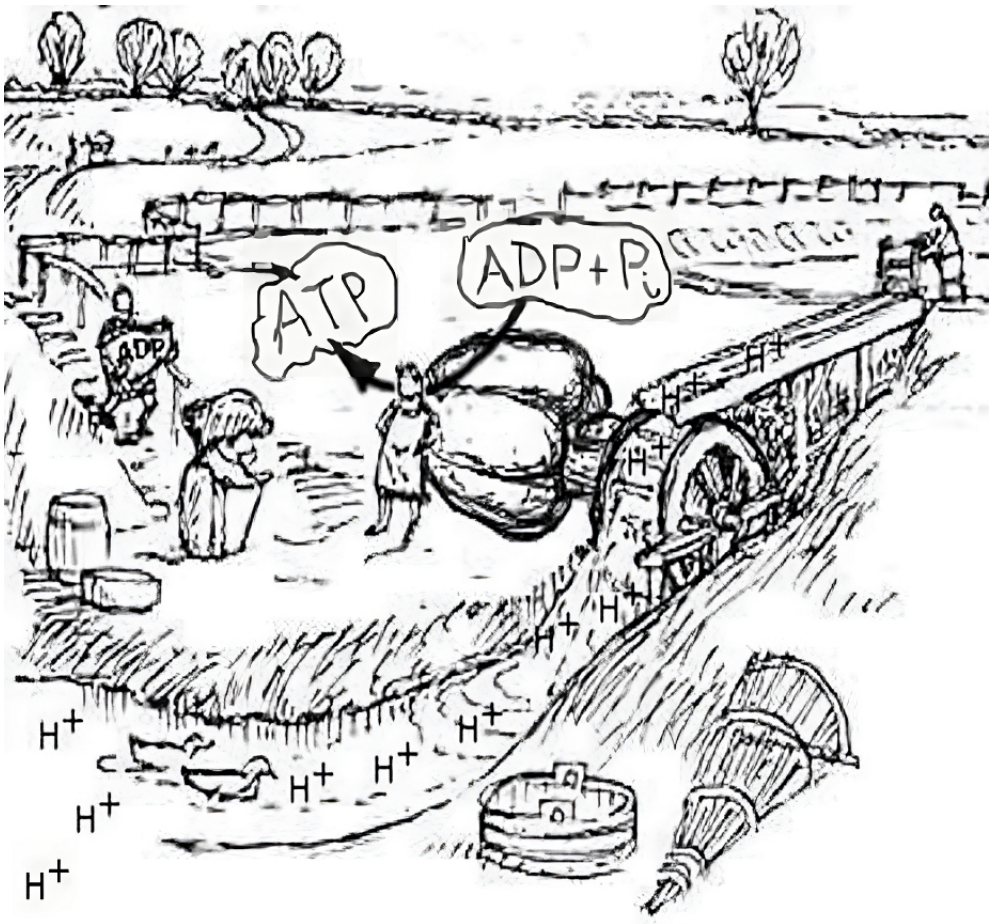


Figure 1.3: The drawing illustrates the energy conversion by ATP synthase. The transmembrane potential energy is replaced by gravitational potential energy. The image is from www.atpsynthase.info, copyright Boris A. Feniouk.

1.2.1 *E. coli* and TA2.A1 F_1F_o: differences

In this project, two different species of F_1F_o were studied in parallel to increase the chances of success; *E. coli* F_1F_o [Ishmukhametov et al., 2005], and F_1F_o from ther-

moalkaliphilic *Bacillus* sp. strain TA2.A1 [Cook et al., 2003]. They differ in the size of the c-ring, *E. coli* c-ring contains 10 monomers, and the TA2.A1 c-ring consists of 13 monomers. TA2.A1 F_1F_o at physiological conditions works at higher pH than *E. coli* F_1F_o, and has an optimal temperature range of 65-70 °C, compared with optimal temperature for *E. coli* F_1F_o 37 °C.

Another difference is that *E. coli* F_1F_o can synthesise and hydrolyse ATP, but TA2.A1 F_1F_o hydrolyses ATP at a much lower rate. However, detergent lauryldimethylamine oxide (LDAO) can activate ATP hydrolysis by TA2.A1 [Cook et al., 2003].

1.2.2 ATP synthase research

The story of ATP synthase research began in the laboratory of Efraim Racker in 1960. Studying beef heart mitochondria, they isolated a submitochondrial water-soluble factor (F_1). They observed that without this component, the oxidative phosphorylation system still catalysed the electron transport, but without the phosphorylation. However, oxidative phosphorylation was restored after the addition of this water-soluble component [Pullman et al., 1960].

A year later, Peter Mitchell postulated a hypothesis that connected the electrochemical potential of protons across the membrane with ATP synthesis [Mitchell, 1961]. Later, in 1978, he received the Nobel Prize for his chemiosmotic hypothesis. The hypothesis was supported by the experiment with chloroplast membranes, where the synthesis of ATP was observed in the absence of light after imposing a pH gradient across the membrane [Jagendorf and Uribe, 1966]. The final confirmation was established by the experiment with ATP synthase reconstituted into lipid vesicles, which confirmed that a transmembrane pH gradient drives the synthesis of ATP [Sone et al., 1977].

In 1973, Paul Boyer described the kinetics of oxygen exchange between the water and ATP molecules involved in oxidative phosphorylation and proposed the binding change mechanism: he identified that the energy-requiring step is not the ATP synthesis itself, but the conformational changes in ATP synthase, creating a difference in the binding affinities of the three binding states [Kayalar et al., 1977], [Gressers et al., 1982]. Moreover, the physical rotation of the central part of the protein was proposed in the later paper without further proof. This idea was revisited after the first molecular structure of bovine F_1 was determined by John Walker's group in 1994 [Abrahams et al., 1994]. Boyer and Walker shared half of the Nobel Prize in chemistry in 1997 "for their elucidation of the enzymatic mechanism underlying the synthesis of adenosine triphosphate (ATP)".

Rotation studies of F_1

Guided by the molecular structure of F_1, scientists proposed a mutation on the β subunit of *E. coli* F_1, which allowed the formation of a disulfide bond between the β and the γ subunit. While the formation of the crosslink resulted in the inactivation of F_1, its reduction restored the full activity. Moreover, they used radiolabelled β subunit to demonstrate the rotation of the γ subunit relative to the β subunit during the ATP hydrolysis [Duncan et al., 1995].

Another demonstration of F_1 rotation was performed by applying polarized absorption relaxation after photobleaching to the eosin-labelled γ subunit of the immobilized molecule during ATP hydrolysis [Sabbert et al., 1996]. They showed that the rotation was blocked when they substituted ATP with non-hydrolysable adenylyl-imidodiphosphate.

Single-molecule direct observations of rotation of immobilized F_1 during ATP hydrolysis were performed using approximately 1 μm fluorescent actin filament at-

tached to the γ subunit [Noji et al., 1997] (Figure 1.4) or by attaching a 40 nm gold bead to the γ subunit [Yasuda et al., 2001] (Figure 1.4). The second experiment with submillisecond resolution confirmed that F_1 rotates in discrete 120° steps, which is consistent with ATP hydrolysis on three β subunits. They also identified 90° and 30° substeps, which they believed were driven by the binding of ATP and release of ADP, respectively.

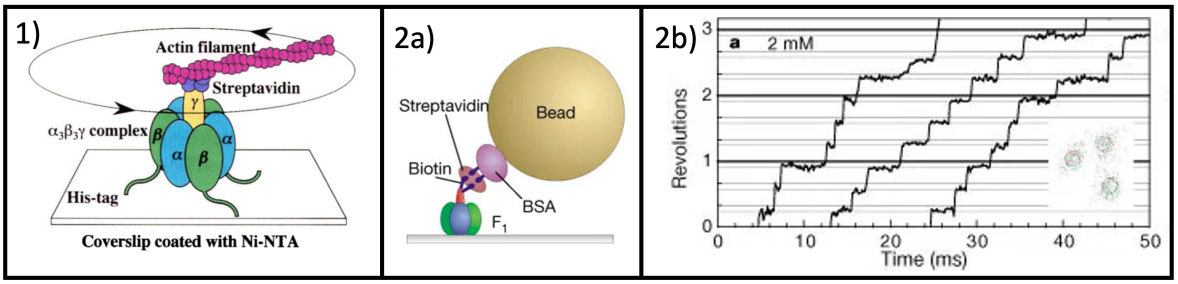


Figure 1.4: 1) Visualisation of F_1 rotation using an actin filament, the scheme of the experiment from their publication [Noji et al., 1997] 2) Visualisation of F_1 rotation using a gold bead, a) the scheme of the experiment, b) a graph of distinct rotational steps on submillisecond scale, adapted from their publication [Yasuda et al., 2001]

Rotation studies of F_1F_o

Actin filaments were also used for the visualisation of rotation of the entire F_1F_o molecule [Sambongi et al., 1999] (Figure 1.5). In this study, *E. coli* F_1F_o was immobilized, and the c subunit was labelled with an actin filament. The rotation was recorded during the ATP hydrolysis. Although the subsecond resolution was not efficient for recording the steps, they were able to conclude virtually lossless energy coupling between the subunit γ and the subunit c.

The rotation of F_1F_o during ATP hydrolysis was also published in [Onoue et al., 2009]. They reconstituted F_1F_o in a giant liposome and immobilized the protein on a glass surface. A micron -sized plastic bead was used for monitoring the rotation of the c subunit inside the giant liposome. Both approaches, however, monitored the function of F_1F_o in a lipid membrane with no transmembrane potential.

Other advances were achieved using single-molecule Förster resonance energy transfer (FRET), in experiments with energized proteoliposomes. FRET labels on the ϵ and the b subunits of *E. coli* F_1F_o revealed that proton transport through the enzyme leads to conformational changes of ϵ [Zimmermann et al., 2005]. Moreover, 36° step size of rotary c subunits was detected during observation of *E. coli* F_1F_o labelled with FRET labels on the a and the c subunits during ATP synthesis [Düsser et al., 2009]. The most significant F_1F_o rotational experiments using single-molecule FRET are summarized in the review [Duncan and Börsch, 2013]. However, these experiments face the problem of the low signal-to-noise ratio and fast photobleaching.

A new experimental strategy was presented in [Watanabe et al., 2013]. They incorporated *E. coli* F_1F_o into a planar bilayer supported by a 200 nm layer of Ni-NTA agarose, which also anchored the c subunit labelled with His tags. They observed rotation of the β subunit through an attached 80 nm gold nanobead in total internal reflection dark-field mode. The transmembrane proton-motive force driving the ATP synthase was created by photolysis of caged photon upon total internal reflection illumination of 1-(2-nitrophenyl)ethyl sulphate by ultraviolet light (404 nm). They presented a rotational trace with 5 nm spatial and submillisecond temporal resolution and identified 120° steps (Figure 1.5).

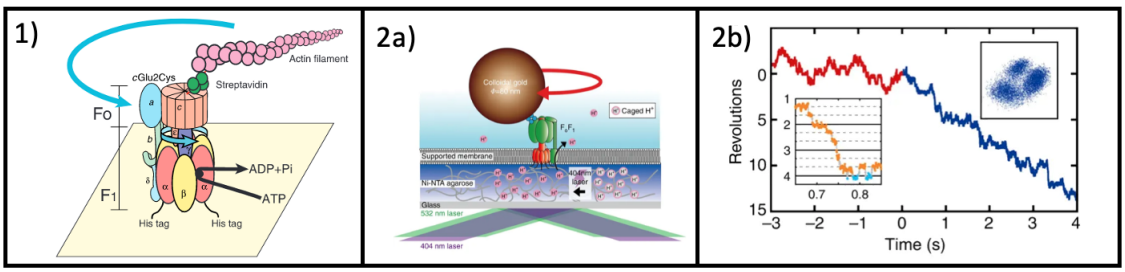


Figure 1.5: 1) Visualisation of F_1F_o rotation using an actin filament, the scheme of the experiment from their publication [Sambongi et al., 1999] 2) Visualisation of F_1F_o rotation using a gold bead, a) the scheme of the experiment, b) a graph of rotational steps, adapted from their publication [Watanabe et al., 2013]

Afterwards, the functional research was mostly focused on single-molecule FRET experiments performed in an anti-Brownian electrokinetic trap, which increased the resolution of the intramolecular distance measurements. With this approach, they measured heterogeneity in enzyme activity under the constant ADP concentration [Perez et al., 2023].

However, the biggest attention was later focused on the structural studies of F_1F_o, especially the research using cryogenic electron microscopy (cryo-EM) to reveal rotational sub-states of the protein, as described in the next section. Progress in functional and structural studies of F_1F_o has also driven the research of possible modulators of this protein for the treatment of human disease. Recently identified compounds are summarized in the review [Patel et al., 2020].

Symmetry mismatch

The mechanism of mechanical coupling of the two molecular motors remains unclear. F_1 with three-fold symmetry and F_o with 8-17 fold symmetry (depending on the species) rotate together, therefore, it was suggested that there must be a place in the protein accommodating for temporal elastic storage of the energy. The proposed candidates are the central stalk [Cherepanov et al., 1999], [Panke and Rumberg, 1999], the peripheral stalk [Stewart et al., 2012] and OSCP subunit in mitochondrial F_1F_o or the corresponding δ subunit in bacterial F_1F_o [Murphy et al., 2019].

An interesting insight was obtained recently in a cryo-EM study of *E. coli* F_1F_o [Sobti et al., 2020]. They tried to lock the rotor of F_1 in a single rotational position by the presence of 10 mM MgADP in the solution. Overall, they presented nine structures with 3.1-3.4 Å resolution, revealing four discrete rotational substates. They were able to visualise bends and twists in the peripheral stalk and torsional flexing of the entire molecule caused by the symmetry mismatch (Figure 1.6).

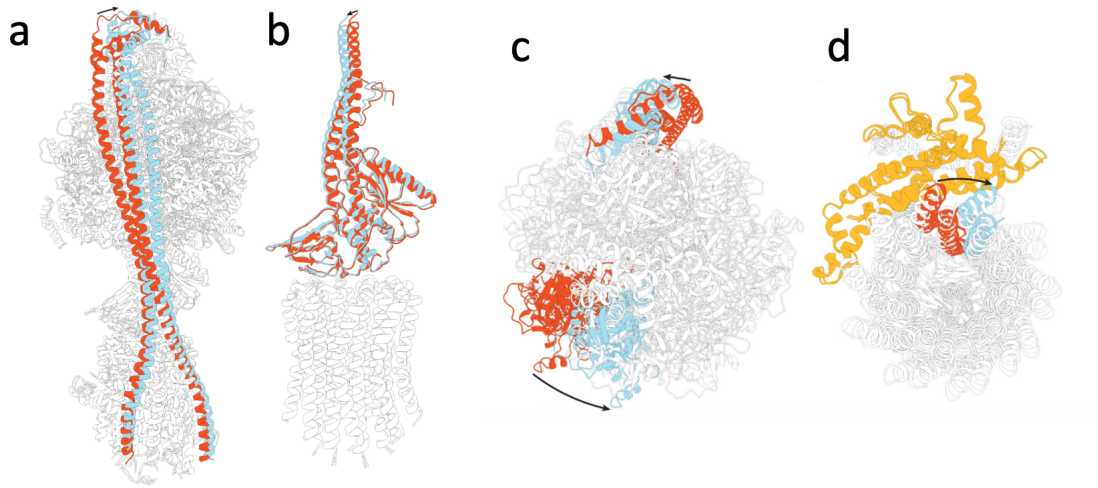


Figure 1.6: Molecular models of *E. coli* F_1F_o published in [Sobti et al., 2020]. In each image, they compared the position of two different rotational substates (orange substate 1A and light blue substate 1E), and the movement is also indicated by the black arrow. a) Superposition on the a subunit viewed from the side. Highlighted peripheral stalk visibly bending and twisting. b) Superposition on the c ring. Highlighted a small movement of the central motor. c) Superposition on the a subunit viewed from above with highlighted α subunit and the peripheral stalk. d) Superposition on the a subunit (yellow) viewed from bellow with highlighted c subunit.

1.2.3 Open questions

Performing rotational studies of F_1F_o under a controlled electrochemical transmembrane potential was shown to be very difficult. Although the attention was lately shifted towards the structural cryo-EM experiments, there are still several questions that can probably only be answered with functional studies.

Some of the open questions regard the minimum transmembrane potential required for the rotation of F_1F_o. We cannot yet tell, if both chemical and electrical potentials are required for the function of this enzyme, and what their roles are. In the past, functional studies often either did not attempt to apply transmembrane potential, or only chemical and not electrical potential was applied. I therefore believe that it would be a useful opportunity to study F_1F_o under the highly accurate and independent control of electrical and chemical potential, as would allow the experimental assay presented in this work.

Furthermore, high-resolution measurements of rotation steps can contribute to the still controversial discussion about the elastic energy storage inside the protein. To be able to resolve the dynamics between the individual 120° steps, we would need to achieve submillisecond resolution. This may be possible by monitoring the rotation via the attached gold nanorods.

1.3 Model lipid membranes

An important part of designing any functional study of membrane proteins is choosing a suitable model lipid system that can mimic the natural environment of the protein. There is indeed a wide range of different approaches, which I summarized below:

- liposomes
    - small unilamellar vesicles
    - large unilamellar vesicle
    - giant unilamellar vesicles
- planar membranes
    - supported
        - with solid support
        - polymer-cushioned and tethered membranes
    - unsupported
        - nanodiscs
        - suspended membranes
        - droplet interface bilayers
        - microdevices with microwells

1.3.1 Liposomes

Liposomes are artificial vesicles composed of one or more lipid bilayers. They are widely used in different experimental assays, including activity measurements of transporter molecules [Veshaguri et al., 2016]. In this single-molecule experiment, proton pumping of P-type ATPase AHA2 is monitored through pH-sensitive fluorophore pHrodo.

It is possible to energize liposome membrane using acid/base assay or by incorporating a proton pump into the membrane (described in section 2.1.5). The main disadvantage is that the inner environment of the liposome is not accessible during the experiments.

1.3.2 Supported planar membranes

Planar membranes with solid support

The first supported bilayers were developed in response to the difficulty of reconstituting transmembrane proteins into lipid monolayers. The experiment included various phospholipid membranes supported on oxidized silicon
[Tamm and Mcconnell, 1985]. The assay was later adapted for studying lipid domain formation [Kirat et al., 2009], protein self-assembly [Carton et al., 1996], membrane-cytoskeleton interactions [Loose and Schwille, 2009], along with others. Although the lipid bilayer is separated from the solid support by a thin water film, the separating distance is limited, which could lead to interaction between the solid support and the protein incorporated into the membrane, and, possibly, loss of functionality or denaturation.

Polymer-cushioned and tethered planar membranes

The problems with the solid support have been addressed by introducing an extra layer of polymer cushion [Sackmann, 1996], or, later, by different types of spacers,

for instance, peptide spacer attached through anchor lipid or biotin-avidin-biotin link of biotinylated bovine serum albumin and biotinylated liposome [Rebaud et al., 2014].

These methods not only allowed the incorporation of large membrane proteins into the membrane without the risk of contact with the solid support but also enabled building of transmembrane potential. The method was later advanced by creating independent compartments (aqueous droplets) in a hydrophobic solution on top of hydrogel-supported bilayer [Leptihn et al., 2013]. The droplet-on-hydrogel bilayer is described in detail in section 1.4.1.

1.3.3 Unsuported planar membranes

Nanodiscs

Nanodiscs are artificial membrane discs encircled by a stabilizing protein [Borch and Hamann, 2009]. With a controllable diameter up to tens of nanometers, they allow proteins incorporated in a membrane to become soluble in a detergent-free aqueous medium. While this is extremely useful for studying receptors or ligand binding, nanodiscs do not define internal and external volume, and, therefore, it is not possible to apply potential gradient through their membrane.

Suspended membranes

Suspended lipid bilayers are formed over micro- or nanosized pores. First suspended membranes were described in 1962 [Mueller et al., 1962] and were referred to as black lipids, due to their dark appearance in reflected light. This method allows free access to the membrane from both sides but offers very limited stability of the membrane.

Droplet interface bilayers

The droplet interface bilayer system employs the advantages of suspended membranes while introducing additional stability [Bayley et al., 2008]. It is created from two aqueous droplets submerged in an oil-lipid solution (lipid monolayer spontaneously assembles on the surface of the droplets) and brought into contact (the process is illustrated in Figure 1.7). Possibilities of this system include the incorporation of membrane proteins into the droplet interface bilayer, attaching electrodes to measure ion current through the embedded channels and pores or applying transmembrane potential, and creating droplet networks.

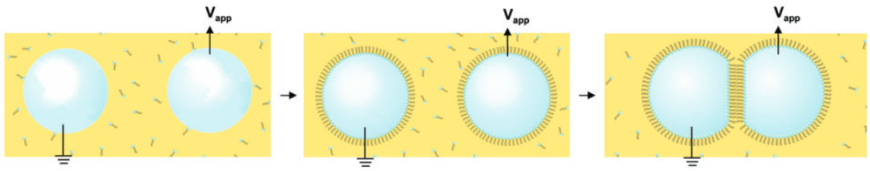


Figure 1.7: Illustration of one type of formation of droplet interface bilayer adapted from [Bayley et al., 2008]. Two aqueous droplets pipetted onto agarose-coated electrodes and submerged in an oil-lipid solution. After the lipid monolayer spontaneously assembles on the surface of the droplets, the droplets are brought into contact and form a bilayer.

Microdevices with microwells

Arrayed lipid bilayer chambers (ALBiC) is a microsystem for quantitative analysis of the activity of transporters [Watanabe et al., 2014a]. It consists of 4 μm lipid bilayers and allows single-molecule analysis of the activity of incorporated proteins. This was demonstrated by recording passive proton transport by α-hemolysin and proton transport by F_1F_o during ATP hydrolysis. Figure 1.8 shows schematic images of the system.

The arrayed lipid bilayer chambers were also used for studying membranes with asymmetric lipid composition, created by consequently injecting two different lipid solutions [Watanabe et al., 2014b]. They reported the formation of 10,000 asymmet-

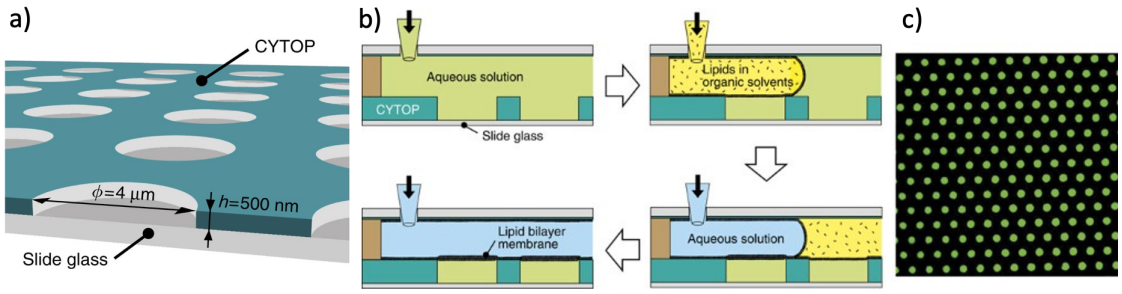


Figure 1.8: Images of the arrayed lipid bilayer adapted from [Watanabe et al., 2014a]. a) Illustration of the microdevice. b) Scheme of the lipid bilayer formation. c) Fluorescent signal from Alexa 488 encapsulated in the microchambers sealed by a lipid membrane.

ric lipid bilayers on a single micro-chamber array with 97 % efficiency.

The same system was later adapted for preparing micro-reactor arrays with a concentration gradient of target molecules (demonstrated with alkaline phosphatase and α-hemolysin), allowing multiple bioassays under the different conditions to be measured in parallel [Watanabe et al., 2018].

1.4 Foundations of the assay

The experimental assay presented in this work is based on the previously published work described below.

1.4.1 Droplet-on-hydrogel bilayer

Droplet-on-hydrogel bilayer is a novel experimental assay for studying membrane proteins in a stable planar lipid bilayer supported by a hydrogel film [Leptihn et al., 2013]. Its formation is explained in Figure 1.9. Briefly, the supporting hydrogel is first spin-coated on a glass cover slip. It is then covered with lipid and oil solution, and a water droplet is immersed in the same lipid and oil solution. When a lipid monolayer is spontaneously formed in oil/water interfaces on the sur-

face of the hydrogel and around the droplet, the droplet falls on the surface. A droplet-on-hydrogel bilayer is formed at the contact of the two monolayers. Finally, a silver/silver chloride electrode is connected to the droplet. The method enables a single-channel electrophysiology and simultaneous optical imaging. Currently, it is mainly used for studying pores, where it is possible to monitor an electrical current through the pore. Naturally, this is not possible for transporter proteins, since the electrical current flowing through transporters is unmeasurably small. We can, however, use the electrodes to apply a transmembrane potential and measure the function of the protein optically.

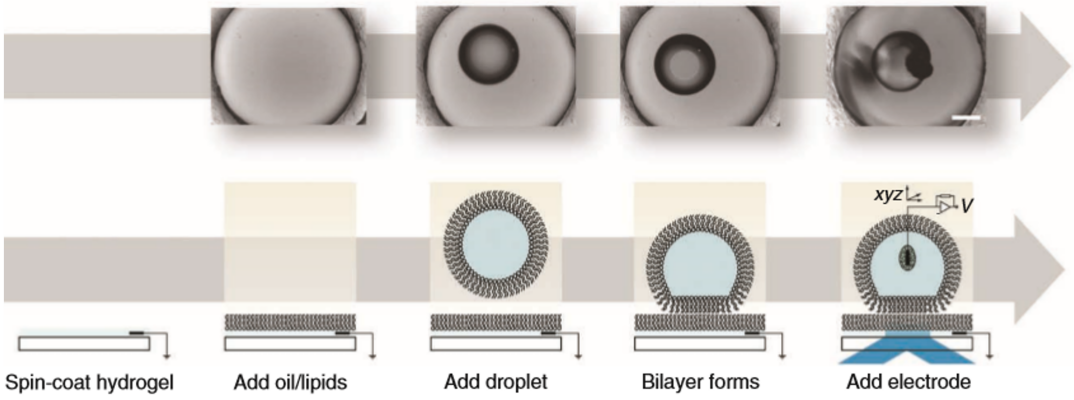


Figure 1.9: Droplet-on-hydrogel bilayer formation: Supporting hydrogel is spin-coated on a glass cover slip and covered with lipid and oil solution. A water droplet is immersed in the same lipid and oil solution, and a lipid monolayer spontaneously forms in oil/water interfaces. The droplet falls on the surface, and a lipid bilayer is formed at the contact of the two monolayers. Finally, a silver/silver chloride electrode is connected to the droplet. An illustration from [Leptihn et al., 2013].

1.4.2 Charged membrane fusion

A single-step delivery of fragile membrane proteins into membranes by fusion of oppositely charged proteoliposomes without a loss of their function was described in [Ishmukhametov et al., 2010]. This method can also work with a perfusion system, transporting the cationic proteoliposomes with reconstructed F_1F_o to the droplet. In a low-salt environment of the droplet, the cationic proteoliposomes will fuse with a negatively charged lipid bilayer, delivering functional protein into the membrane.

1.4.3 Gold nanorods

A potential way how to increase the resolution of rotation of F_1F_o would be using gold nanorods instead of spherical gold nanobeads to label the protein. While the spherical shape of the beads allows only for localisation of the label, the structural anisotropy of the rods provides also information about their orientation.

Ashely Nord in her doctoral thesis [Nord, 2013] compared the noise in signal from a 100 nm gold nanobead attached to a spinning hook of the bacterial flagellar motor and in signal from a 110 nm by 53 nm gold nanorod attached to a hook of the bacterial flagellar motor, which is not energized, and the rod diffuses freely. Figure 1.10 shows the comparison of the traces from the experiments, with red lines showing the relative size of a single step. Gold nanorods improved the angular resolution of the hook in comparison with gold nanobead labels.

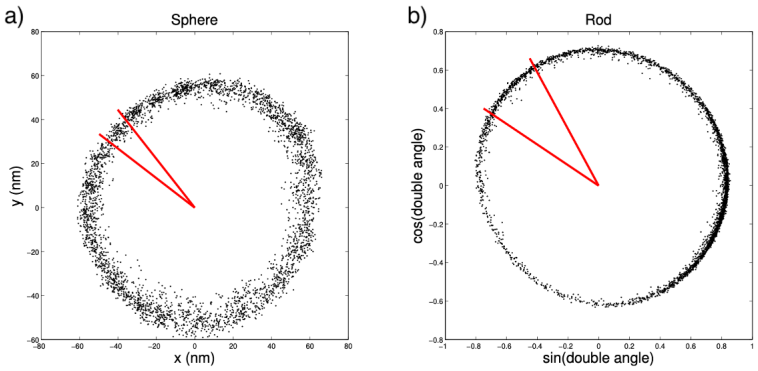


Figure 1.10: A comparison of the noise in a) the x and y position of a 100 nm gold nanobead attached to a spinning hook of the bacterial flagellar motor and b) sine and cosine of the double in-plane angle (calculated from intensities of four polarisation channels) of a 110 nm by 53 nm gold nanorod attached to a hook of the bacterial flagellar motor, which is not energized, and the rod diffuses freely. The red lines indicate the relative size of the single step. The frame rate in both experiments was 4500 Hz.

Chapter 2

Preparation of proteins for functional study of F_1F_o

The main motivation for creating an experimental assay for the functional study of membrane proteins in energised lipid membrane was a desire to observe the molecular motor F_1F_o in conditions mimicking the protein's natural environment. The first chapter of my thesis is therefore dedicated to this protein. I learned how to express, purify, analyse, quantify, characterise, and mutate F_1F_o, and how to functionalise agarose to anchor F_1F_o to the agarose layer. Here I describe the main principles and methods I used, along with the results I obtained. The detailed protocols can be found in the Methods.

2.1 Protein preparation

I learned how to express and purify F_1F_o with the kind help and guidance from Dr Cornall. We used the protocol from [Ishmukhametov et al., 2005] for *E. coli* F_1F_o and the protocol from [McMillan et al., 2007] for TA2.A1 F_1F_o.

2.1.1 *E. coli* F_1F_o

I used *E. coli* DK-8 strain transformed with plasmid pFV23, containing a cysteine-free F_1F_o mutant with one cysteine added after the second amino acid of the α subunit, one cysteine after the second amino acid of the c subunit, and a His Tag (six histidine residues) after the fourth amino acid of the β subunit (courtesy of Dr Ishmukhametov).

A single colony was incubated in lysogeny broth (LB) supplemented with 100 μg/ml ampicillin and grown overnight at 37 °C. Cells were then diluted in fresh culture media and grown for 6-8 hours, harvested by centrifugation, and the pellet was stored at -80 °C.

First, we used a French press for lysing the bacteria. Cell debris was removed by centrifuging, and the supernatant was subsequently ultracentrifuged to remove water-soluble proteins. The pellet was resuspended with added detergent for dissolving the membrane proteins, homogenised in a homogeniser, and incubated for 90 minutes. We then collected the solubilised protein by ultracentrifugation.

Further purification was conducted at 4 °C using a Ni-NTA gravity-flow chromatography column. As the last step, cysteine residues on the α and the c subunits were biotinylated. I flash-froze the sample dropwise in liquid nitrogen and stored it in a liquid nitrogen dewar. The detailed protocol can be found in Methods, section 6.1.

2.1.2 TA2.A1 F_1F_o

I used *E. coli* C43 strain transformed with vector pET-3, containing cysteine-free TA2.A1 F_1F_o mutant with a His Tag (six histidine residues) after the fourth amino acid of the β subunit, a single cysteine after the second amino acid of the α subunit and a single cysteine after the second amino acid of the c subunit. The details about the mutations can be found in section 2.2.

A single colony was incubated in lysogeny broth (LB) supplemented with 100 μg/ml ampicillin and grown overnight at 37 °C. Cells were then diluted in fresh culture media and grown with monitoring absorbance (optical density) at 600 nm, until a value between 0.35 and 0.40 was reached. Protein expression was then induced by adding 1 mM of β-D-1-thiogalactopyranoside (IPTG), and the cells were incubated for another 5 hours. Cells were then harvested by centrifugation, and the pellet was stored at -80 °C.

Like in the *E. coli* F_1F_o protocol, we used a French press for lysing the bacteria. Cell debris was removed by centrifuging, and the supernatant was subsequently ultracentrifuged to remove water-soluble proteins. The pellet was resuspended with added detergent for dissolving the membrane proteins, homogenised in a homogeniser, and incubated for 90 minutes. We then collected the solubilised protein by ultracentrifugation.

Further purification was conducted at 4 °C using a Ni-NTA gravity-flow chromatography column. As the last step, cysteine residues on the α and the c subunits were biotinylated. I flash-froze the sample dropwise in liquid nitrogen and stored it in a liquid nitrogen dewar. The detailed protocol can be found in Methods, section 6.2.

2.1.3 Protein concentration assays

I used several different bicinchoninic acid (BCA) assays for quantifying the concentration of the protein samples. They are based on the reduction of divalent copper cations (Cu^{2+}) to monovalent copper cations (Cu^{+}) by the peptide bonds from the protein. Cu^{+} chelates with bicinchoninic acid to form a light-absorbent complex, therefore light absorbed by the sample is proportional to the protein concentration. First, I measured a calibration curve using samples with different (known) concentrations of bovine serum albumin. I fitted the data points with a line, and I used the

line equation to convert light absorbance from the protein sample to protein concentration.

The results reported in Figure 2.1 were obtained with the Pierce Rapid Gold BCA Protein Assay Kit from Thermo Fisher Scientific, and the protocol adapted from the manual is described in detail in the Methods, section 6.3.

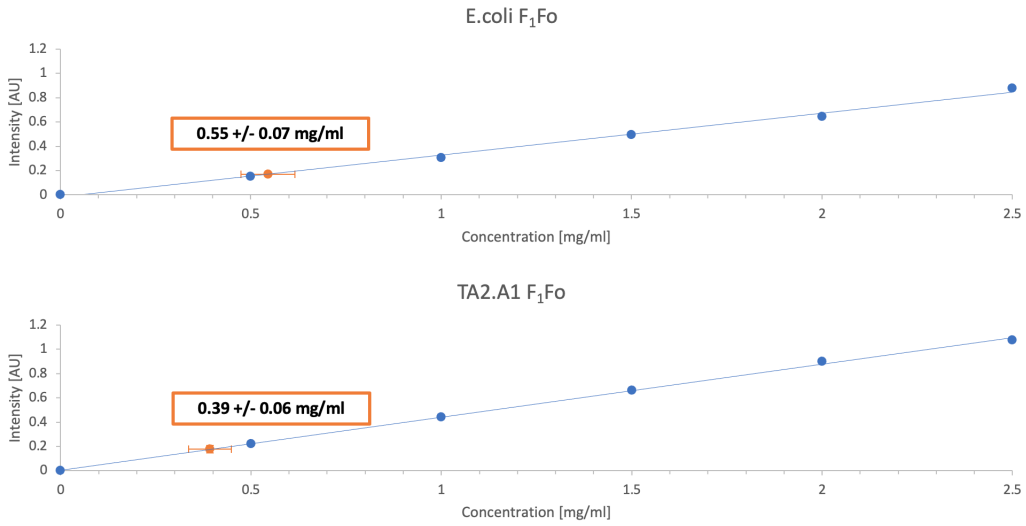


Figure 2.1: Measurement of the concentration of *E. coli* F_1F_o sample and TA2.A1 F_1F_o sample which I expressed and purified. I used the Pierce Rapid Gold BCA Protein Assay Kit. I measured the intensity from two samples of the same protein, and the protein concentration was calculated from an average of the two measurements. A conservative estimate of the confidence interval was calculated from the difference between these measurements.

2.1.4 Polyacrylamide gel electrophoresis (PAGE)

Another standard method for the examination of protein samples is protein gel electrophoresis. In contrast with the bicinchoninic acid (BCA) protein concentration assays, it does not measure the concentration of the protein. In fact, we need an estimation of protein concentration to run a PAGE gel. The advantage of PAGE is that it separates protein subunits according to their electrophoretic mobility (a function of molecular weight). It is then possible to calculate the ratios between concentrations

of subunits with different electrophoretic mobility. I examined several of my protein samples, with the kind help of Dr Rieu and buffers provided by Dr El Sayyed.

We used Mini-PROTEAN TGX Precast Protein Gel with 4-20 % gradient, the detailed protocol is described in the Methods, section 6.4.

Figure 2.2 shows SDS-PAGE (sodium dodecyl sulfate - polyacrylamide gel electrophoresis) gels, containing two different *E. coli* F_1F_o preparations and two different TA2.A1 F_1F_o preparations. Samples names and different bands are annotated to indicate the position of individual subunits on the gel. The difference in intensities of the bands between the samples only reflects the amount of the protein used in the experiment. I can see that the purification process was not perfect as indicated by the presence of other proteins in the sample. Nevertheless, for the droplet-on-hydrogel functional F_1F_o study it may not be necessary to optimise the purification protocol. Correctly functioning F_1F_o molecules, which are labelled with a gold nanorod, will produce a rotating signal, which is extremely unlikely to be mimicked by impurities. However, if I later find out that the impurities cause any unexpected problems, I will need to further purify the sample.

I speculated whether the lines above 60 kDa, which are especially strong in TA2.A1 F_1F_o samples, indicate incomplete denaturation of the protein. I have therefore repeated the experiment and found out that denaturation at room temperature and at 90 °C gave me the same results, which indicates that it probably is not the case.

2.1.5 F_1F_o activity assays: overview

There are several possibilities for examining the function of F_1F_o after expression and purification, or even to test it after long storage. Here I summarised some of the different activity assays:

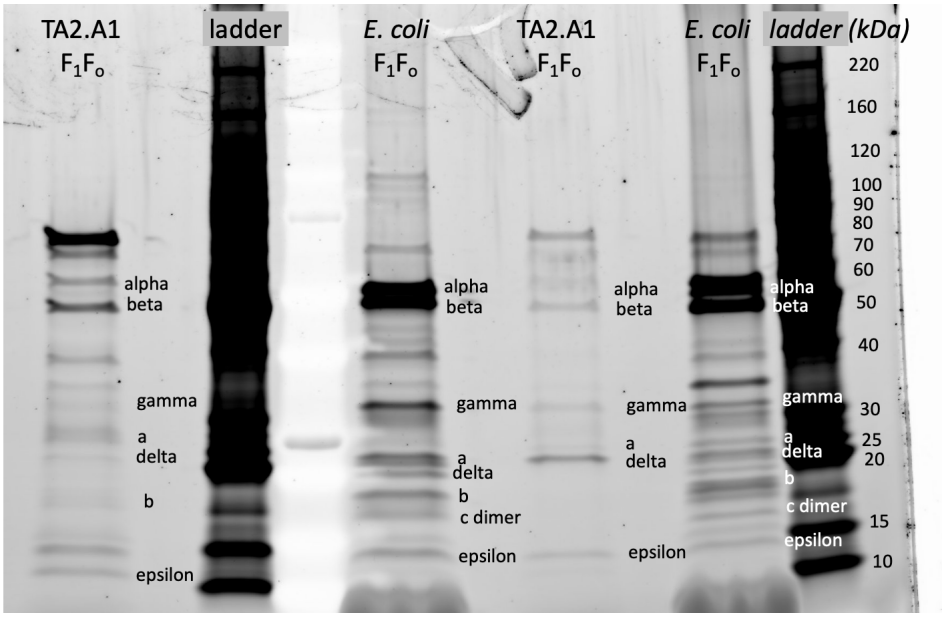


Figure 2.2: SDS-PAGE gels showing four samples, two different preparations of TA2.A1 F_1F_o and two different preparations of *E. coli* F_1Fo. I indicated possible positions of individual subunits, using two protein ladders. Extra lines are suggesting the purification process was not perfect, but that should not negatively affect the experiment.

- **adenosine triphosphate (ATP) hydrolysis:** (TA2.A1 F_1F_o hydrolyse ATP much slower than *E. coli* F_1F_o, unless detergent LDAO is added)

  - **<u>in solution:</u> phenol red assay** (described in section 2.1.6) and **oxidation of NADH (nicotinamide adenine dinucleotide (NAD) + hydrogen (H))** (a scheme is presented in Figure 2.3, and more details can be found in [Bublitz, 2015]) - they only verify activity of the water-soluble F_1, and not the membrane protein F_o

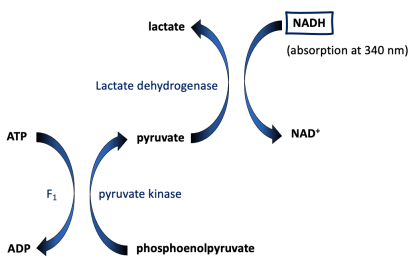


Figure 2.3: The main principle of NADH oxidation activity assay.

- **in proteoliposomes:**

  9-Amino-6-Chloro-2-Methoxyacridine (ACMA) quenching

  ACMA is a fluorescent probe which, under the physiological pH range, exists in two forms: an intensively fluorescing neutral and a less intensively fluorescing mono-cationic form (Figure 2.4). However, only the neutral form can permeate the membrane of the proteoliposomes. ATP hydrolysis by F_1F_o drives a proton transport through the proteoliposome membrane and thus causes acidification inside the proteoliposomes. With decreasing pH, the ratio of mono-cationic and neutral ACMA molecules inside the proteoliposomes increases, which is measurable in bulk as a fluorescence quenching of the sample [Schwamborn, 2017].

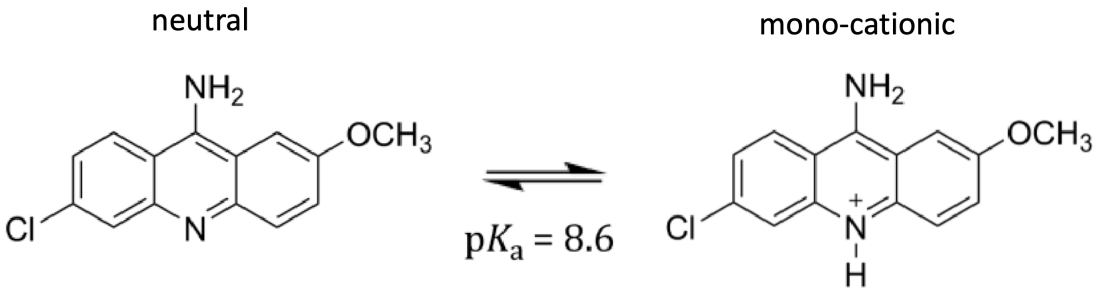


Figure 2.4: Structures of the neutral and the mono-cationic form of ACMA, coexisting at physiological pH range. Acidification of the inside of liposomes powered by ATP hydrolysis shifts the ratio towards the less intensively fluorescent mono-cationic form, which is demonstrated in bulk by fluorescence quenching of the sample. The image is adapted from [Schwamborn, 2017].

- **adenosine triphosphate (ATP) synthesis:**

  - **in proteoliposomes:** the proton motive force driving the ATP synthesis could be generated by:

    - **acid/base assay:** transmembrane pH gradient can be created by the increase of the pH in solution (outside of the proteoliposomes) [Schmidt and Gräber, 1985]
    - **proton pump:** transmembrane potential can be created by light-sensitive

proteorhodopsin, photosystem II [Lee et al., 2018] or bo_3-oxidase [Nilsson et al., 2016]

2.1.6 Phenol red activity assay

The following experiment was performed with the kind help and guidance of Dr Gonzalez, who also prepared the reaction medium. We measured the rate of ATP hydrolysis by the *E. coli* F_1F_o sample. Since there is a proton generated during hydrolysis of the terminal phosphate group of each ATP molecule (Figure 2.5), the rate of hydrolysis could be monitored using a pH indicator phenol red. The detailed protocol can be found in the Methods, section 6.5.

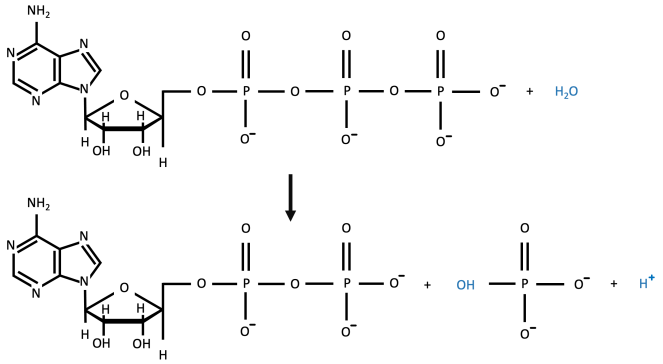


Figure 2.5: Hydrolysis of the terminal phosphate group of an ATP molecule creates ADP, inorganic phosphate, and a proton.

We monitored the change of light absorbance by the sample at 557 nm caused by two separate effects: ATP hydrolysis by 20.4 μg of F_1F_o, and adding 0.5 μmol of hydrochloric acid (HCl). To approximately estimate the rate of ATP hydrolysis, we will compare the changes caused by the two effects, neglecting the buffering effect of the reaction medium and any non-linearity in light absorbance:

HCl calibration:

absorbance before adding 0.5 μmol of HCl: 1.662

absorbance after adding 0.5 μmol of HCl: 1.359

Change in absorbance 0.303 is equivalent to adding 0.5 μmol of H^+.

ATP hydrolysis by F_1F_o:

change in absorbance during hydrolysis: 0.04 per minute

amount of ATP hydrolysed by 20.4 μg of F_1F_o per minute: $\frac{0.04}{0.303} \times 0.5 = 0.066$ μmol

amount of ATP hydrolysed by 1 mg (= 0.002 μ mol) of F_1F_o per minute: $\frac{0.066}{20.4} \times 100 =$ 3.24 μmol

1 mg of *E. coli* F_1F_o hydrolysed 3.24 μmol of ATP per minute.

This is approximately 20 times lower than the values reported in the literature ([Ishmukhametov et al., 2005]), which could be explained by the impurities in the samples observed in SDS-PAGE gel, and by long storage of the sample in liquid nitrogen (more than two years) before activity assay was performed, so it may have slowly denatured over time. Given the fact that the absorbance was stable, and it only started to decrease after adding the F_1F_o, we can exclude the possibility that the observed change in absorbance can be explained by spontaneous ATP hydrolysis.

2.2 Protein labelling: Site-directed mutagenesis

For my experimental assay, it is important to be able to label the protein in a specific way, which was achieved by adding cysteines and histidines to the suitable position on the protein (the positions of cysteins are indicated in Figure 2.6). While this was already done for *E. coli* F_1F_o by Dr Ishmukhametov, I performed mutagenesis of TA2.A1 F_1F_o.

I used a cys-free F_1F_o from thermoalkaliphilic *Bacillus* sp. strain TA2.A1 [Cook et al., 2003] in pET-3 vector, with a His-Tag (six histidine residues) inserted after the first amino acid on the N-terminus of β_3 subunit - courtesy of Dr Ishmukhametov.

The His-Tag on the β_3 subunit enable the use of a nickel - nitriloacetic acid (Ni-NTA) gravity-flow chromatography column for protein purification. My task was to mutate the protein by inserting a cysteine after the second amino acid on the N-terminus of the α_3 subunit, and another cysteine after the second amino acid on the N-terminus of the c_{10} subunit. The α_3 subunit was modified with a cysteine to enable attachment of a biotin-maleimide linker through the reaction of the maleimide with the thiol group on the cysteine. The other end of the linker, the biotin, attaches to the streptavidin on the surface of the gold nanorods. The c_{10} subunit was also modified with cysteine to allow the same protein-maleimide-biotin-streptavidin linking, anchoring the c_{10} subunit to the agarose gel functionalized with streptavidin.

pET-3 vector containing TA2.A1 has 11 524 base pairs, and I chose to perform two subsequent single base pair insertions using a site-directed mutagenesis kit. Alternatively, I could have used the Gibson assembly method, which would allow me to modify fragments of the vector in parallel.

2.2.1 Site-directed mutagenesis

Site-directed mutagenesis is an *in vitro* method for changing, inserting, or deleting one or multiple base pairs of a double-stranded DNA (deoxyribonucleic acid) plasmid (template DNA), originating in the publication [Kunkel, 1985]. There are now several types of commercially available kits using the same principle, from which I tried the QuickChange II XL (I would like to thank Dr Pulcu for providing me with the chemicals) and the QuickChange Lightning site-directed mutagenesis kits.

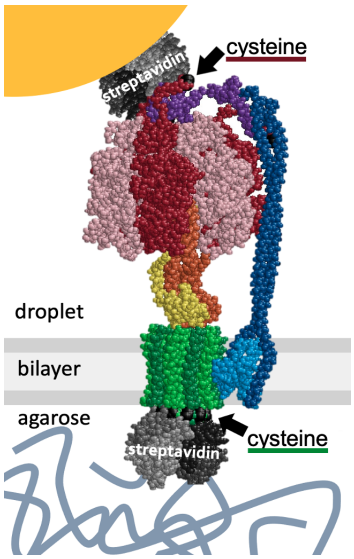


Figure 2.6: A structural model of *E. coli* F_1F_o, PDB ID 5T4O [Sobti et al., 2016], and streptavidin (grey), PDB ID 6J6J [Fan et al., 2019], edited using the RasMol software. The position of cysteines (black spheres) on the α subunit (dark red) and the c subunit (green) are indicated by black arrows. For simplification, there is only one streptavidin molecule shown to be attached to the gold nanorod, and only one streptavidin molecule anchoring F_o to the agarose layer.

This work was completed thanks to the kind help and advice from Dr El Sayyed, Dr Pulcu and Dr Mazumder.

Since I have succeeded with the QuickChange Lightning site-directed mutagenesis kit, in the following text I focus on this method - the principles are similar for both.

I used the protocol in the Instruction manual for the QuickChange Lightning Site-directed mutagenesis kit by Agilent Technologies, and optimised the conditions several times, until the mutagenesis was successful. The final protocol is detailed in the Methods, section 2.7.

Basic principles

Site-directed mutagenesis uses primers, short synthetic pieces of deoxyribonucleic acid (DNA) sequence, which are complementary to the part of the template DNA around the place where we want the mutation to occur, and they contain the desired

mutation (in my case, 3 additional base pairs). These primers are extended during a PCR (polymerase chain reaction) amplification by DNA polymerase, resulting in a nicked copy of the template plasmid with the required mutation (mutagenized plasmid). Subsequently, the template DNA is digested with the restriction enzyme Dpn I. This enzyme is specific for methylated DNA, such as our template DNA produced from *E. coli*, and leaves unmethylated DNA, such as our mutagenized (biosynthesized) plasmid, intact. This process is schematically shown in Figure 2.7.

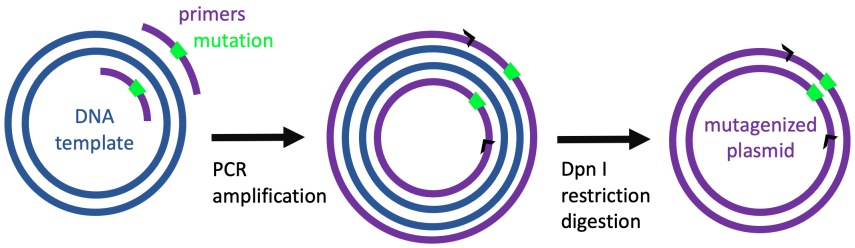


Figure 2.7: A scheme of the site-directed mutagenesis. Primers (purple) complementary to the DNA template (blue) containing the desired mutation (green) are extended during PCR amplification, thus creating a nicked copy of the DNA template with the desired mutation. The methylated template is then digested with a restriction enzyme.

Primer design

As explained in the Instruction manual for QuickChange Lightning Site-directed mutagenesis kit by Agilent Technologies, there are several considerations for primer design:

- both primers must be complementary to the opposite strands of the same sequence of the DNA template
- the desired mutation should be in the middle of the primers, and there should be around 10 to 15 unmutated bases on both sides
- the length of the primers should be between 25 and 45 bases (longer primers are also possible, but it is important to check for secondary structure formation)

- melting temperature (T_m), calculated by an empirical formula for insertion (Equation 2.1), needs to be at least 78 °C

$$T_m = 81.5 + 0.41(\%GC) - \frac{675}{\text{primer length in bases}} \tag{2.1}$$

- guanine (G) cytosine (C) content needs to be at least 40 %, and primers should terminate with one or more guanine or cytosine bases

- primers cannot be 5′ phosphorylated

I tried two different sets of primers, and the following one worked. Inserted bases are:

α subunit:

5′-3′ forward primer: gtgaacgagatgagcTGCatcagacctgaagaaat

5′-3′ (reverse) complementary primer: atttcttcaggtctgatGCAgctcatctcgttcac

length: 35 bases (between 25 and 45)

GC %: $\frac{17}{34} = 45.7$ % (minimum 40 %)

melting temperature: $81.5 + 0.41 \times 46 - (\frac{675}{35}) = 81.16$ °C (minimum 78 °C)

c subunit:

5′-3′ forward primer: gaggaattataatgggaTGCgtcttagctgcagc

5′-3′ (reverse) complementary primer: gctgcagctaagacGCAtcccattataattcctc

length: 34 bases (between 25 and 45)

GC %: $\frac{17}{34} = 47.1$ % (minimum 40 %)

melting temperature: $81.5 + 0.41 \times 47 - (\frac{675}{34}) = 80.9$ °C (minimum 78 °C)

PCR amplification

During this crucial step, the biosynthesis of the mutagenized plasmid takes place at carefully controlled temperatures. Table 2.1 summarises the cycling parameters from the Instruction manual for QuickChange Lightning Site-directed mutagenesis kit by Agilent Technologies:

Segment	Cycles	Process	Temperature	Time
1	1	initialisation	95 °C	2 minute
2	18	denaturation	95 °C	20 seconds
		primer binding	60 (55) °C	10 (20) seconds
		extension	68 °C	0.5 (1) minute /kbp
3	1	final elongation	68 °C	5 minutes
4	1	storage	4 °C	

Table 2.1: Cycling parameters for PCR: temperatures and times recommended by the manual, and, in the brackets, the values which worked for me after the troubleshooting.

The first segment of the polymerase chain reaction (PCR) heats the reaction chamber and starts the DNA denaturation process. The second segment is responsible for the biosynthesis itself. Initially, the hydrogen bonds between the complementary bases break at 95 °C, resulting in the denaturation of the DNA plasmids. Lowering the temperature allows the primers during the second step to bind to the single-stranded DNA template. Finding the proper temperature is crucial: if the temperature were too high, the primer may not bind to the template, and if it were too low, it may be able to bind non-specifically. In Table 2.1, there are temperatures and times recommended by the manual, but I also added the values, which worked for me after the troubleshooting, in the brackets. The third step is when the extension of the primers takes place, eventually creating a copy of the entire plasmid with the desired mutation. The length of this step depends on the size of the plasmid, I allowed 1 minute per 1,000 base pairs of plasmid length. Segment 2, consisting of the denaturation, the primer binding, and the extension, is repeated 18 times, resulting in an exponential amplification of the mutagenized plasmid, before the temperature is lowered and the final storage phase takes place.

2.2.2 Calcium competent cells

After the mutation and amplification of the DNA plasmid using PCR, I used competent cells to take up the DNA from their environment for plasmid storage. I used the commercial XL-10 Gold Ultracompetent cells, but, for long-term storage of the mutated plasmid, I prepared my own calcium competent cells with the kind help of Dr El Sayyed. The detailed protocol can be found in the Methods, section 6.7.

Following the heat-shock transformation described in the Methods, section 6.6, I used one bacterial colony to inoculate an ampicillin medium and cultured the cells overnight. Finally, the cells were diluted with glycerol to 30 *vol*% final concentration, aliquoted, and stored at -80 °C.

2.2.3 DNA extraction and sequencing

To verify the success of mutagenesis, I needed to extract the DNA from bacterial cells, purify it, and have it sequenced. With the kind help of Dr El Sayyed, who provided me with chemicals and advice, I used the Thermo Scientific GeneJET Plasmid Miniprep Kit, according to the protocol described in the Methods, section 6.7.

The concentration of the extracted DNA, measured by Nanodrop, was 137.2 ng/μl. Since the sample looked suitable, I had it sequenced by Source Bioscience, who confirmed the successful mutation of both α and c subunit.

2.3 Agarose-streptavidin

The purpose of mutagenesis of the c subunit of F_1F_o was to be able to anchor the F_o to the agarose layer, and thus observe a rotation of the water-soluble motor F_1 against the membrane motor F_o. Here I describe how I modified agarose with streptavidin, so the biotinylated F_o can be attached to the agarose through a biotin-streptavidin bond, one of the strongest non-covalent bonds.

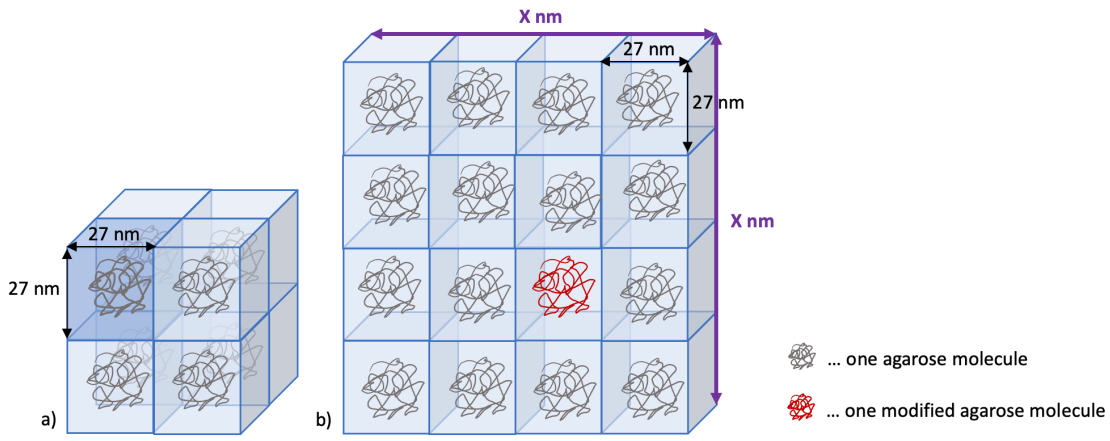


Figure 2.8: a) In 1 % agarose solution, a single agarose molecule occupies on average a cube with a side of 27 nm. b) I divided the upper layer of agarose into cubes with a side of 27 nm, and there is, on average, one modified agarose in each cube with a side of X nm.

The first step was to calculate how much streptavidin I need, by finding the appropriate ratio of agarose and agarose-streptavidin.

2.3.1 Calculation of fraction of modified agarose

The average molecular weight of a single agarose molecule is 120,000 g/mol [1], corresponding to 2×10^{-19} g. In 1 % solution, a single agarose molecule corresponds to approximately $100 \times 2 \times 10^{-19}$ g $= 2 \times 10^{-17}$ g of water, or 2×10^{-23} m^3 (given the water density 1,000 kg/m^3). A single agarose molecule, therefore, occupies, on average, a cube with a side of 2.7×10^{-8} m = 27 nm. To find out how many modified agarose molecules we need to have in the upper layer of agarose, let's divide the layer into cubes with a side of 27 nm, so there is (on average) one modified agarose molecule in each square with a side X nm (Figure 2.8).

The lipid bilayer - approximately a circle with a radius of 360 μm (approximated

[1] https://www.thermofisher.com/uk/en/home/life-science/cloning/cloning-learning-center/invitrogen-school-of-molecular-biology/na-electrophoresis-education/na-electrophoresis-workflow.html

from the volume of the droplet) - has an area of around 0.4 mm^2, corresponding to roughly 5×10^8 cubes with a side of 27 nm.

Based on the experience from different experiments in our laboratory, let us estimate the labelling efficiency to be $\frac{1}{10}$ (one in 10 molecules modified with streptavidin will have F_1F_o anchored to it), and spinning efficiency to be $\frac{1}{100}$ (one in 100 anchored F_1F_o molecules will spin). Therefore, to see 100 anchored spinners on the bilayer, we need at least $100 \times 10 \times 100 = 10^5$ modified agarose molecules in the upper layer of agarose below the lipid bilayer. Using the total number of agarose molecules in contact with the lipid bilayer calculated from the previous paragraph, we find out the minimum fraction of agarose molecules which need to be modified with streptavidin (F_{min}):

$$F_{\text{min}} = \frac{10^5}{5 \times 10^8} = \frac{1}{5000} \tag{2.2}$$

From a different perspective, we can, given the ratio above, calculate an average distance between two labelled spinners - in Figure 2.8 marked as X.

$$X = 27\ \text{nm}\sqrt{\frac{1}{F_{\text{min}}}} = 27\ \text{nm}\sqrt{5000} \approx 1909\ \text{nm} \approx 1.9\ \mu\text{m} \tag{2.3}$$

2.3.2 Preparing agarose-streptavidin

I adapted the protocol from [Ho, 2010], who modified agarose with nitrilotriacetic acid (NTA) to attach a hexa-histidine mutant of his protein of interest. He used carbonyldiimidazole (CDI) to modify the hydroxyl group on the agarose, creating an imidazole carbamate intermediate. This compound can react with an amine group of streptavidin (Figure 2.9). Excess CDI and the free imidazole were removed by dialysis.

The gelated agarose-streptavidin was dried and stored in the form of powder at room temperature. The protocol is described in the Methods, section 6.8.

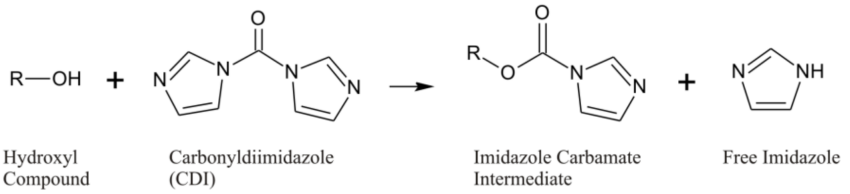


Figure 2.9: The key step of the agarose modifying protocol: the hydroxyl group on agarose molecules was modified with CDI, forming an imidazole carbamate intermediate, which reacts with the amine group of streptavidin. The free imidazole was then removed together with the excess CDI by dialysis. The scheme of the reaction is adapted from [Ho, 2010].

2.3.3 Control experiments

We checked the agarose-streptavidin protocol in two different ways. Both control experiments were performed with the kind help of Dr Helen Miller, who did all the imaging on her microscope setup.

The goal of the experiments was to observe whether biotinylated fluorescent dye and the biotinylated fluorescent beads stick to the agarose-streptavidin surface more than to the agarose surface. The protocol for the experiment is described in the Methods, section 6.9. I prepared simple flow channels by using glass slides, double sided tape and cover slips. The glass slides were covered with a thin layer of agarose-streptavidin or a thin layer of agarose for negative control. Biotinylated fluorescent dye fluorescein or biotinylated fluorescent beads were injected into the channel using a pipette, and the channel was consequently rinsed twice with a buffer, to remove free dye or beads, while making 2-4 recordings of the fluorescent signal from the surface in each stage of the experiment.

The glass slides were observed under the microscope using a 473 nm laser with an output power of 1.6 mW. Images were saved in a 16-bit TIFF (Tag Image File Format) and analysed in the ImageJ software. In the experiment with fluorescein, I analysed the mean grey value of the pixels (black=0, white=65536), and I normalised

the image, so the lowest pixel value (551) became 1. In the experiment with beads, video recordings were inspected for the presence of static (attached) beads in both samples after rinsing with the buffer.

Fluorescent dye

We compared the intensity from agarose and agarose-streptavidin samples presented with the dye and flushed with the buffer twice (Figure 2.10). In the agarose sample, we cannot see any significant increase in intensity during the experiment, although we did observe fluorescein molecules after injecting the dye. However, we did observe an increase in intensity after injecting the dye into the agarose-streptavidin sample. Although we were expecting clearer results, this is not contradicting the hypothesis that the biotinylated fluorescein is attached to the agarose-streptavidin on the surface of the glass slide.

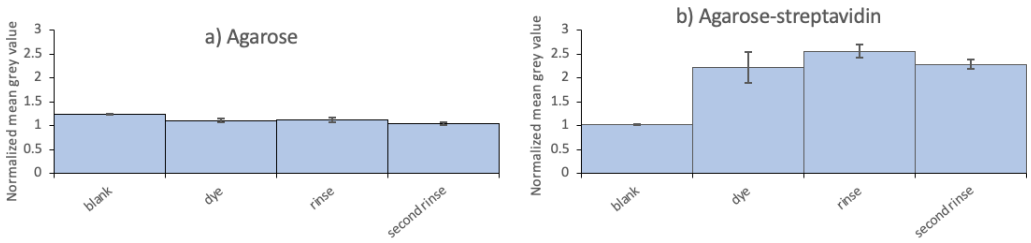


Figure 2.10: Experiments with a layer of a) agarose and b) agarose-streptavidin on the surface of a glass slide (blank), and consequently covered with biotinylated fluorescein (dye) and rinsed with buffer twice to remove free dye (rinse, second rinse).

Fluorescent beads

In the experiment with the fluorescent beads, we analysed several recordings of the agarose and the agarose-streptavidin samples. We only observed one diffusing bead in the agarose sample, while the agarose-streptavidin sample had several static beads (Figure 2.11), and their photobleaching rate was comparable to the photobleaching rate of the control videos of the same beads which we took beforehand

(Figure 2.12).

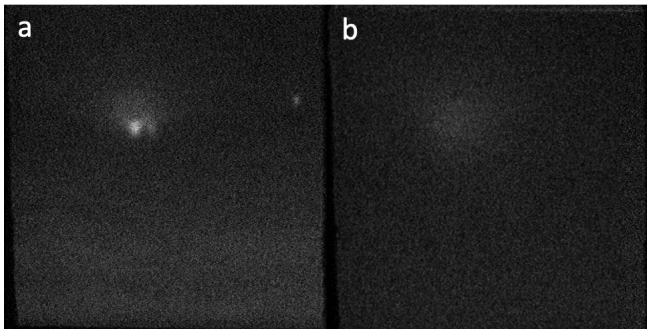


Figure 2.11: a) Observation of the agarose-streptavidin covered with fluorescent beads and consequently flushed several times with the buffer. We saw several beads attached to the surface, bleaching rate was comparable to control experiments. One of the attached beads is recorded in the photo. b) Same experiment, but there was no streptavidin on the agarose. We could not find any beads attached to the surface.

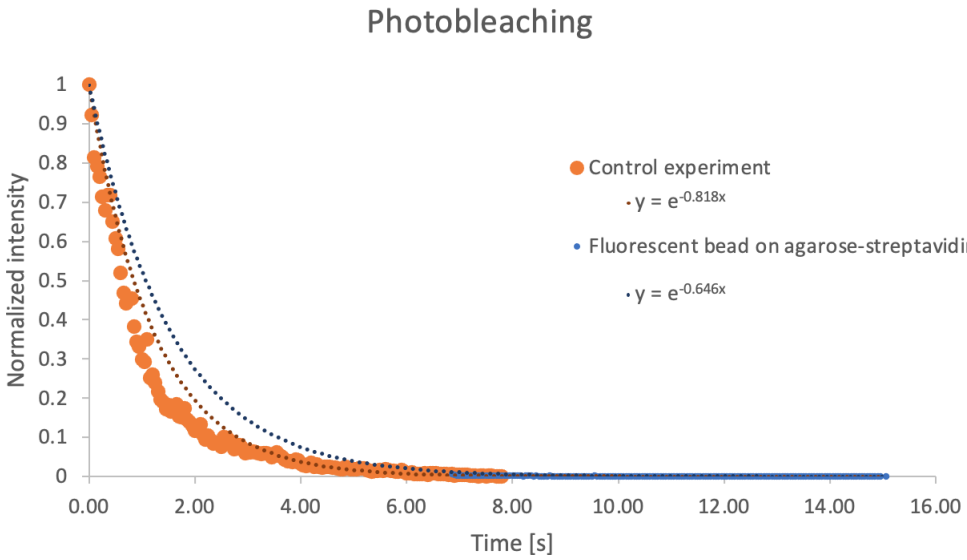


Figure 2.12: Normalized traces of intensity of fluorescent beads decreasing in time due to photobleaching. The intensity of the fluorescent bead attached to agarose-streptavidin is represented in blue, and the intensity of the fluorescent bead recorded during the control experiment is orange.

These two control experiments convinced me that the tested agarose-streptavidin preparation can be used in the hydrogel layer, which is supporting the lipid bilayer, for anchoring the biotinylated c subunit of F_1F_o. By anchoring the rotor of the protein, we will force the stator labelled with gold nanorod to rotate, and the rotation can be recorded in the form of periodically changing polarized light produced by

the gold nanorod.

2.4 Conclusion

In this chapter, I documented the process of expression and purification of *E. coli* F_1F_o and TA2.A1 F_1F_o, and the consequent examination of protein concentration, quality and activity. Furthermore, I have described a successful attempt to mutate the TA2.A1 F_1F_o in two places to be able to label and anchor the protein for the high-resolution functional study experiment. Finally, following the calculations, I have modified agarose with streptavidin, so anchoring can take place in the agarose layer. This was verified by two different experiments.

Chapter 3

Development of protocol for lipid bilayer formation

The previous chapter covered the preparation and testing of the protein of interest, ATP synthase F_1F_o. The protein consists of two coupled molecular motors: F_1 is a water-soluble protein, and F_o is a membrane protein. Therefore, a suitable lipid environment is needed to keep the protein active and accessible at the same time.

Several different approaches were used to study F_1F_o, and some of them are described in the Introduction, section 1.2.2. However, to study F_1F_o under a controlled transmembrane potential, we need to have an electrically conductive connection to both sides of the lipid membrane. For this reason, we work with planar membranes, which are supported by hydrogel. I adapted the droplet-on-hydrogel bilayer protocol by exploring different compositions of lipid and oil mixture and duration of monolayer formation. It would be very difficult to explore entire multi-parametric space, but the goal was different: to find a set of parameters which would produce a lipid bilayer stable for more than 10 hours - this is more than enough stability for any planned experiments.

3.1 Droplet-on-hydrogel bilayer formation

First, I describe the process used for forming a lipid bilayer, as shown in Figure 3.1. More details can be found in the Methods, section 6.15. Agarose gel is spin-coated on a glass cover slip, and this cover slip is secured on the bottom of the polymethyl methacrylate (PMMA) chip. The chip creates several separated wells with the agarose layer on the bottom (more details about the chip can be found in section 4.1.1). The agarose layer is hydrated from the agarose reservoir at the bottom of the chip.

Next, the lipids of interest are dissolved in a suitable oil, and this mixture is used to fill the wells above the agarose, and a small, separated incubation compartment on the chip. The compartment is used for preparing water droplets. Using a syringe, 200 nl of water is injected into the oil mixture and left until a lipid monolayer spontaneously forms on the surface. Another lipid monolayer is meanwhile formed on the surface of the agarose. The droplet is then transferred to the wells above the agarose with a pipette and let sink to the bottom. Below the droplet, the two monolayers combine, forming a droplet-on-hydrogel bilayer.

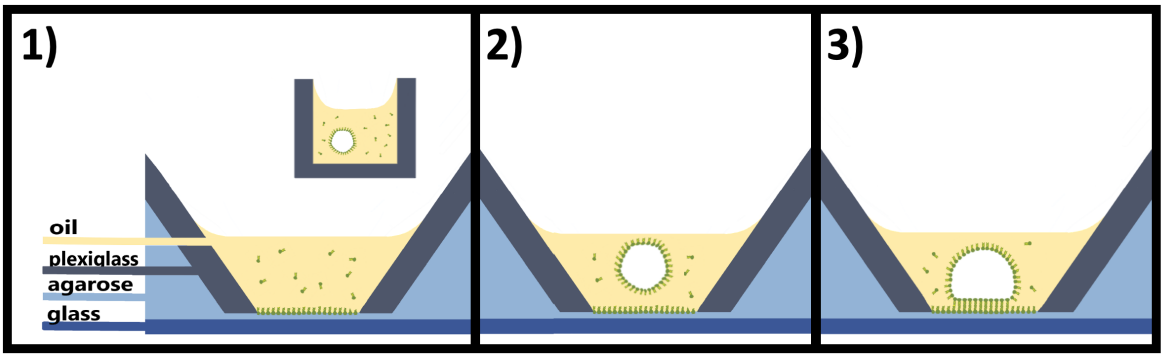


Figure 3.1: Schematic representation of the process of formation of droplet-on-hydrogel bilayer: 1) lipids dissolved in oil spontaneously assemble into a lipid monolayer on the interface of oil and water (on the surface of the droplet and on the agarose surface) 2) droplet with the lipid monolayer is transferred into the oil above the agarose layer 3) water droplet sinks to the bottom of the well, and a bilayer is formed at the contact of the two monolayers.

3.2 Optimising conditions of bilayer formation

Experimental parameters for creating a stable bilayer suitable for the functional study of F_1F_o are lipid composition, lipid concentration, duration of monolayer formation, and oil composition.

3.2.1 Lipid composition

To find a suitable lipid composition, I considered two main factors: the activity of F_1F_o in a given lipid membrane, and the stability of this membrane. Wei-Meng Ho approached this problem in his thesis by preferring a mixture of natural lipids, known for their higher proton translocating activity in proteoliposomes. He tested different lipid mixtures, and, following a complex argumentation, he proposed the following [Ho, 2010]:

For 1 ml of lipid mixture, he used

- 7.7 mg of *E. coli* polar lipids
- 0.85 mg of diphytanoyl phosphatidylcholine (DPhPC)
- 0.85 mg of cholesterol
- 7.8 mg of egg phosphatidylcholine (PC)
- 0.78 mg of egg phosphatidic acid (PA).

Although Dr Ho succeeded in preparing a stable lipid membrane with this composition, his results were not replicated after several years of effort. I can only speculate what may have been the reason, but replicating precise ratios of delicately balanced lipids, which are, moreover, stored in a rapidly evaporating chloroform, seems to be an extremely difficult task. Therefore, I have decided to approach this problem from the other side and find a stable synthetic lipid mixture, which can be tolerated by F_1F_o.

The new lipid mixture consists of two components: neutral lipids with highly branched hydrophobic tails, 1,2-diphytanoyl- sn-glycero-3-phosphocholine (DPhPC), as the main component of the bilayer, and the negative charge was introduced by adding 1-palmitoyl-2- oleoyl-sn-glycero-3-phosphate ($POPA^-$). The chemical structure of both lipids is shown in Figure 3.2.

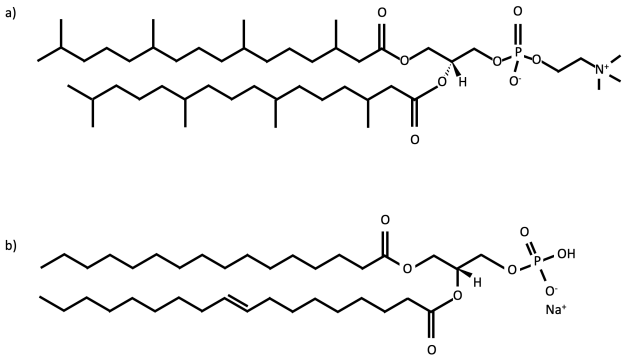


Figure 3.2: Chemical structure of a) DPhPC, a neutral lipid with highly branched hydrophobic tails, and b) $POPA^-$, an anionic lipid.

DPhPC contributes to the stability of a planar membrane, and so DPhPC lipids are widely used for forming planar membranes, for example floating bilayers [Su et al., 2020], droplet interface bilayers [Gross et al., 2011], or droplet-on-hydrogel bilayers [Leptihn et al., 2013]. Moreover, proteoliposomes made with 75 wt% of DPhPC and 25 wt% of $POPA^-$ maintains the activity of *E. coli* F_1F_o (unpublished data of Dr Ishmukhametov).

3.2.2 Lipid concentration and duration of monolayer formation

With a suitable choice of lipid composition, it is equally important to ensure that the lipids dissolved in oil create a robust monolayer on the surface of the water droplet and on the agarose-oil interface, so the fusing of these two monolayers creates a lipid bilayer. It is straightforward to see that the duration of monolayer formation is coupled with the lipid concentration, therefore I tried different durations for each concentration. In Table 3.1, I summarised the stability of droplet-on-hydrogel bilay-

1 mM DPhPC in hexadecane:

monolayer formation duration	15 min	30 min	60 min	100 min
stable for 1 min	0/4	0/4	1/4	3/4
stable for 2 min	0/4	0/4	0/4	1/4
stable for >10 hours	0/4	0/4	0/4	1/4

10 mM DPhPC in hexadecane:

monolayer formation duration	30 min	70 min
stable for 1 min	0/4	2/12
stable for >10 hours	0/4	0/12

5 mM DPhPC in 1:1 hexadecane and silicone oil:

monolayer formation duration	30 min	45 min	60 min	75 min
stable for 1 min	4/4	4/4	4/4	4/4
stable for >10 hours	4/4	2/4	1/4	2/4

Table 3.1: Stability of droplet-on-hydrogel bilayers. Numbers represent the number of bilayers, out of the total number with the same experimental conditions, which did not rupture during the given time.

ers created with DPhPC in hexadecane or 50 vol% of hexadecane and 50 vol% of silicone oil, and milliQ water. Reported numbers represent the number of bilayers which did not rupture during the given time, out of the total number of bilayers formed in the same experimental conditions. If a bilayer ruptures, there is nothing to compensate for the surface tension of the droplet, and the water from the droplet leaks into the agarose layer, resulting in a seemingly disappearing droplet. This is easy to observe with the naked eye.

From the presented experiment, the most optimal concentration seems to be 5 mM, and the monolayer forming time is 30 minutes.

3.2.3 Oil composition

The final parameter to adjust was a choice of oils to dissolve the lipids in. From the literature, I found that, for similar experiments, the usual choices were hexadecane ($C_{16}H_{34}$), decane ($C_{10}H_{22}$) or AR20 silicone oil (polyphenyl-methylsiloxane).

In studies of droplet interface bilayers, it was found that the DPhPC bilayers formed in 50 vol% of hexadecane and 50 vol% of AR20 silicone oil are more solvent-free than bilayers formed in pure hexadecane or decane [Taylor et al., 2015], and are more stable compared to pure hexadecane [Wauer et al., 2013]. I therefore continued with this mixture and tried 5 mM of 75 mol% DPhPC and 25 mol% $POPA^-$ in 50 vol% of hexadecane and 50 vol% of AR20 silicone oil, with a monolayer forming time of 30 minutes. The resulting droplet-on-hydrogel bilayers were so stable that **14 out of 16 remained intact for 21 hours, and two of them did not rupture for 3.5 days** when I stopped the experiment.

3.2.4 Image of bilayer

Figure 3.3 shows an example of a stable bilayer, formed from a 5 mM solution of 75 mol% DPhPC and 25 mol% $POPA^-$ in 50 vol% hexadecane and 50 vol% AR20 silicone oil solution, and I used milliQ water as the aqueous solution. Monolayers were formed for 30 minutes before the droplet was transferred to the oil mixture above the agarose layer, and a droplet-on-hydrogel bilayer was formed.

3.3 Charged membrane fusion

After designing a protocol for forming a stable droplet-on-hydrogel bilayer, the next step would be to test the method for protein delivery into the bilayer. As was described in the Introduction, section 1.4.2, I will use a method called charged membrane fusion [Ishmukhametov et al., 2010], which was shown to be successful in delivering F_1F_o molecules into a lipid membrane while maintaining their activity. I have designed a two-colour fluorescent control experiment to verify that fusion takes place. In the following text, there is a description of the design of the control experiment and the steps I have already completed, as well as the future work.

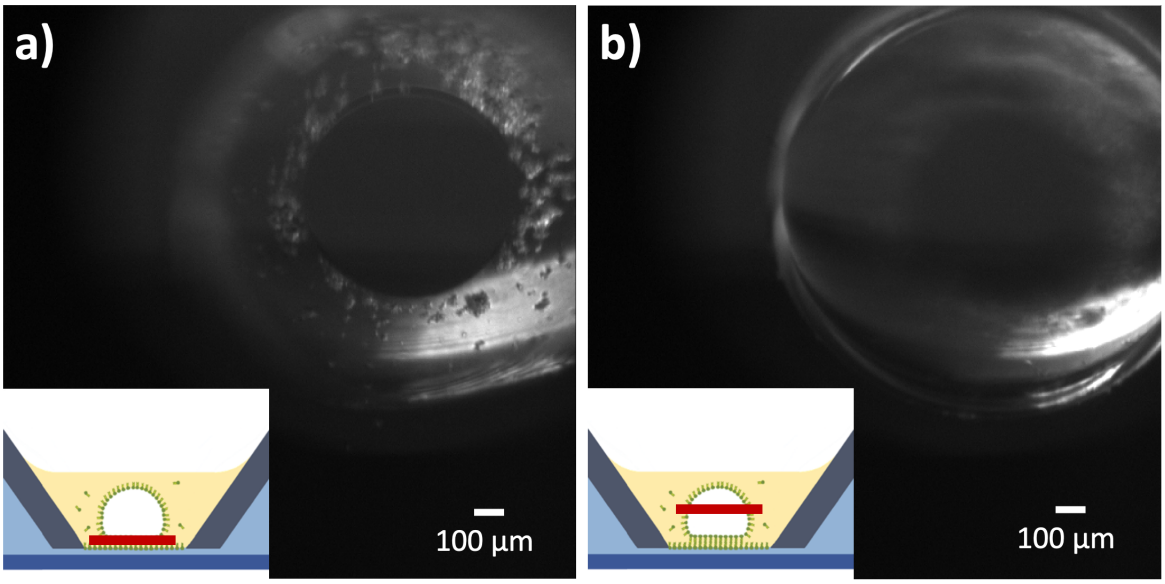


Figure 3.3: Example of a droplet-on-hydrogel bilayer observed through the microscope objective from below. The red bar on the schematic image shows the position of the focal plane in the droplet: a) black circle in the middle indicates the position of the lipid bilayer, inhomogeneities on the oil-agarose interface around the bilayer scatter the incoming light, and therefore are visible on the image b) photo of the water droplet on the top of the bilayer, the droplet is visible due to the light reflecting from the oil-water interface.

3.3.1 Control fusion experiment: the design

I designed an experiment with liposomes made with cationic lipids and labelled with two fluorescent dyes: green pyranine (excitation 460 nm, emission 511 nm), a water-soluble dye which marks the inside of the liposomes; and red mCherry (excitation 587 nm, emission 610 nm) attached to the membrane protein proteorhodopsin, which marks the position of the liposome membrane. The process of fusion of the cationic liposomes with the anionic membrane is explained in Figure 3.4.

Using a two-colour fluorescent microscope, we can observe co-localized red and green signals from the liposomes moving freely in the liquid. Since a liposome is attracted to the membrane via opposite charge electrostatic attraction, it starts to fuse with the membrane, while the liposome membrane opens up, allowing the water-soluble green dye to diffuse into the agarose reservoir. The membrane of the cationic liposome then fuses with the anionic planar membrane, and prote-

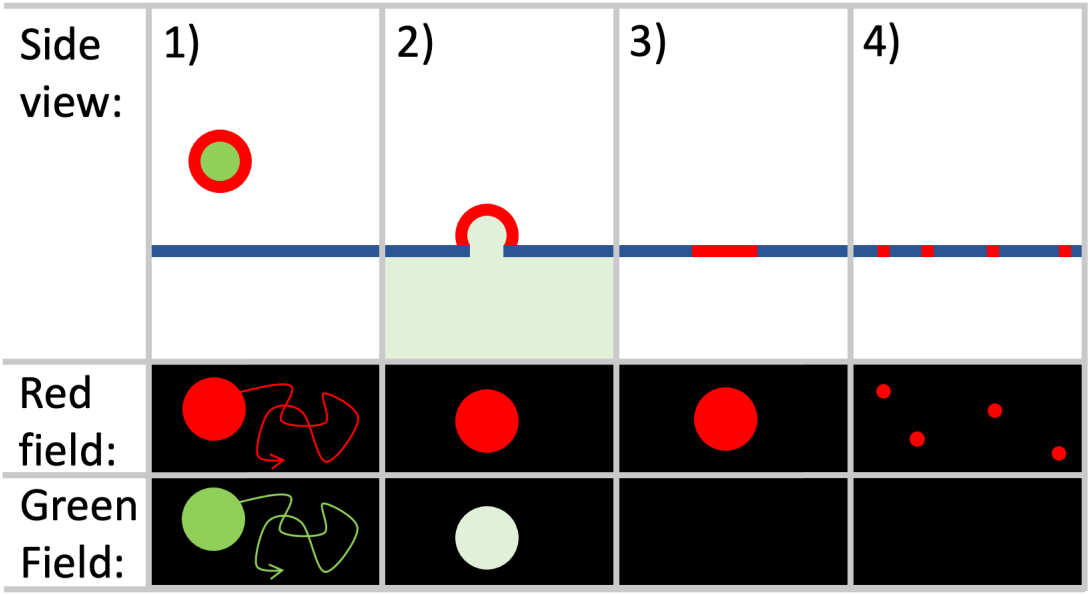


Figure 3.4: Simplified scheme of fusion experiment, a side view and a top view of the red and green field: 1) a cationic liposome labelled with green water soluble dye and red membrane dye is attracted to the anionic membrane (blue); we can see a moving spot in both fields 2) the liposome has partially fused with the membrane, part of the green dye has diffused out of the liposome; there is a static bright spot in the red field, the green spot disappears 3) the liposome has just completely fused with the membrane, the green dye has diffused into the reservoir; there is a static bright spot in the red field, and nothing in the green field 4) red membrane dye is diffusing through the membrane, with is much slower than diffusing in liquid; in a single molecule microscope, we would be able to see individual mCherry molecules diffusing through the bilayer, and nothing in the green field.

orhodopsin molecules labelled with the red fluorescein dye diffuse through the membrane. Using simple approximations, I can show that the two events happen on different time scales:

Diffusion of pyranine in water

This is a case of 3D Brownian motion. Pyranine molecules in water will have the mean squared displacement equal to $< r^2 >$ after the time t_1:

$$t_1 = \frac{< r^2 >}{6D_1}, \tag{3.1}$$

where D_1 is a diffusion coefficient:

$$D_1 = \frac{k_B T}{6\pi\eta R}, \tag{3.2}$$

where η is the dynamic viscosity of water, R is the size of the diffusing particle, $T = 298$ K is temperature and $k_B = 1.38 \times 10^{-23}$ J/K is Boltzmann constant.

Given the dynamic viscosity of water 8.91×10^{-4} Pa $\cdot$ s and the size of pyranine molecule 1 nm, we can calculate that molecules of pyranine in water will have the mean square displacement 10^4 μm^2 after time $\boldsymbol{t_1 = 6.8\ s}$

In this calculation, I neglected the effect of agarose on the viscosity of the absorbing medium and did not consider the thickness of the agarose layer the pyranine is diffusing into, which I estimated to be above 100 μm.

Diffusion of mCherry-proteorhodopsin in lipid bilayer

Here I calculate a 2D diffusion. To simplify the situation, I consider a diffusion of rhodamine labelled phosphatidyl- ethanolamine in DPhPC bilayer, which was measured using fluorescence correlation spectroscopy [Horner et al., 2009]. I expect this to be a lower estimate of the diffusion rate of mCherry-proteorhodopsin, since the cross-section area of the membrane part of the protein is much larger, and possibly have a stronger interaction with DPhPC lipids, than phosphatidylethanolamine, and both parameters contribute to slower diffusion. I neglect the effect of anionic POPE molecules (25 mol%, or 20.5 wt% of the bilayer).

2D version of the equation for the time t_2 until the mean squared displacement is $< r^2 >$:

$$t_2 = \frac{< r^2 >}{4D_2}, \tag{3.3}$$

where $D_2 = 8.1 \pm 0.4 \mu\text{m}^2/\text{s}$ is a diffusion coefficient of rhodamine labelled phosphatidyl-

ethanolamine in DPhPC bilayer published in [Horner et al., 2009]. A lower estimate of the time needed for the molecules of mCherry-proteorhodopsin in a lipid bilayer to have the mean square displacement 10^4 μm^2 is $\boldsymbol{t_2 = 308.6\ s}$.

Although both calculations are very approximate, they were only done to show that the two effects are happening on different time scales. I can therefore expect that in the control fusion experiment, after a liposome fuses with the membrane, the water soluble green fluorescent dye pyranine will diffuse away much faster than the membrane protein labelled with the red fluorescent dye mCherry.

To summarise, after a few minutes after injecting the proteoliposomes into the liquid above the lipid bilayer, there are three possible outcomes of the control experiment:

- no static particles, neither red nor green
  - liposomes diffusing in the solution
- co-localized red and green static particles
  - liposomes attached to the surface, but not fused
- only red particles are static
  - liposomes fused with the membrane

Photobleaching

An obvious question would be, how we can differentiate between pyranine molecules diffusing into the reservoir, or simply bleaching out due to the prolonged laser excitation. Therefore, the rate of photobleaching needs to be measured prior to the fusion experiments.

3.3.2 Liposomes with two fluorescent labels

To prepare liposomes for the control fusion experiment, I used a low salt buffer to minimize shielding the polar lipid head groups. Water soluble pyranine was mixed

with the buffer before adding the lipids, so after liposomes formation, the buffer inside and outside of liposomes was dyed. Redundant pyranine from the outside was removed by the Sephadex G50 gravity-flow chromatography column. A detailed protocol can be found in the Methods, section 6.16. I verified the presence of both dyes in the liposomes using Nanoimager (a single molecule localisation microscopy), but I have not succeeded in recording a liposome fusion event.

3.3.3 Two colour fluorescent microscope setup

For the control fusion experiment, I have built a two-colour fluorescent microscope setup under the supervision of Prof. Berry and Dr Rieu.

I used the Nikon Eclipse TE200 inverted microscope with an infinite conjugate oil immersion $100\times$ objective and without a condenser; the Andor iXon electron-multiplying charge-coupled device camera; and two lasers: a 440 nm laser with output power 5.04 mW for exciting the fluorescent dye pyranine and a 561 nm laser with output power 36.7 mW for exciting the fluorescent dye mCherry. I started with the image part of the microscope first, and then I mounted and aligned the lasers.

Emission path

To align the emission path of the setup, I used a white collimated source of light, carefully positioned above the microscope objective, making sure that the light beam is vertical. I was imagining a pen mark on a glass cover slip in the object plane of the objective.

A scheme and a photo of the emission part of the setup are in Figure 3.5. First, I placed an iris in the image plane. One of the two lenses with the same focal length (f) was positioned after the iris in the distance f, the other one was mounted in front of the camera, so it focused the light on the camera chip. The light beam was then

split into two perpendicular beams using a dichroic mirror.

I first aligned the green path using kinematic mirror mounts. The green beam just misses the mirror in front of the camera lens and goes through the middle of the camera lens and parallel with the lens tube, and it was focused on the camera chip. The red beam was aligned so it is also parallel with the lens tube, and it was focused right next to the green beam on the camera chip. A photo of the red and the green signals alignment can be seen in Figure 3.6

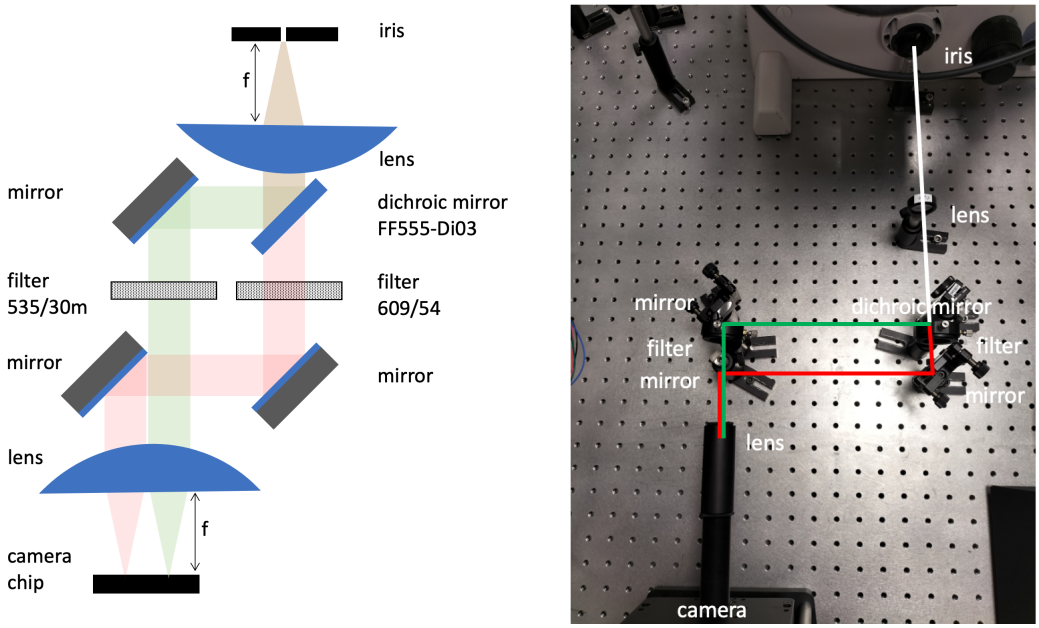


Figure 3.5: The emission path: a scheme (left), and a photo (right). The scheme is not in scale, I exaggerated the size of the beam, so it is easier to see where it is collimated and where it is focused.

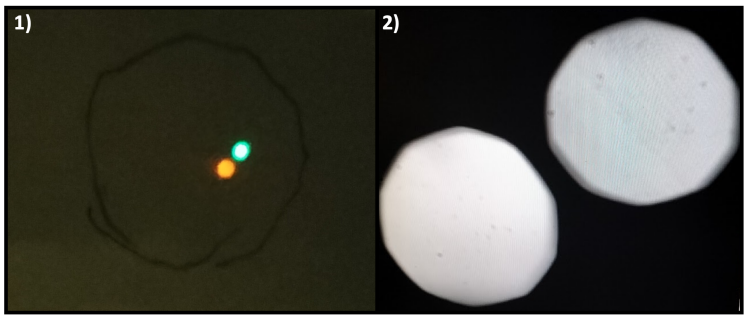


Figure 3.6: A photo of the green and the red signal positioned next to each other: 1) on the paper placed on the lens tube of the camera during the alignment, 2) captured by the camera. I used a white collimated light as a light source. Asymmetry in the shape of one of the signals is caused by imperfect alignment.

Excitation path

A scheme and a photo of the excitation path of the setup are in Figure 3.8. The challenge of the laser alignment was to align the two lasers so they enter the microscope at the same place and perfectly parallel. I used two mirrors mounted on kinematic mirror mounts for each laser, so I could "walk" the beam. If two laser beams meet at two points which are far from each other, I can be sure that the position and the angle of both lasers are the same. I used laser spots on the dichroic mirror and on the ceiling above the objective as the two reference points.

After the lasers were aligned, I installed a beam expander for the green (561 nm) laser. The expander consists of two lenses with focal lengths f_1 and f_2. If the width of the beam before the expander was w_1, then the new width of the laser after the expander w_2 could be calculated using similar triangles (see Figure 3.7) according to Equation 3.4.

$$w_2 = w_1 \frac{f_2}{f_1} \tag{3.4}$$

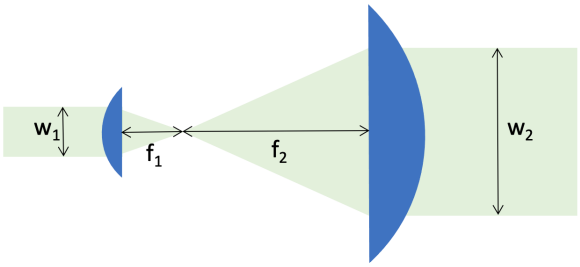


Figure 3.7: A scheme of a laser expander. The width of a beam can be calculated using similar triangles.

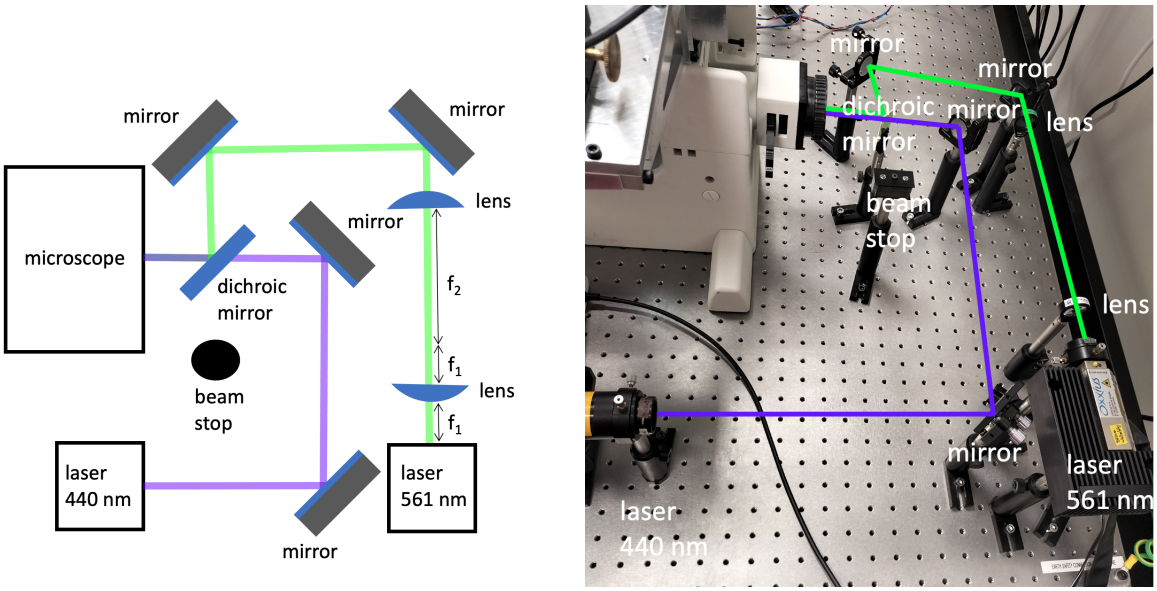


Figure 3.8: The excitation path of the microscope setup: a scheme (left), and a photo (right). Green (561 nm) laser has a beam expander installed in its path.

3.4 Conclusion

In the first part of this chapter, I described a process of finding parameters for constructing a stable planar hydrogel-supported bilayer which would support the activity of F_1F_o . Using 5 mM of 75 mol% DPhPC and 25 mol% $POPA^-$ in 50 vol% of hexadecane and 50 vol% of AR20 silicone oil, and allowing monolayer formation for 30 minutes, I was able to create droplet-on-hydrogel bilayers stable for 21 hours. I designed a control experiment to test liposome fusion with the membrane with opposite charge, the method I plan to use for protein delivery. Although I did not have time to perform the actual experiment, I managed to create liposomes with

two fluorescent labels marking the internal space of the liposomes, and the membrane. I also built a fluorescent microscope setup using two different lasers and two channels for the output signal.

Chapter 4

Design, building and testing of the perfusion system

In the previous chapters, I have described how to prepare the proteins and a stable lipid bilayer for droplet-on-hydrogel bilayer experiments. To deliver proteins, labels, substrates, or ions to droplet above the bilayer, I designed a perfusion system, which is described in detail in this chapter.

The main objectives of the design are to enable highly accurate independent control of electrical and chemical transmembrane potential and reliable delivery inside the droplet with a low-cost apparatus, which is easily reproducible on any microscopy setup.

The liquid flow through the droplet is created by two syringes with attached micropipettes. I aimed for an electronically controlled system - both for the fine positions of micropipettes and for the liquid flow. Exchange of the liquid in the droplet without disturbing the bilayer can be achieved by synchronising inlet and outlet rates, and by avoiding any manual manipulation. Since the volume of the droplet is only around 200 nl, the perfusion system must be extremely precise and stable. Elastic materials, such as plastic tubing or any air bubbles inside the system would

cause time-delayed flow, which could rupture the droplet.

After experimenting with different technical realisations of the perfusion system, I was able to summarise the requirements for the hardware:

- No manual manipulation should be required; I used linear actuators for controlling the syringes to achieve a stable flow with minimal vibrations
- The fine position of the micropipettes in three axes is remotely controlled by piezoelectric NanoCubes to avoid vibrations, which may rupture the droplet
- The syringes and the tubing are completely filled with liquid and do not contain any air, because the air compressibility results in unstable flow; similarly, I avoided flexible tubing due to its elasticity
- A commercial patch clamp electrode holder was adjusted for my experiment to make an electrical contact between the electrode and the inside of the droplet
- Position of the micropipettes in the droplet

A schematic picture of the final design of the perfusion system can be seen in Figure 4.1, and a photo in Figure 4.2. The chip containing the droplet-on-hydrogel bilayer is framed in dark red. Inlet and outlet pipettes are attached to syringes controlled by actuators, and NanoCubes are used for fine positioning of the pipettes. The bilayer is observed through the objective below. The top view microscope, which helps with positioning the pipettes, was omitted from the schematic picture for simplicity.

4.1 Mechanical support for droplet-on-hydrogel bilayer

The supporting part of the hardware includes a polymethyl methacrylate (PMMA) chip, an electrode holder, a platform, stages and holders. All the individual components are described in the following text.

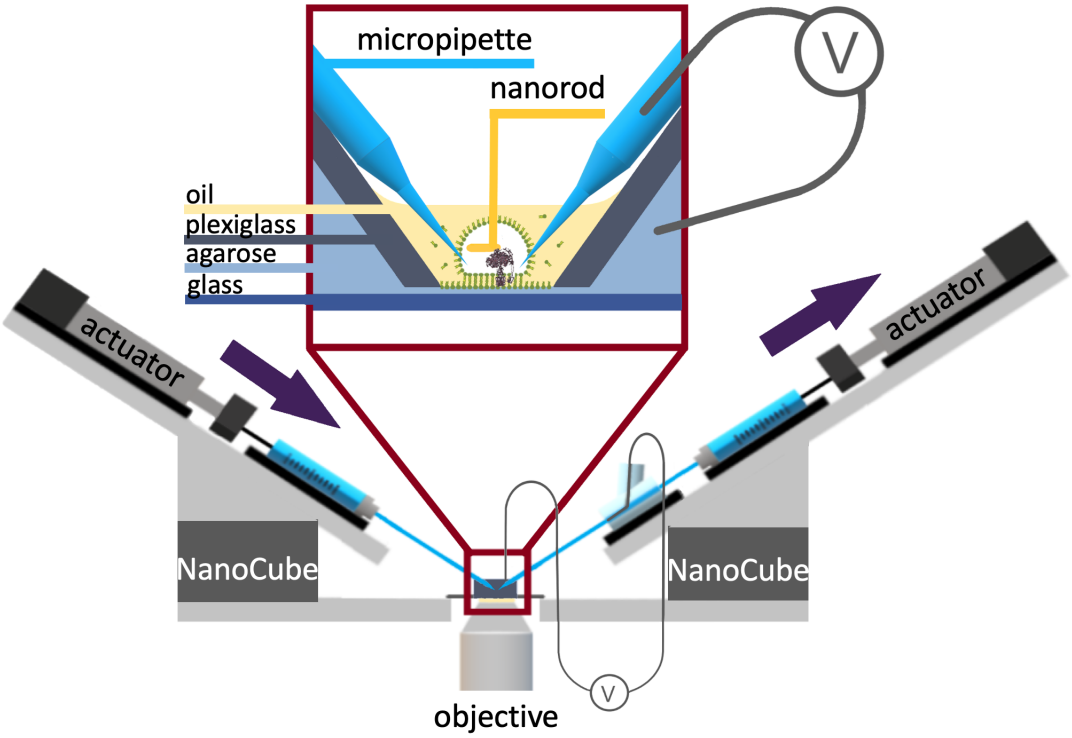


Figure 4.1: A schematic picture of the perfusion system. The droplet-on-hydrogel bilayer is zoomed in and framed in dark red. The top view microscope was omitted for simplicity.

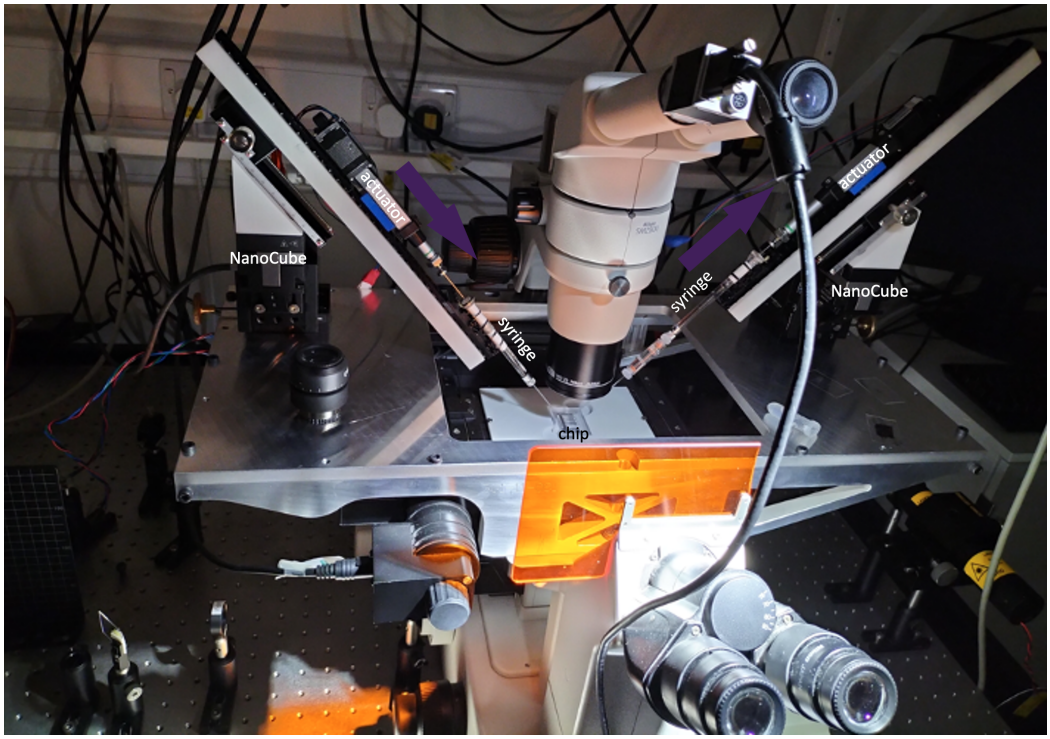


Figure 4.2: A photo of the perfusion system, with the top view microscope for positioning of the pipettes.

4.1.1 Chip

Droplet-on-hydrogel bilayers are formed in wells of a polymethyl methacrylate (PMMA) chip attached to a glass cover slip. The original design published by [Leptihn et al., 2013] was modified to allow micropipettes of the perfusion system to reach all the wells under 50° angle (from the horizontal axis). However, the key features of the chip were preserved:

- the chip is made of polymethyl methacrylate (PMMA) by a computer numerical control (CNC) machine
- the bottom of the chip fits a 24 $\times$ 40 mm cover slip
- the holes in the middle of the chip work as wells for the droplets
- the wells are surrounded by a microfluidic channel, which is filled with agarose through two filling holes, and provides hydration of the thin agarose layer spin-coated on the cover slip (Figure 4.3)
- the space between the compartments and the microfluidic channel is elevated from the surface of the cover slip by 50 μm to allow agarose to fill the space around the wells
- the third hole next to the filling hole allows an electrode to be connected with the agarose, without mechanical disturbance of the agarose
- a small chamber was prepared for incubation of the droplet - the original model has it separately from the chip, the modified model has an incubation chamber on the chip

Figure 4.4 shows the original model published by [Leptihn et al., 2013], and the adjusted model. The model was designed in the AutoCAD software with the kind help of Dr Alcinesio, who also made the chips on a CNC machine (chips b) and c) in Figure 4.5). I also tried to 3D print the chip, but the spatial resolution of the printer was not sufficient (chip e) in Figure 4.5). The final version of the chip was manufactured by Protolabs (chip d) in Figure 4.5).

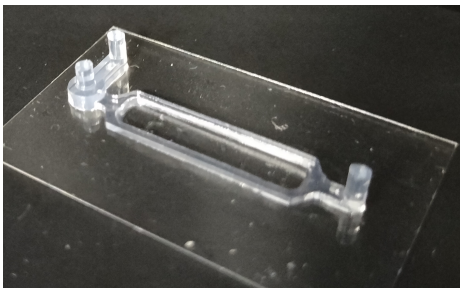


Figure 4.3: After removing the chip from the cover slip, the agarose shows the shape of the microfluidic channel used for hydrating the thin agarose layer.

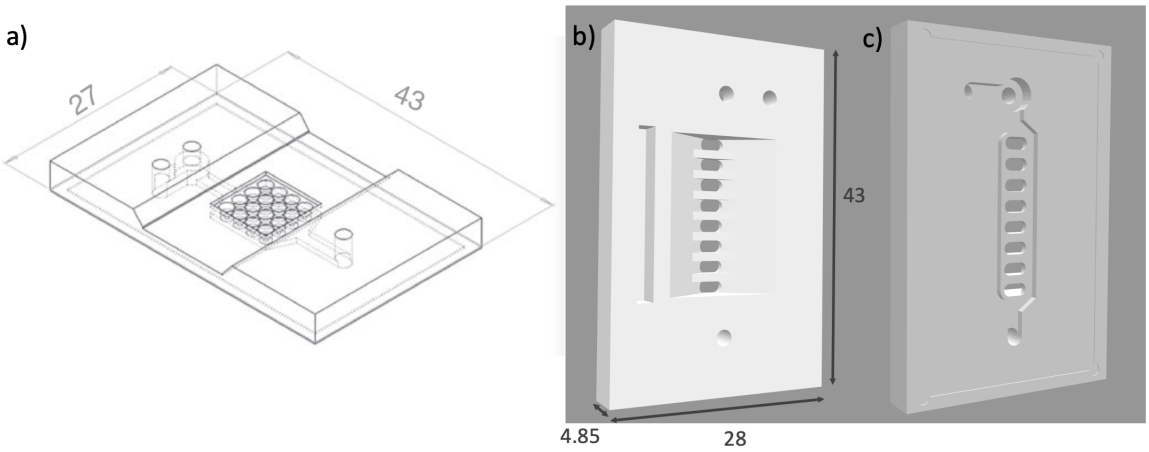


Figure 4.4: The original and the modified models of the chip: a) the original model published in [Leptihn et al., 2013]; b) the modified model created by adapting the original model for the use with perfusion system, top view; c) the modified model, bottom view. All the measures are provided in millimetres.

Cover slip coating

The polymethyl methacrylate (PMMA) chip is placed on the top of a cover slip covered with a thin layer of agarose. The cover slips were cleaned according to the protocol described in the Methods, section 6.10, which was adapted from single molecule research procedures, with small alterations (e.g. the cover slips were stored in milliQ water, not in ethanol). I find it likely that a less extensive cleaning procedure, perhaps just a single flush with ethanol, could be also sufficient for these experiments.

The agarose could be spread on the cover slip using another clean cover slip, but

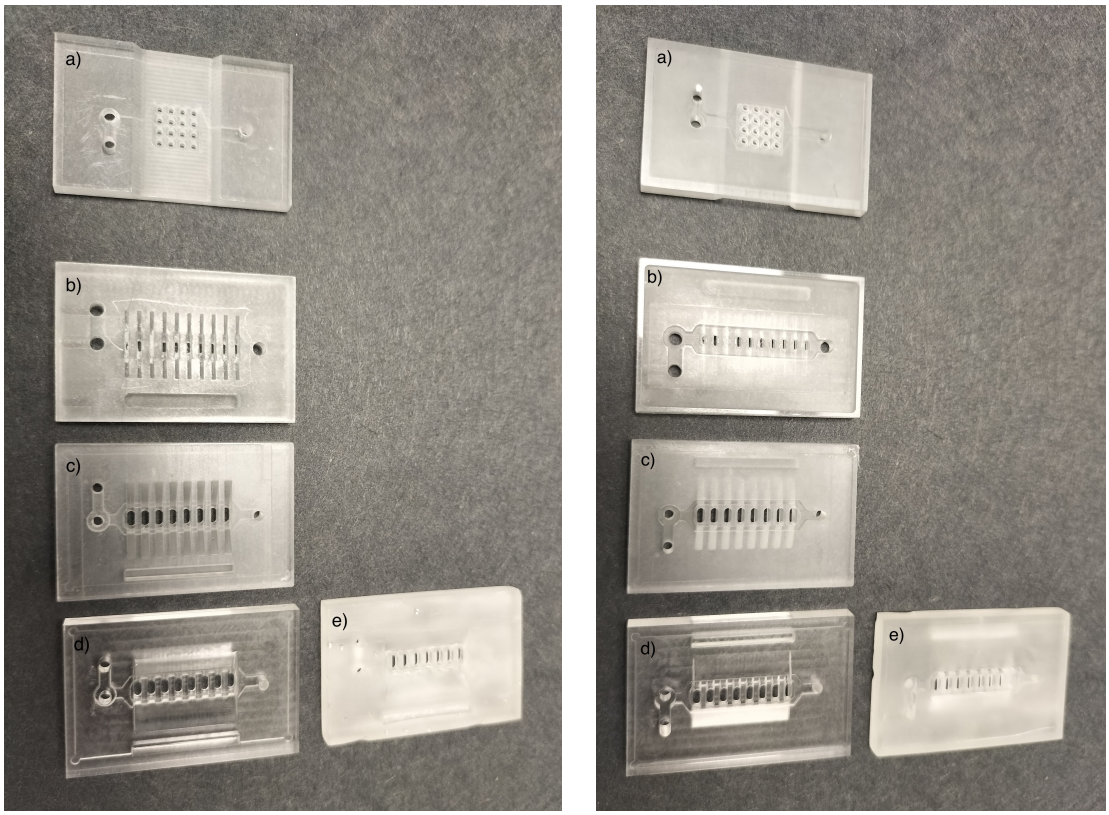


Figure 4.5: The different versions of the chip, the top view on the left, and the bottom view on the right: a) the original design of the chip published in [Leptihn et al., 2013]; b) a CNC machined chip, with the wells being too narrow; c) a CNC machined chip with the wells being too tall; d) the final design, CNC machined; e) the final design, 3D printed - the resolution was not sufficient.

I decided to use a spin coater for more reproducible results and a thinner agarose layer. The protocol is described in the Methods, section 6.13. Briefly, a cover slip was plasma cleaned in 0.5 bar oxygen stream at 95 W and then transferred into a spin-coater. I added 140 μL of 1 % agarose solution at 70 °C and spin-coated at 3000 rpm for 60 seconds. The coated cover slips can be stored in a sealed container for several months.

Assembling the chip

A step-by-step procedure is documented in the Methods, section 6.15. A critical step is the filling of the microfluidic channel with agarose. I start with 70 °C liquid, but the agarose cools down and solidifies quickly. I use a pipette tip with an enlarged opening to push the agarose through the channel with a gentle and steady flow. Any

air bubbles in the channel needs to be avoided. After the agarose solidification, it is important to check whether the wells were not flooded with the agarose by inspecting the bottom of the chip. The thin agarose layer below each well reflects light differently than the thick layer of agarose in the microfluidic channel, so it is easy to spot any flooding. In case of flooding, we can either only use the wells which were not flooded, or clean the chip and assemble it again.

Another critical step is the droplet transport from the incubation compartment to the well of the chip. The droplets cannot come in contact with the air, therefore I always keep a small amount of oil and lipid mixture in the pipette tip during the droplet transport. When releasing the droplet from the pipette tip, I aim for the middle of the well. A photo of the assembled chip with droplets can be seen in Figure 4.6.

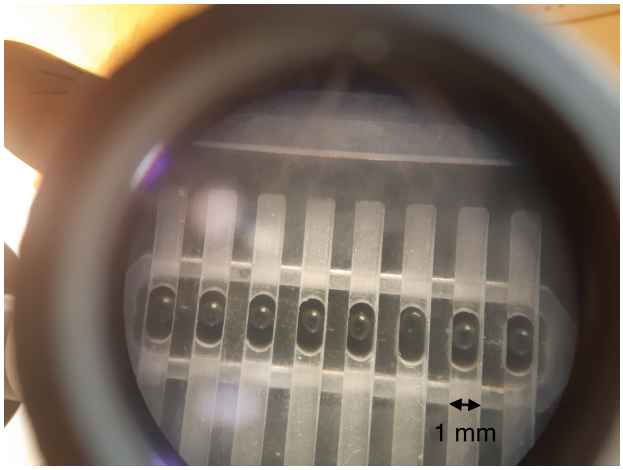


Figure 4.6: An assembled chip with droplets in each well, observed under the microscope.

4.1.2 Chip adapter

To secure the chip on the motorised stage, I designed an adapter and had it 3D printed from polyamide 12 (PA 12) by selective laser sintering (SLS) at 3D Hubs BV. This is a quick and simple solution, with a sufficient result. I designed a larger space for the chip, and I used two wedges to secure the chip in place. This enables a

comfortable manipulation with the chip, but also makes the model less sensitive to the printing precision. The model and the photo of the adapter are shown in Figure 4.7.

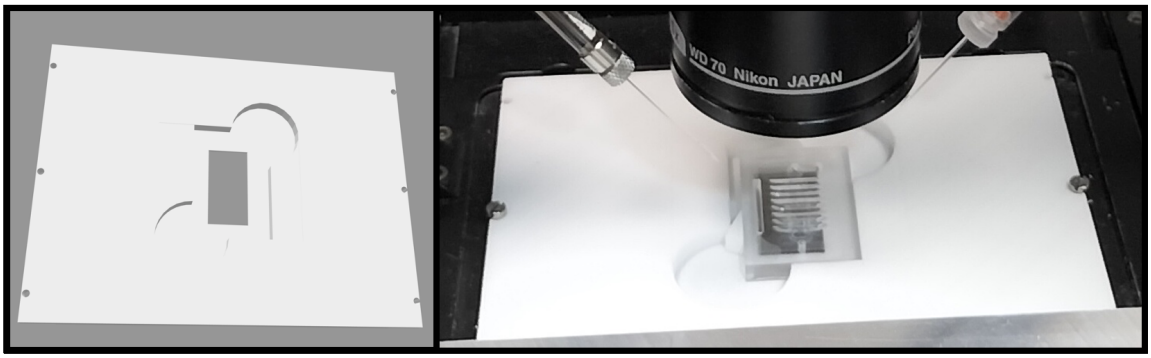


Figure 4.7: A 3D model (left) and a photo (right) of a mounted chip adapter with the chip. Using a 3D printer was a quick and simple solution.

4.1.3 Platform

The perfusion system was built on a Nikon Eclipse TE200 inverted microscope with a removed condenser. It is held by an aluminium platform which is static relative to the microscope objective, and the chip can move relative to the platform using a motorised microscope stage. This allows easy switching between different compartments of the chip.

After I tried several prototypes, the design was finalised by Adam Lowe, and manufactured in the Mechanical workshop of the University of Oxford. A 3D model of the platform can be seen in Figure 4.8.

4.1.4 Stages, holders, and NanoCubes

On the top of the platform, there are two Thorlabs three-axis stages, each holding a NanoCube (Physik Instrumente), a piezoelectric system for nanopositioning, with a travelling distance of 120 μm in three axes. The three-axis stages are used for a

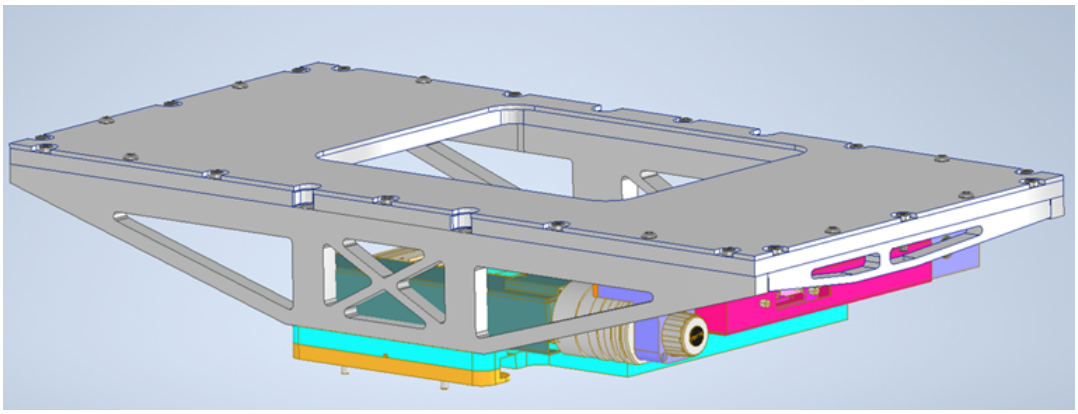


Figure 4.8: A model of the platform, created by Adam Lowe. The model (grey) is shown with the motorised microscope stage.

coarse positioning of the pipettes, and after the initial alignment, they should not be needed. The NanoCubes, contrarily, are used for fine position adjustments while inserting the pipettes into the droplet.

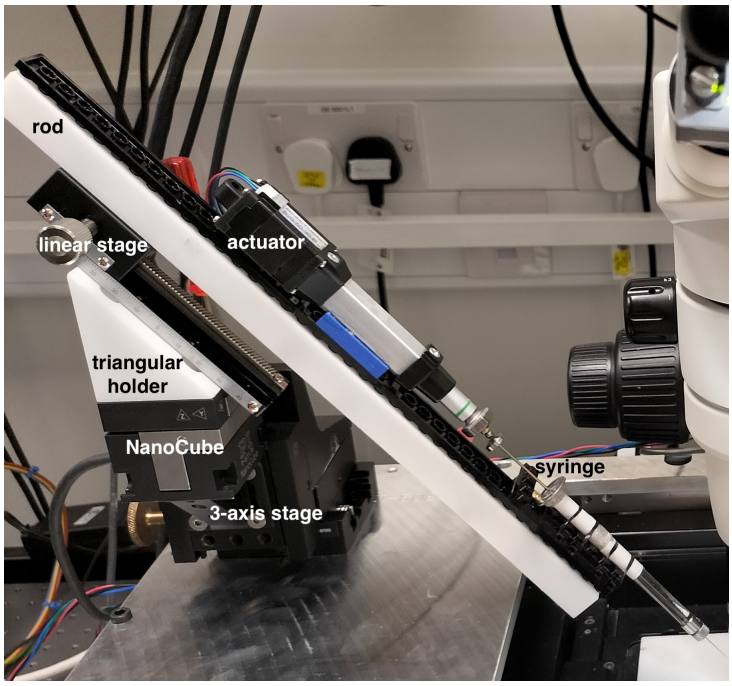


Figure 4.9: Parts of the perfusion system: the 3-axis stage is mounted directly on the platform, and it holds a nanopositioning piezoelectric system NanoCube, and a triangular holder; a linear stage is mounted on the triangular holder and controls the position of the rod with actuator and syringe. The same setup is used for the second pipette.

On the top of each NanoCube, there is a triangular holder printed from polyamide

12 (PA 12) by selective laser sintering (SLS) by 3D Hubs BV. The triangle holds the rod under the 50° angle - defining also the angle under which the pipettes enter the droplet. Between the triangular holder and the rod, I used a manual dovetail rack and pinion linear stage made of aluminium alloy by Optimal Engineering Systems (Figure 4.10). This is the only moving part of the setup with the translation axis orientated along the pipette. This is important for a simple exchange of the liquid in the pipette, or the pipette itself. After removing a pipette from the droplet by NanoCube, I can use the linear stage to move the pipette out of the chip, detach the rod, and make any required changes to the pipette. The rod can be then re-attached to the same position by neodymium magnets and moved back to the initial place just outside of the droplet, using the micrometre on the linear stage. The fine positioning of the pipettes could be done subsequently with NanoCubes.

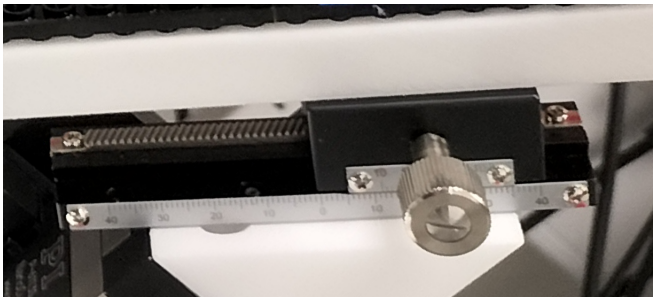


Figure 4.10: A manual dovetail rack and pinion linear stage for positioning of the pipettes. The only moving part of the setup with the translation axis orientated along the pipette. The micrometre helps to bring the pipettes back to the initial position.

4.1.5 Rod

The remaining parts of the setup are all mounted to the rod. I trialled different options to find a rod which does not vibrate at the end, and is not too heavy. After comparing aluminium rod and rods made of different 3D printing materials, I decided to use a rod 3D printed from polyamide 12 (PA 12) by selective laser sintering (SLS) at 3D Hubs BV. I designed the rod with three pairs of neodymium magnets

mounted to it, so the rod can be secured to the pair of neodymium magnets mounted on the linear stage in three different positions (Figure 4.11). The top of the rod has a layer of Lego bricks glued on it, complementing the Lego bricks on the bottom of the actuators and syringe holders. This solution, in contrast with other mechanical connectors I tried, has minimal room for wiggling, it is easy to attach and detach, and it is very easy to install. Together with the magnets, this made the system versatile but quite robust and stable.

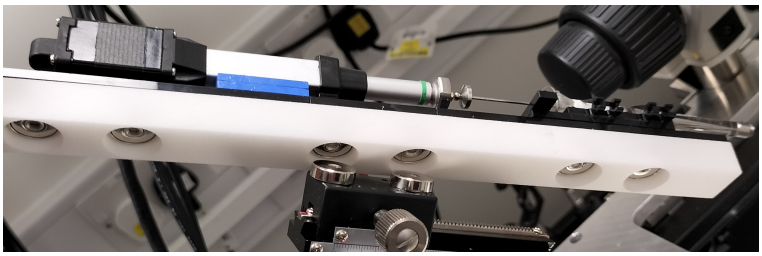


Figure 4.11: A photo of the rod to which the actuator and the syringe are mounted. There are three pairs of neodymium magnets on the rod, and any of the pairs can be connected to the pair of magnets mounted to the linear stage. The top of the rod is covered with Lego bricks, allowing stable but versatile mounting of the actuator and the syringe.

4.1.6 Syringe holder

Since the syringe plunger is being pushed or pulled by the actuator, I needed to minimise the possibility for the syringe to move around, causing changes in the position of the pipette and an uneven liquid flow. I tried a 3D-printed holder fitting the syringe tightly, but for the final design, I decided to use neodymium magnets to hold the syringe - one of them is glued on the Lego structure, and the second one is glued on the syringe. There are additional rubber bands to secure the syringe in place (Figure 4.12).

For similar reasons, a neodymium magnet is also used to attach the end of the syringe plunger to the actuator. The magnet glued on the actuator is attracted to a small steel bearing ball glued to the end of the plunger, ensuring that the force from

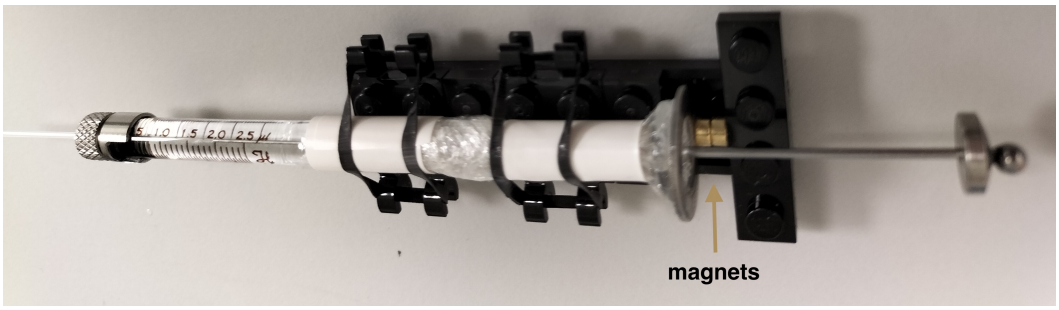


Figure 4.12: The syringe is held in place using neodymium magnets glued on a Lego structure. Additional rubber bands are used to secure the syringe in place.

the actuator is transferred in the correct direction.

4.1.7 Electrode holder

The chip was designed to allow control over the transmembrane potential applied on the droplet-on-hydrogel bilayer. Two electrodes are needed: one is placed in the agarose microfluidic channel through the hole in the chip and the agarose creates an electrical connection to the bottom side of the bilayer; the second electrode needs to be conductively connected to the water droplet. To avoid further mechanical disturbance of the droplet, I decided to connect the electrode between the pipette and the syringe. I used a custom-made electrode holder made of polycarbonate with a silver electrode and BNC (Bayonet Neill-Concelman) connector from the A-M systems (Figure 4.13). The connector was glued on the outlet syringe, rather than the inlet syringe, to minimise the possibility of contamination of the droplet.

As it is common for similar experiments, we can use silver/silver chloride (Ag/AgCl) electrodes. The electrodes are prepared by immersing a silver wire into the 20 vol% sodium hypochlorite solution, as described e.g. in the protocol in [Leptihn et al., 2013].

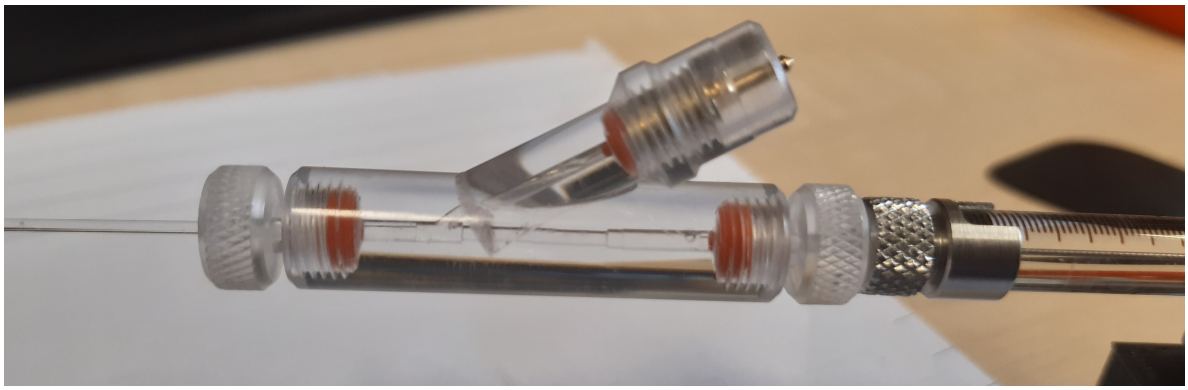


Figure 4.13: Custom-made electrode holder from A-M systems. The silver wire is visible in the arm of the holder. The holder is glued to the outlet syringe.

4.2 Top view microscope

To navigate the micropositioning of the pipettes, a second microscope is needed above the chip. I used a Nikon SMZ800N stereo microscope, mounted to the back of the platform. A custom-made adapter mounted a small Basler Ace camera to the place of one of the eyepieces, and I watched the magnified live image on a laptop screen.

The microscope needed to be mounted right above the objective of the microscope underneath. Figure 4.14 shows the mounting designed by Adam Lowe and manufactured by the Mechanical workshop at the University of Oxford. This mounting allows small adjustments in any direction on the horizontal plane. I aligned the microscope by focusing on the objective of the microscope underneath and moving the microscope until the objective was exactly in the middle of the field of view (Figure 4.15) The vertical position can be adjusted easily by moving the microscope up or down on the mounting pole.

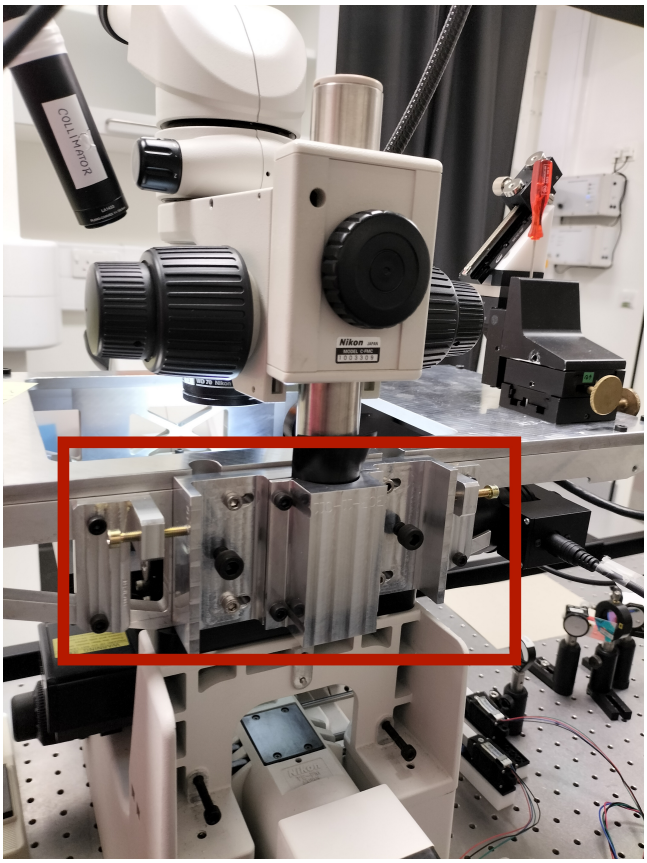


Figure 4.14: The microscope mount (framed in red) was designed by Adam Lowe and manufactured by the Mechanical workshop at the University of Oxford. By adjusting the screws, we can make small adjustments in any direction on the horizontal plane.

Figure 4.15) shows a droplet and a micropipette before entering the droplet, observed through the top view microscope. The microscope makes it much easier to control the position of the pipettes. The droplet on the photo has an elliptical shape because we are looking at it through an air-oil surface, which is curved due to capillary force.

4.3 Microfluidic control

In the previous sections, I wrote about the platform supporting the droplet-on-hydrogel bilayer and holding it in the right place relative to the objectives of the microscopes and pipettes of the perfusion system. Now I focus on the parts of the setup contributing to the microfluidic control: pipettes, syringes, and actuators with

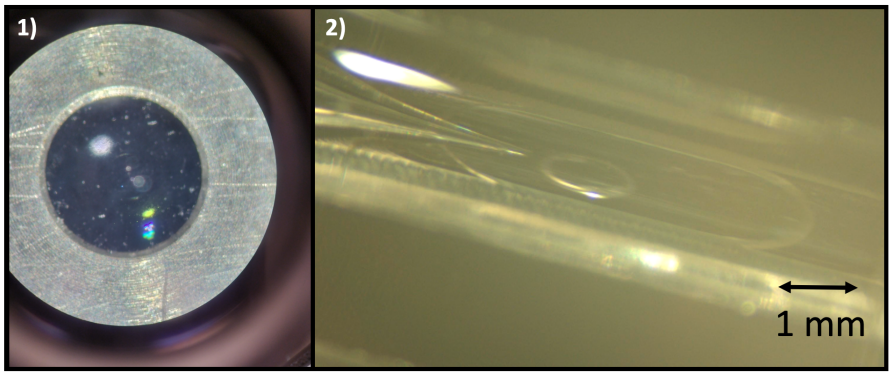


Figure 4.15: 1) The top view microscope was aligned by focusing on the objective of the microscope underneath. I secured the microscope in the position when the objective was in the middle of the field of view. 2) Micropipette approaching a droplet, observed through the top view microscope. The elliptical shape of the droplet is caused by the curved surface of oil due to capillary force.

all the necessary electronics to control them. At the end of this section, it will be demonstrated that I can steadily perfuse a 200 nl droplet in 27 nl steps.

4.3.1 Pipettes

In contrast with many perfusion systems which are using flexible tubes, I focused on minimising the elasticity of the system and thus simplifying the relation between the pressure applied on the liquid and the flow rate. This is extremely important in the case of very small volumes, where the flow rates in and out of the droplets need to be very similar to avoid disturbance of the droplet and rupture of the bilayer. The entire working liquid is therefore contained either in the droplet or in glass: I used glass syringes and glass pipettes attached via an adapter.

Pulling

I prepared the glass pipettes from borosilicate glass capillaries from World Precision Instruments (1B100-3), with an outer diameter 1 ± 0.1 mm, an inner diameter of 0.58 ± 0.1 mm, and a length of 76 mm. The capillaries with constant diameter were pulled using a micropipette puller, to create a thin tip which does not disturb the

droplet significantly. With the kind help and advice from Dr Nematian, Dr Conrad and Dr Cloake, I used the Sutter Instrument Micropipette Puller located in Prof. Tucker's laboratory. The principles of glass pulling are described in Pipette Cookbook 2018 by the Sutter Instrument. The puller uses a heat filament to soften the glass prior to the pulling, and this cycle is repeated with various parameters:

- Heat

  This parameter represents the amount of current supplied to the heat filament. Too much heat can burn the filament, and too little can damage the puller. To determine the amount of heat required to melt the glass capillary, a ramp test needs to be completed whenever we change the heat filament or the glass.

- Pull

  The puller can either only use the gravitational weight of the plunger, where the current supplied to the pull solenoid is zero, creating a shorter tip, or the pull of 50-150 AU is performed by the proportional amount of current supplied to the pull solenoid, creating a sharp electrode or a needle.

- Velocity

  The rate of separation of puller bars. Low velocity typically results in a shorter tip, and the lower the velocity is, the more cycles of pulling are needed.

- Time

  When using the Time mode, the glass is cooled with air during the pulling, since the velocity trip point is reached. One time unit is equivalent to 0.5 ms of cooling air.

- Delay

  An alternative mode of cooling provides a longer duration of cooling than the Time mode, so the cooling continues after the glass is pulled.

- Pressure

In both Time and Delay modes, this setting varies the pressure of air used to cool the filament and the glass. 500 units are equivalent to 2 psi of cooling air.

The ramp test showed that the heat needed for melting the glass was 588 AU. After a series of optimisation, I found the following pulling parameters:

Cycle	Heat	Pull	Velocity	Time	Pressure
1	587	0	25	250	500
2	587	0	25	250	500
3	587	0	25	250	500
4	587	0	25	250	500
5	587	0	10	250	500

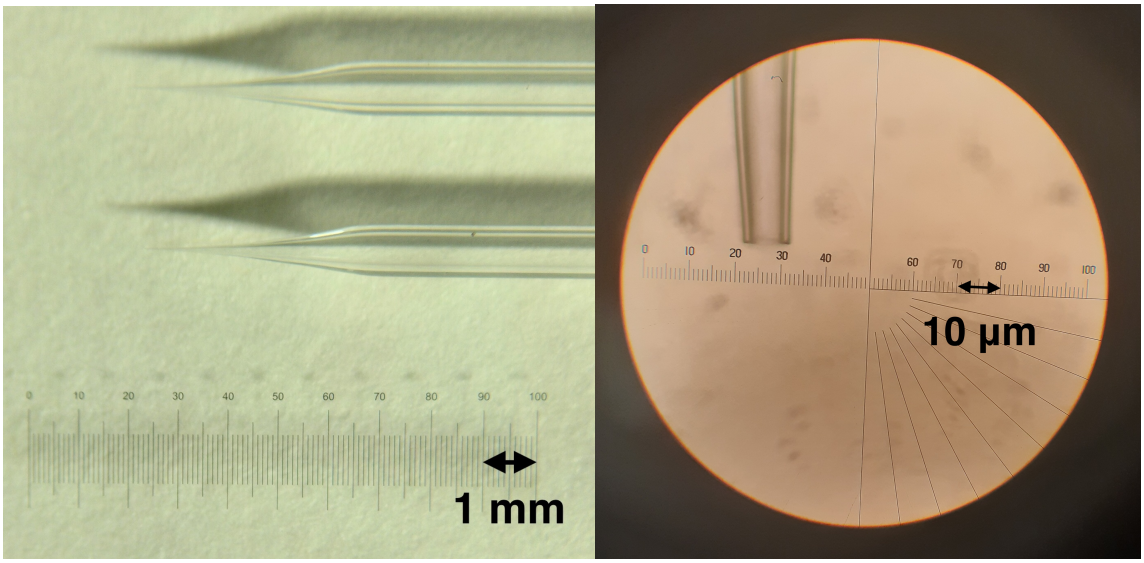


Figure 4.16: Glass pipettes observed under the microscope. Using the parameters presented above, I managed to consistently produce pipettes with approximately 4 mm long and 10 μm thick tips.

Hydrophobic coating

Having a pipette with the right size and shape, there is one more problem to solve: a water adhesion to the glass pipette, which can disturb the bilayer below the droplet. This phenomenon is caused by the values of surface tensions of oil-water, oil-glass

and water-glass interfaces, and I will outline the problem using simple calculations.

Let's consider the situation sketched in Figure 4.17: a water droplet (I neglected the effect of the ionic strength of the buffer on the value of surface energy) in hexadecane (I neglected the effect of silicone oil, and, much more importantly, lipid molecules), with a glass pipette immersed in the droplet. Although the surface tension values vary in the literature, depending on the specific type of material and experimental conditions, I built an approximated picture based on the following data:

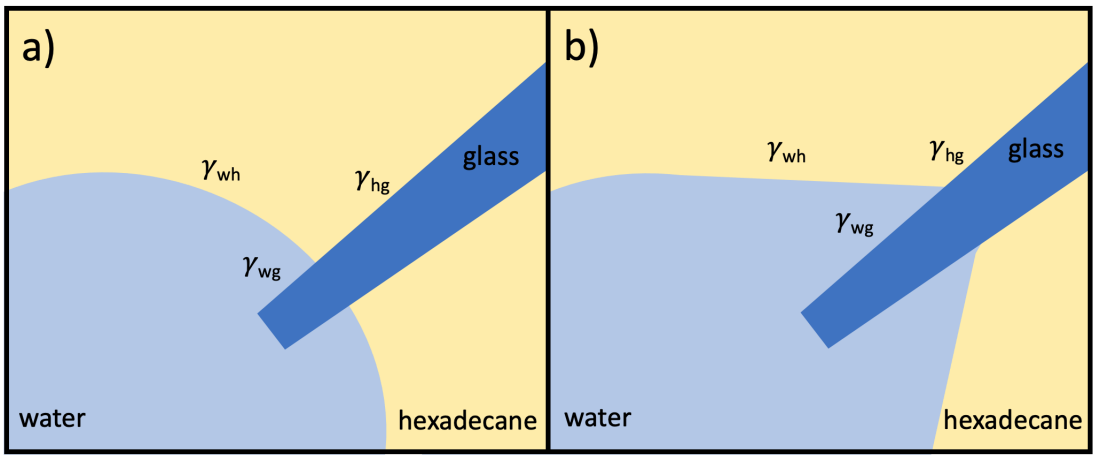


Figure 4.17: An illustration of a water droplet (light blue) in hexadecane (yellow), with a glass pipette (darker blue) immersed in the droplet. Depending on the geometry and surface tension values, option a) or option b) could be realised. However, the values of surface tensions above suggest option b), which is consistent with my observation.

- Hexadecane-glass surface tension: $\gamma_{hg} = 56.3$ mN/m
  calculated using the Young equation (Equation 4.1), the contact angle of hexadecane on glass 15.6° [Sbeih et al., 2021], the surface tension of hexadecane in air 28.12 mN/m [Rolo et al., 2002], and the surface tension of glass on air 83.4 mN/m [Rhee, 1977]

- Water-hexadecane surface tension: $\gamma_{wh} = 52.4$ mN/m
  the interfacial tension measured between 0.01 M phosphate buffer (pH 7.4) and n-hexadecane [Lee et al., 2000]

- Water-glass surface tension: $\gamma_{wg} = 14.9$ mN/m
  calculated using the Young equation (4.1), the contact angle of water on glass 18° [Sbeih et al., 2021], the surface tension of water in air 72.8 mN/m [Rhee, 1977], and the surface tension of glass on air 83.4 mN/m [Rhee, 1977]

From the Young equation, we can get a relation for surface tensions between three phases (solid, liquid and gas), and the contact angle of a liquid drop on a solid material in gas:

$$\gamma_{SG} - \gamma_{SL} - \gamma_{LG} cos\theta = 0, \tag{4.1}$$

where γ_{SG} is the surface tension of a solid in gas, γ_{SL} is the surface tension of a solid-liquid interface, γ_{LG} is the surface tension of a liquid in gas, and θ is the contact angle of a liquid drop on a solid material in gas.

From the values above, it can be concluded that it can be energetically favourable for the system to increase the area of the water-glass and the hexadecane-water surface and decrease the area of the hexadecane-glass surface by adhesion of the water to the glass pipette, which is consistent with my observations.

To avoid this scenario, I tested a few options for hydrophobic coating, as can be seen in Figure 4.18. The coatings include silicone glue, which was used for this purpose before, grease, a siliconizing reagent Sigmacote, and water repellent, but I also experimented with coating the layer of silicone glue with pencil dust. My observations were performed in the air. I found out, that although most coatings work for increasing the surface energy of the coated pipette, which was demonstrated by a decreased contact area between the pipette and water, some of the options are more practical than others. I decided to proceed further with the siliconizing reagent Sigmacote.

Sigmacote is a solution of a chlorinated organopolysiloxane in heptane. On the glass, it forms a thin covalent film, which repels water. Due to its liquid form, it

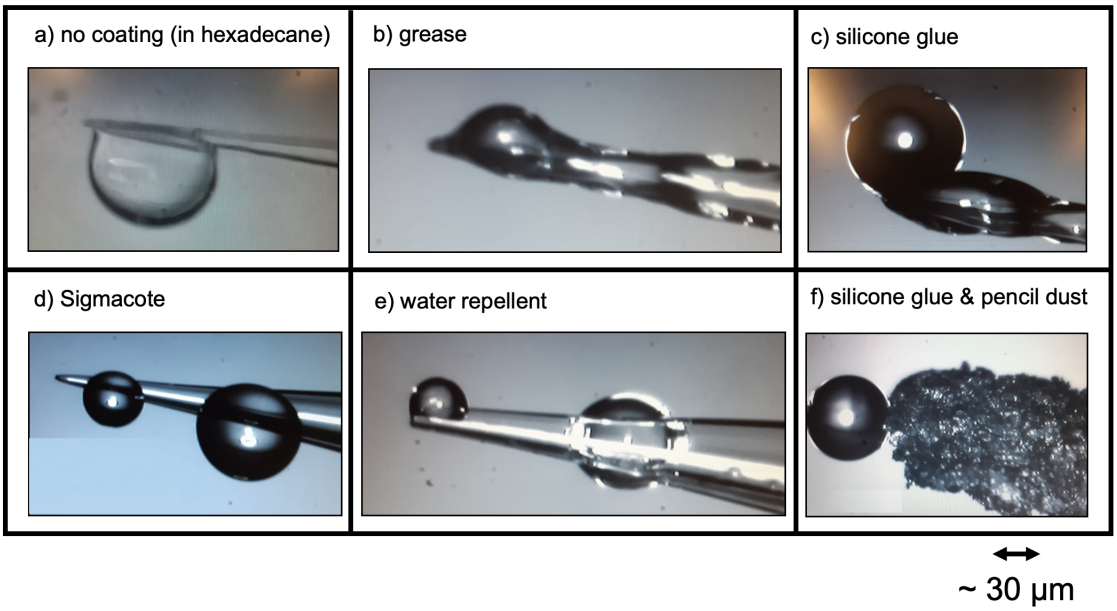


Figure 4.18: Water droplets released from a glass pipette: a) immersed in hexadecane, with no coating of the pipette; b)-f) in air, the pipette is coated with a hydrophobic coating. While most of the coatings work, Sigmacote was the most practical to use.

is very easy to apply: First completely filled the pipette with a buffer used in the experiment. Next, I dipped the tip of the pipette in the Sigmacote solution, let it dry completely, and repeated it two more times. The pipette was then ready to be used. A photo of a water droplet in the air, being held by two pipettes coated with Sigmacote during a perfusion experiment, can be seen in Figure 4.19.

Attachment of pipette to syringe

Glass pipettes were attached to the syringes using Hamilton Removable Needle Compression fittings. This ensures minimum elasticity on the connection points, and easy replacement of the pipettes.

4.3.2 Actuators

Due to my commitment to avoiding flexible tubing, it would be very difficult to use commercial syringe pumps. Instead, I found a solution, which minimises the resid-

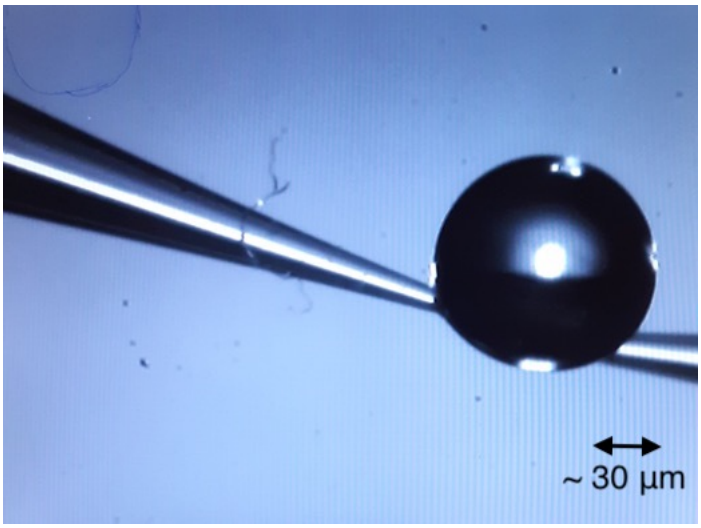


Figure 4.19: A photo of perfusion testing. A water droplet suspended in air, being held by two immersed pipettes coated with Sigmacote solution.

ual ("dead") volume, and elasticity of the tubing by using only short glass pipettes. I used small actuators to push and pull the syringes, and made the electronics and the software for controlling these actuators. I experimented with two types: actuators with a permanent magnet direct current (PMDC) motor, and with a stepper motor.

Actuator with a permanent magnet direct current (PMDC) motor

Actuonix L12-50-50-12-P is a micro linear actuator with a stroke length of 50 mm, a gear ratio of 50 : 1, a DC voltage of 12 V, and potentiometer position feedback. When it is controlled with the Linear Actuator Control board, the correct position is achieved in several cycles of moving closer to the target position and measuring the actual position through the position feedback. I observed that the vibrations caused by quick forward and backward movement are potentially disruptive for the droplet, and therefore decided to write a simpler protocol for controlling the actuators in LabVIEW. I used the National Instruments voltage output module NI-9263 and built current amplifiers.

Current amplifier

I used a high-power monolithic operational amplifier OPA541 to build current amplifying circuits. The circuits use an external power supply, take input from the NI-9263 voltage output module, and the outputs are connected directly to the actuators. Figure 4.20 shows a scheme of the circuit (left) and a photo of two circuits I soldered to run the actuators.

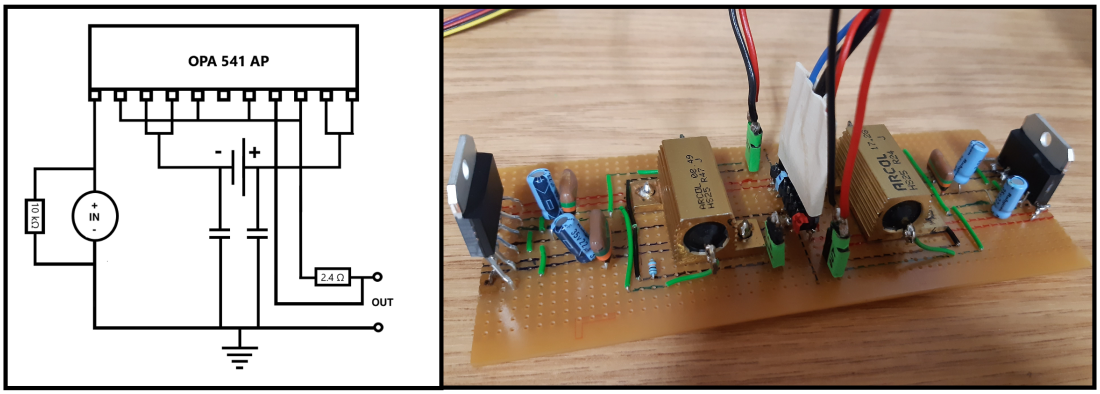


Figure 4.20: A current amplifying circuit: a scheme (left), and a photo of two circuits for running two permanent magnet direct current (PMDC) motor actuators. I used the operational amplifier OPA541 for amplifying the current.

The operating principle of the PMDC actuator is simple: when a sufficient voltage is applied, the actuator moves, and reverse polarity of the voltage causes a movement in the opposite direction. I measured the minimum voltage required for moving the actuator in my setup to be 1.2 V, and the minimum signal duration was 50 ms.

Position feedback

In addition to controlling the actuators, I also wanted to track their positions, using the potentiometers in the actuators. I applied a reference voltage on the potentiometer reference rails, and the voltage difference between the reference voltage and the voltage on the potentiometer wiper pin was linearly proportional to the position of the actuator. The position was monitored through the National Instruments voltage

input module NI 9215 and visualised using LabVIEW.

Software

I wrote a LabVIEW software which takes an amplitude and a duration of the signal and a number of cycles as inputs, moves the actuator, and plots the position of the actuator. This allowed me to analyse the variability of the step sizes under the same conditions (without engaging the syringes - an example of such analysis for a 1.3 V signal with a duration of 100 ms is shown in Figure 4.21).

I ran the analysis for two different models (they differ in size) of actuators with permanent magnet direct current (PMDC) motors. I analysed the expansion and contraction of the actuators, and I found a 10 % variability of the step sizes 0.2-0.8 mm.

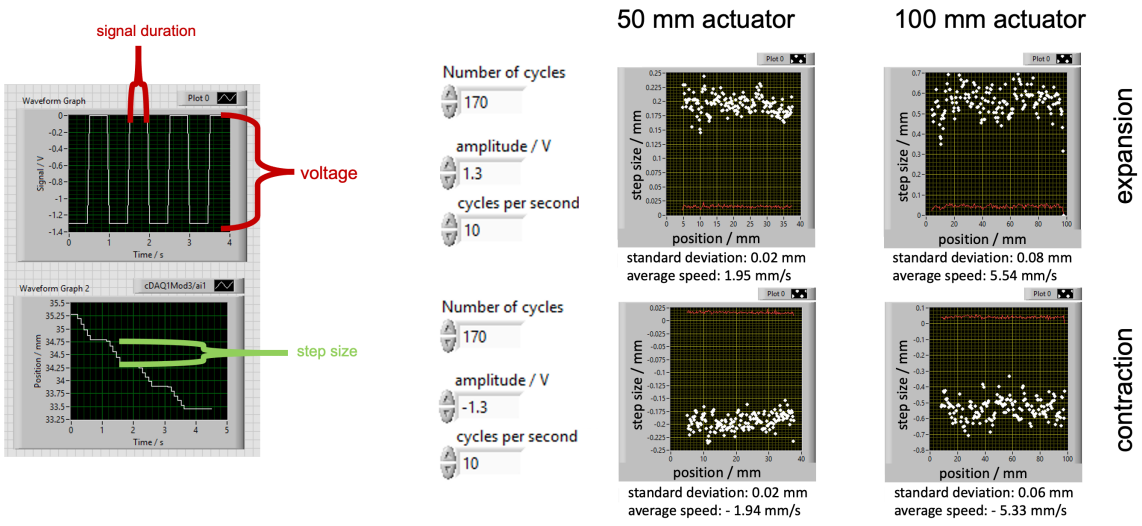


Figure 4.21: Analysing the variability of step sizes for two different actuators during expansion and contraction (without engaging the syringes). I used a 1.3 V signal with a duration of 100 ms. The standard deviation was found to be 10 % of the step size.

The variability of the step sizes is given by the type of the actuator motor. A permanent magnet direct current (PMDC) motor provides constant torque, and therefore

the position of the rotor and the velocity of the actuator depend on the load. In contrast, a stepper motor provides a constant angle, and, consequently, a constant velocity independent of the load. This option will be explored in the following section.

Actuator with stepper motor

I used Actuonics S20 Linear Stepper Actuator with NEMA8 (National Electrical Manufacturers Association) hybrid bipolar stepper motor with a step size of 1.8° and a stroke length of 50 mm. The velocity of this actuator is determined by the step frequency, and the maximum force by the input current. It is controlled by four inputs, two for each of the two independent coils sets (Figure 4.22), which effectively become electromagnets, as the current in the coils produces a magnetic field. The rotor rotates to align with the changing magnetic field produced by the coils.

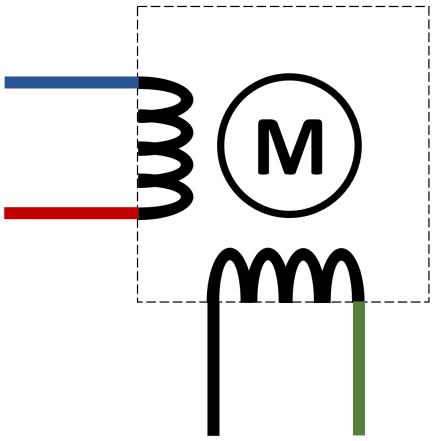


Figure 4.22: An actuator with a stepper motor is controlled via four inputs, two for each of the two independent coil sets. The velocity of the actuator is determined by the step frequency.

The table below shows the sequence of the inputs for the full-step rotation of the motor, where magnets on the rotor are always aligned with the coils. Value 1 represents the input voltage in reference to the ground (0). If the input voltage is positive, the step sequence 1-2-3-4 represents a clockwise and the step sequence 4-3-2-1 a counterclockwise rotation of the motor.

Step	blue (coil A)	red (coil A)	black (coil B)	green (coil B)
1	1	0	1	0
2	0	1	1	0
3	0	1	0	1
4	1	0	0	1

However, the rotor does not always need to align with the coils, but it can also be in between the full step positions. This is called a half-stepping, and it is shown in the table below:

Step	blue (coil A)	red (coil A)	black (coil B)	green (coil B)
1	1	0	1	0
2	0	0	1	0
3	0	1	1	0
4	0	1	0	0
5	0	1	0	1
6	0	0	0	1
7	1	0	0	1
8	1	0	0	0

In the work presented further, I used the half-stepping mode, with one half-step moving the actuator by 5 μm.

Amplifier

To amplify the current provided by the National Instruments voltage output module NI-9263, I used a quadruple high-current half-H driver L293D. It takes four voltage inputs from the NI-9263 and returns four outputs for the four pins of the actuator. The scheme of the circuit is shown in Figure 4.23, and a photo of two circuits for running the two stepper motor actuators is in Figure 4.24.

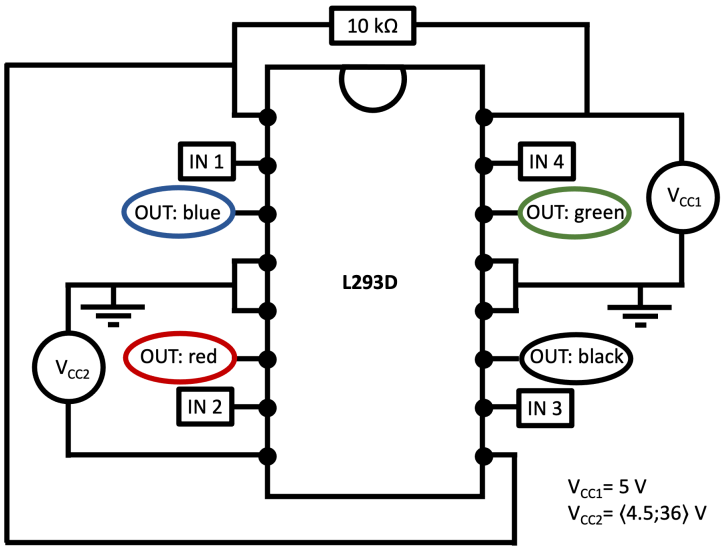


Figure 4.23: A scheme of a current amplifying circuit for a stepper motor, using a quadruple high-current half-H driver L293D for amplifying the current.

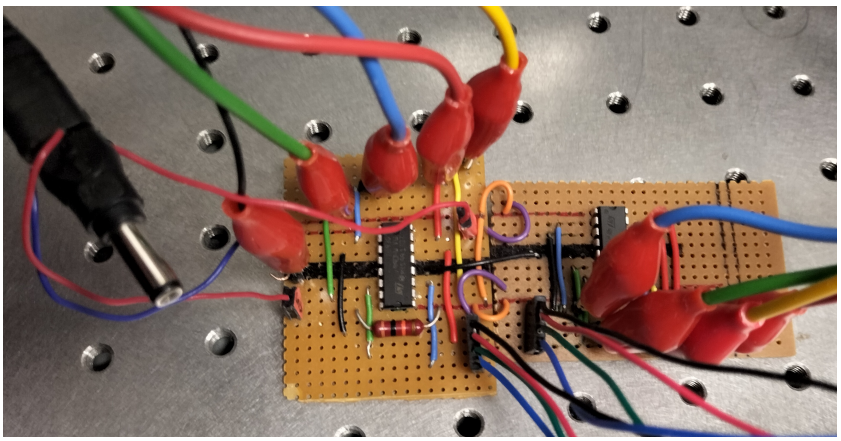


Figure 4.24: A photo of the two current amplifying circuits for running the stepper motor actuators. Each of them is an externally powered circuit, with four inputs from NI-9263 module, and four outputs connected to the actuators.

Software

The software for controlling the stepper motor actuators was also written in LabVIEW, with the kind help of Professor Berry.

To be able to move a stepper motor actuator by a defined distance, we need to know the position of the rotor in regard to the coils (for half stepping, it could be one of steps 1-8 from the table above). The first task before moving the actuators is therefore moving the motor into a defined position. After this, the position of the rotor would be updated and stored after each movement. The software runs continuously and the movement is initiated each time we prompt it. It is adapted for controlling the liquid flow, therefore the input variables include the ratio between the velocities of the two actuators (value -1 means the same velocity, but in the opposite direction, resulting in a stable flow), the total time of the movement, the number of steps (one step corresponds to 5 μm), and the voltage (I used 4 V).

4.3.3 Perfusion

4.3.4 Qualitative experiments

First, I tested the perfusion system qualitatively - these experiments were performed using the actuators with permanent magnet direct current (PMDC) motors. I used water coloured with blue food colouring, so I can track the water flow, and I was visually inspecting the size of the droplet during the perfusion. If the droplet grows, the inlet volume is larger than the outlet volume, and the opposite is true if the droplet shrinks. I performed the experiments in air and also in oil inside a well of an assembled chip (Figure 4.25). In both experiments, I used a series of 2.25 nl steps. The experiment in the air shows that the coloured water from the droplet moved into the outlet pipette, while the volume of the droplet has not visually changed. The experiment in the oil shows the water droplet coloured by the coloured water

from the inlet pipette, while the original size of the droplet (in comparison with a droplet of the same size in the well below) has not changed.

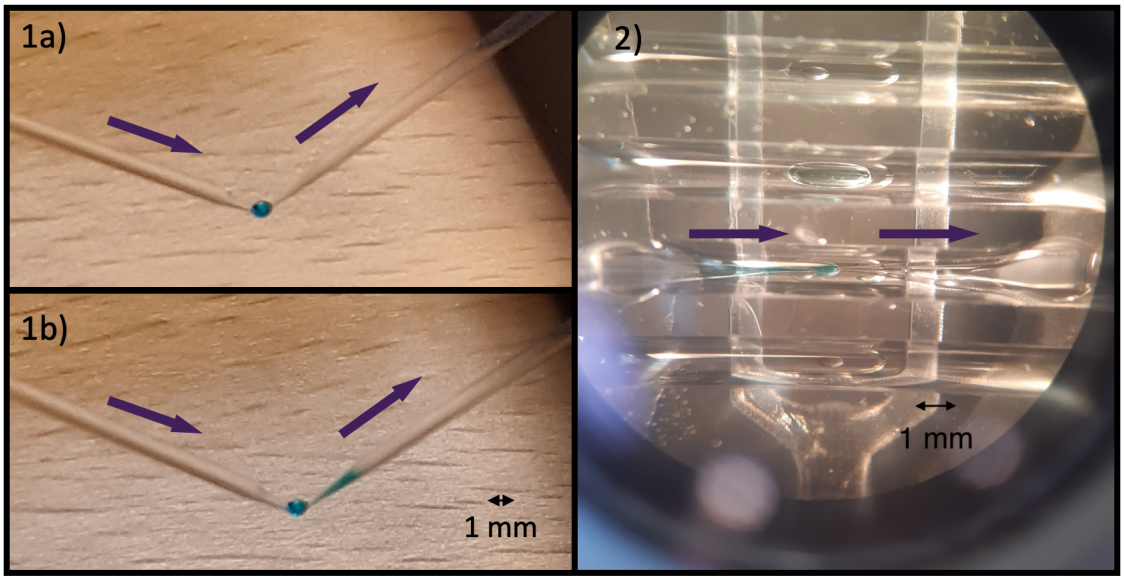


Figure 4.25: Qualitative tests of the perfusion system. I used blue food colouring to visualise the movement of the water. 1) Experiment in the air: a 400 nl coloured water droplet was attached to the tips of the pipettes and perfused by a series of 2.25 nl steps. Figure a) shows the droplet before, and figure b) after the perfusion. The coloured water is visible in the outlet pipette, while the size of the droplet has not visibly changed. 2) Experiment in oil a well of an assembled chip: the inlet pipette was filled with coloured water, the outlet pipette with clean water; both pipettes were then moved into a 200 nl droplet and the droplet was perfused by a series of 2.25 nl steps. The figure shows the droplet after the perfusion, visibly coloured by the liquid from the inlet pipette, and maintaining the original size.

Figure 4.26 shows frames from a video capturing a perfusion experiment. This time, the experiment was performed with the actuators with stepper motors. I was perfusing a 200 nl water droplet on a glass slide, with the inlet pipette filled with coloured water. The step size was 27 nl.

4.3.5 Quantitative experiments

The quantitative experiments were also performed with the actuators with stepper motors. I perfused a water droplet in the air and analysed the video from the exper-

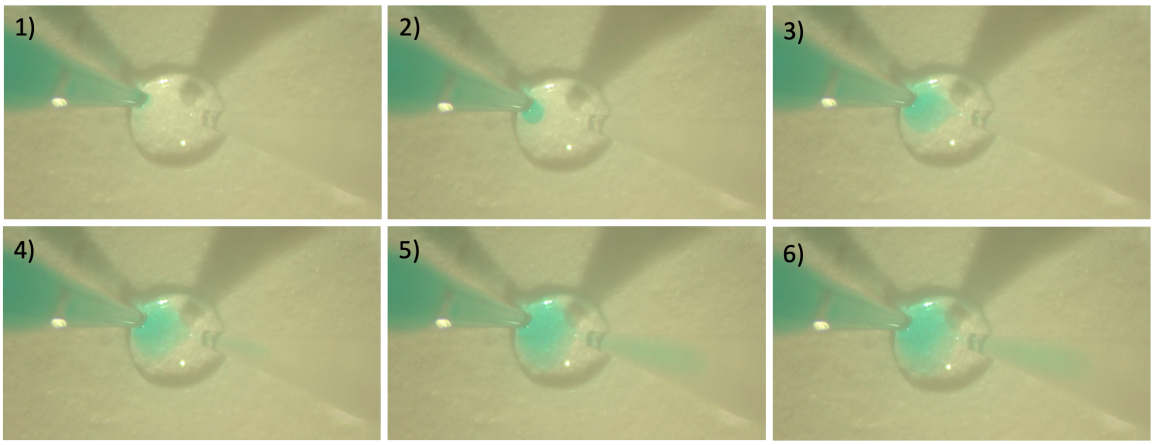


Figure 4.26: Frames from a video of qualitative perfusion experiment. A 200 nl water droplet on a glass slide was perfused using 27 nl large steps. The inlet pipette contains coloured water. We can see the coloured water entering the droplet, while it maintains its size.

iment using software called Videotracker. This software does an automated object tracking, producing a graph of a position of an object in time. I was tracking at least three positions on the surface of the water droplet and fitted the points with a circle (example is shown in Figure 4.27). Using the circle fits, I plotted a graph of the radius of the droplet in time, and, from this graph, I calculated the volume of the droplet in time. To set a scale, I used the known thickness of the pipette. The choice of the origin and the orientation of the axes does not influence the volume of the droplet.

Perfusion step size

During the first experiment, I was filling the droplet through the inlet pipette, and the outlet pipette was inserted, but not used. The graph of the volume of the droplet increasing in time is shown in Figure 4.28 a). Green arrows indicate the beginning of each step. I repeated the experiment and recorded in total 17 step sizes, which are presented in a histogram (Figure 4.28 b)). Despite a small number of data points, the shape of the histogram is close to the expected Gaussian function. The average step size is 26.68 nl, and the standard deviation is 2.99 nl.

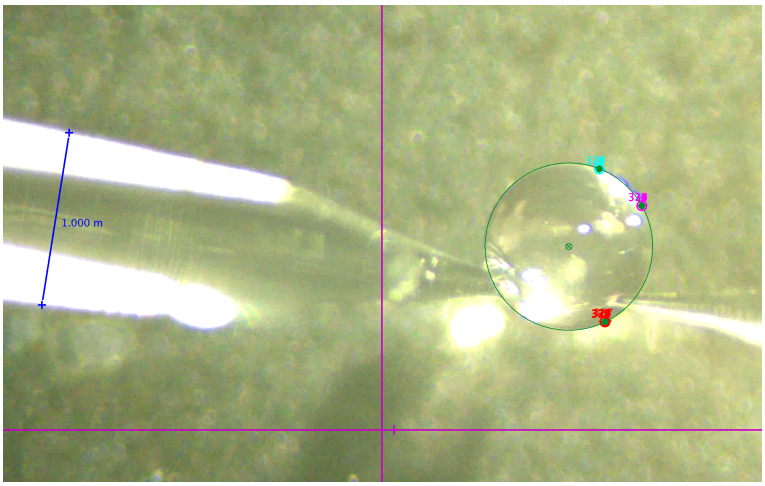


Figure 4.27: A quantitative measurement of the perfusion system during perfusion of a water droplet in the air using image analysis by Videotracker. On every frame, the software tracked three or more points on the surface of the droplet and fitted them with a circle (green). The radius of the circle in time was recorded in a graph. The blue line defines a scale, and the pink lines mark the position and orientation of the axes.

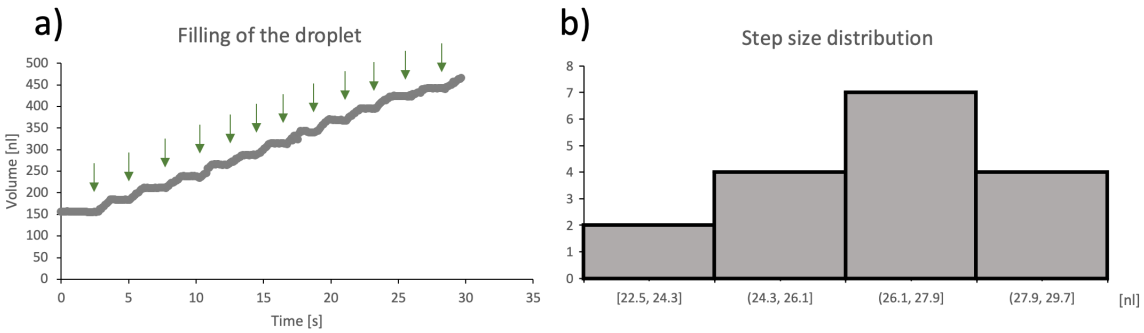


Figure 4.28: a) Graph of the volume of a droplet filled through the inlet pipette. Green arrows indicate the beginning of each step. b) Histogram of step sizes from two experiments. I found the average step size 26.68 $\pm$ 2.5 nl.

During the second experiment, the droplet was perfused, engaging both the inlet and outlet pipette. Since the incoming flow was balanced with the outgoing flow, the expectation was that the volume of the droplet will not change. Figure 4.29 shows two perfusion experiments. For each experiment I show a) graph of the volume of the droplet during the perfusion, fitted with a linear fit, and b) a histogram of residual values. The beginning of each step is indicated by a green arrow. We

can see a very stable flow without noticeable disturbance around the beginning of individual steps. The standard deviation of the volume was 0.70 nl in the first experiment, and 1.59 nl in the second experiment.

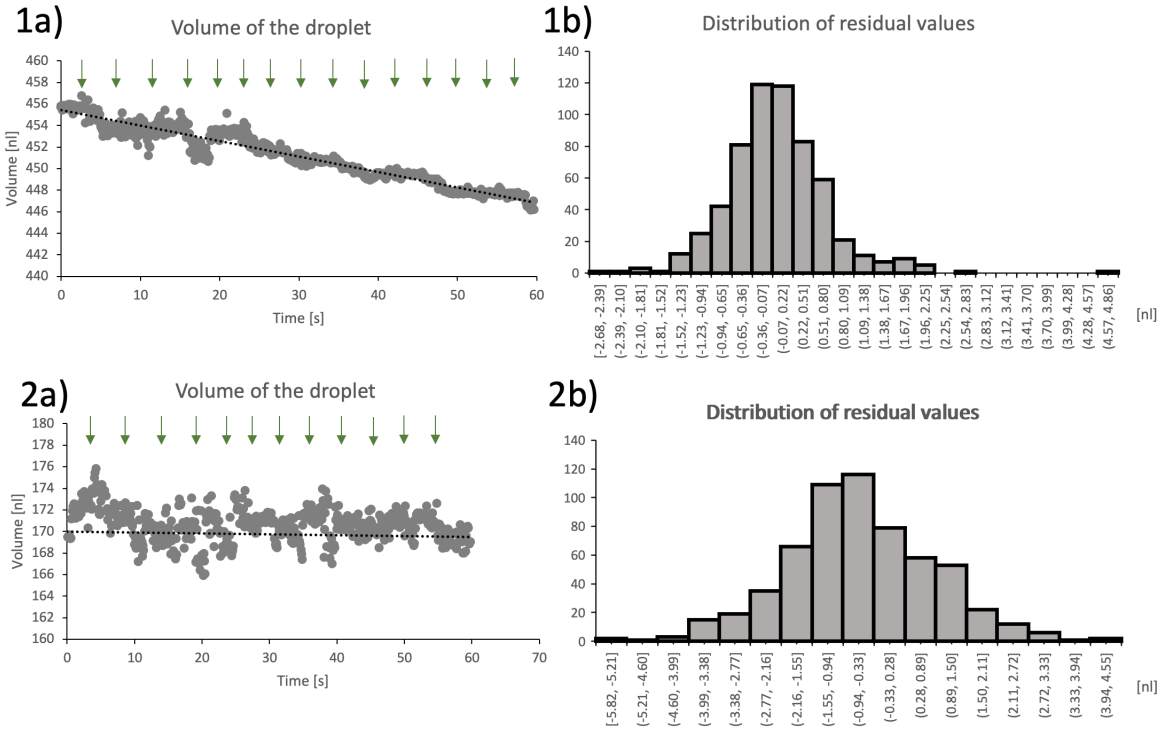


Figure 4.29: For two experiments, I reported a) a graph of the volume of the droplet during the perfusion, fitted with a linear fit (the beginning of each step is indicated by a green arrow), and b) a histogram of residual values. The standard deviation of the volume was 0.70 nl in the first experiment, and 1.59 nl in the second experiment.

The noise recorded during the experiment could either come from a mechanical disturbance of the droplet during the perfusion or the noise introduced by image processing. In an attempt to quantify the second source, I analysed a short video recording of a droplet without perfusion. The graph of volume of the droplet, fitted with a linear fit, is shown in Figure 4.30. The standard deviation of the volume was 0.32 nl.

The results of the control experiment indicate that the noise in the perfusion data could be partially caused by a mechanical disturbance of the droplet by the perfu-

sion, but it is extremely small and unnoticeable without the video analysis. I therefore conclude that the perfusion is very stable and reliable for experiments with droplet-on-hydrogel bilayer.

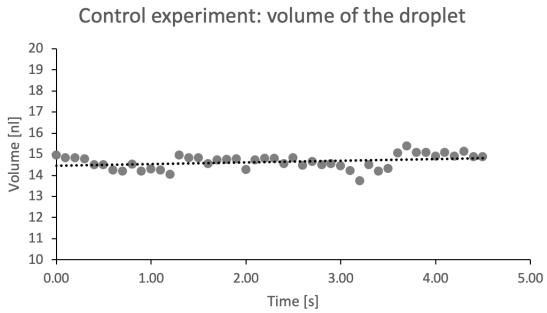


Figure 4.30: The graph of the volume of the droplet without perfusion, fitted with linear fit (black). The standard deviation of the volume is 0.32 nl.

4.4 Conclusion

In this chapter, I have described the building of the hardware necessary for the perfusion of the droplet during experiments with a droplet-on-hydrogel bilayer. I adapted the published design of the microfluidic chip for use with the perfusion pipettes. The next step was the building the mechanical support on the top of an inverted microscope, so the perfusion system was vibrational-free and could be operated remotely. Another microscope was aligned on the top of the first one for easier control of the pipettes' position.

Next, I have described the process of pulling and coating the micropipettes. The flow of the perfusion is controlled by actuators pushing and pulling the plunger of the syringes, and I tested two different types: actuators with permanent magnet direct current (PMDC) motors and actuators with stepper motors. For both types, I soldered suitable current amplifiers and wrote software in LabVIEW to control them. I analysed the expansion and contraction of the actuators with a PMDC mo-

tor, and I found a 10 % variability of the step sizes 0.2-0.8 mm.

At the end of this chapter, I presented the results of the perfusion tests, showing that the setup can reliably perfuse droplets as small as a few hundred nanoliters, with a stable step size of 26.68 $\pm$ 2.5 nl.

Chapter 5

Conclusion and future directions

During my doctoral project, I was building an experimental assay, which can be used for a high-resolution single molecule study of membrane proteins in an energised lipid membrane. The main motivation for this work was a study of ATP synthase F_1F_o. The first chapter of this thesis was therefore designated to this protein.

I started with expression and purification protocols for both *E. coli* and TA2.A1 F_1F_o and then analysed the outcomes of these protocols. I presented the results of protein concentration assay, gel electrophoresis, and phenol red activity assay, and concluded that the expression of F_1F_o was successful.

Next, I used the site-directed mutagenesis to alter the TA2.A1 F_1F_o, so it can be labelled with a gold nanorod and anchored to the agarose layer. The mutagenesis was confirmed by sequencing. I functionalized agarose with streptavidin to enable the anchoring and tested the product using fluorescent microscopy methods.

The second chapter was designated to the lipid bilayer. I found parameters for forming bilayers, which are stable for more than 10 hours, and maintain the activity of F_1F_o. The parameters are: 5 mM of 75 mol% DPhPC and 25 mol% $POPA^-$ in 50 vol% of hexadecane and 50 vol% of AR20 silicone oil, and monolayer formation time 30

minutes.

I also built a double-colour fluorescent microscope setup, with two different lasers, and two channels for the output signal. The setup can be used for a control fusion experiment with two colour liposomes, or, perhaps in the future, for FRET experiments, or other types of fluorescent experiments with F_1F_o.

The last chapter covers all the important steps in building a versatile and low-cost perfusion system for highly accurate independent control of electrical and chemical transmembrane potential and reliable delivery inside the droplet. I modified the published version of the microfluidic chip to be compatible with pipettes perfusing the droplet and designed stable mechanical support for the system, including Lego and magnetic holders. I also prepared micropipettes with a hydrophobic coating.

For controlling the liquid flow, I used actuators attached to the plungers of the inlet and the outlet syringe. I experimented with actuators with permanent magnet direct current (PMDC) motors and with position feedback and I made a suitable current amplifier and LabVIEW software. The analysis of the step sizes of the actuator (without engaging with the syringe) has shown 10 % variability on 0.2-0.8 mm steps.

I also used actuators with stepper motors and made different current amplifying circuits and a different LabVIEW software for them. Using the stepper motor actuators, I recorded a stable perfusion with a consistent step size of 26.68 ± 2.5 nl.

To summarise, my most important contributions to this ongoing project were finding a protocol for a stable and suitable lipid bilayer, preparing a way to anchor the membrane part of the protein, and building a low-cost system for stable perfusion of the droplet.

5.1 Future directions

As was explained in the Covid impact statement at the beginning of this thesis, the schedule of this project was massively affected by the pandemic, and, later, by one year delay in delivery of the crucial parts of the perfusion system, and, therefore, it did not progress as fast as initially planned. There are several experiments planned but not performed yet. In this section, I detail my very next experimental plans, but also other ideas for using the droplet-on-hydrogel based assay.

5.1.1 Next steps

In Chapter 3, I described a design of a control experiment to verify the protein delivery method via charged membrane fusion. I prepared liposomes with membrane fluorescent labels and water-soluble fluorescent labels, and a two-colour fluorescent microscope setup. The first step therefore will be to use the perfusion system to inject the labelled liposomes into the droplet while observing the fluorescent signal from the bilayer in two emission channels. Co-localising of the signals from the two channels will allow me to conclude whether the liposomes are fusing with the bilayer. In case of success, the same lipid composition, but without the labels, will be used for preparing proteoliposomes containing *E. coli* F_1F_o labelled with gold nanorods.

There are several possible strategies for labelling the protein with gold nanorods. To make sure that we only label the α subunit and not the c subunit, the protein must be embedded in proteoliposomes or a supported bilayer prior to labelling. If we used the perfusion system to inject gold nanorods into the droplet after the proteoliposomes fused with the bilayer, we would need to then perfuse the droplet with several droplet volumes, with suitable waiting time in between the individual pulses, to allow diffusion of the gold, so most of the free nanorods can be removed. While this can work, I find it simpler to label the proteoliposomes before they are

injected into the droplet. It is not possible to separate labelled proteoliposomes from free gold nanorods due to the negligible mass of the proteoliposomes in comparison with gold nanorods, and, therefore, I will need to use similar molar concentrations of nanorods and proteoliposomes. Proteins are relatively stable in proteoliposomes, so I can increase the labelling efficiency by increasing the waiting time to one hour.

Another necessary step is energizing the lipid membrane. I will use silver/silver chloride electrodes to apply transmembrane potential up to approximately 150 mV. A lipid membrane, a structure with two parallel sheets of water-soluble lipid heads separated by a layer of hydrophobic lipid tails, can be considered as a parallel plate capacitor. Monitoring the capacitance of the membrane provides information such as possible multilaminarity of the membrane or presence of solvent in the hydrophobic layer, or possibly even single vesicle fusion events. The capacitance is measured using a picoammeter; the application of a triangular wave voltage input creates a square wave capacitive current output.

A 2D projection of the orientation of the gold nanorod attached to an F_1F_o molecule rotating in an energized lipid membrane will be monitored via four avalanche photodiodes, with relative orientation 0°, 45°, 90° and 135°. Analysis of the signal from the four photodiodes will provide the angular velocity of F_1.

Once I will be able to identify a signal from rotating gold nanorods, I will also be able to explore what is the activation potential at different conditions, especially with different transmembrane proton gradients. By adopting the transmembrane potential and the ATP/ADP concentration, I would be able to reverse the direction of the rotation and compare ATP synthesis with ATP hydrolysis by the same molecule.

5.1.2 Ideas for future experiments

Another goal of the experiment outlined in the previous section is to produce high-resolution traces of rotating F_1F_o in the energised membrane during the ATP synthesis. Analysis of these traces, together with the recent results of cryo-EM studies of F_1F_o, can reveal more details about the temporal storage of the energy from the proton transport in the elastic parts of the protein until the energy is used for conformational changes necessary for catalysing the ATP synthesis. The proposed regions are the peripheral stalk, the central stalk, and the OSCP subunit in mitochondrial F_1F_o) or the corresponding δ subunit in bacterial F_1F_o, but their role was not yet reliably confirmed.

In the future, I would find it very interesting to also employ Förster resonance energy transfer (FRET) to study the rotation of F_1F_o, which should be compatible with the presented setup. Using the published cryo-EM structure, it is possible to carefully select the appropriate positions for fluorescent labels so they do not block the rotation of F_1F_o during ATP synthesis, but reveal the conformational changes in the individual subunits in between the rotor steps, which are used for temporal energy storage to compensate for symmetry mismatch between the F_1 and F_o.

Besides the F_1 and F_o, the presented assay could be used also for studying other molecular motors, such as bacterial 5:2 rotary motors, driven by ion flow into the cell, which rotation has never been directly observed [Rieu et al., 2022]. The advantage of independent control of electrical and chemical potential can be used in research of proteins undergoing conformational changes during their function (the movements can be monitored by gold nanoparticles), or to study ligand binding (using fluorescent labels). It is also possible to use this setup for studying various properties of the lipid membrane, including protein diffusion or mechanical properties, and their dependence on electrical and chemical potential.

Chapter 6

Methods

6.1 Expression and purification of *E.coli* F_1F_o

We use DK 8 strain transformed with plasmid pFV23: cysteine-free mutant with added

- CYS after the second amino acid of the α subunit
- CYS after the second amino acid of the c subunit
- 6 HIS after the fourth amino acid of the β subunit

Protocol

1. prepare 50 ml of LB with ampicillin (200 μg/ml)
2. inoculate the medium with bacteria
3. incubate at 37 °C with shaking (200 rpm) overnight

   NEXT DAY

4. prepare two flasks of LB with ampicillin (200 μg/ml), 1 l each
5. add 10 ml of the culture to each of the two flasks

6. incubate at 37 °C with shaking (120 rpm) for **6-8 hours**

7. centrifuge the solution at 4,000 g for 20 min at 4 °C

8. remove the supernatant and store the pellet at -80 °C
   (the day before extraction remove from freezer and keep on ice in the fridge overnight)

   ON ICE

9. resuspend the pellets in 25 ml of French press buffer (200 mM TRIS, 100 mM NaCl, 0.1 mM EDTA, pH 8, 5 mM $MgCl_2$)

10. homogenise the solution in a glass homogeniser

11. add DNase I (from bovine pancreas)

12. disrupt the cells by three passages through a French press cell

13. centrifuge at 8,000 rpm for 20 min at 4 °C

14. centrifuge the supernatant at 80,000 rpm for 1 hour at 4 °C

15. discard the supernatant and resuspend the pellets in 15 ml of extraction buffer (0.5 % sodium cholate, 0.5 % sodium deoxycholate, 1.5% octyl-β-D-glucopyranoside (OG), 0.8 % L-α-phosphatidylcholine from soya beans, 50 mM TRIS, 100 mM NaCl, 250 mM sucrose, 40 mM ϵ-aminocaproic acid, 15 mM 4-aminobenzamidine dihydrochloride, 2.5 % glycerol, 30 mM imidazole, pH 7.5, 5 mM $MgCl_2$)

16. homogenise the solution in a glass homogeniser

17. incubate with gentle stirring for 90 min

18. centrifuge the solution at 80,000 rpm for 45 min at 4 °C

IN FRIDGE

19. assemble a gravity-flow chromatography column and fill it with milliQ water
20. add 750 μl of Ni-NTA
21. add another 750 μl of Ni-NTA
22. let the water through, wash with milliQ water
23. add 2 ml of 0.5 M imidazole
24. wash with milliQ water
25. wash with extraction buffer
26. run supernatant through the Ni-NTA column
27. wash with extraction buffer
28. incubate with 100 mM 2-mercaptoethanol (BME) for 5 min
29. wash twice with extraction buffer
30. incubate with 60 μM biotin for 5 min
31. wash with extraction buffer
32. add 2 ml of elution buffer: extraction buffer with 150 mM imidazole (and keep some of the elution buffer for BCA protein concentration assay)
33. discard the first 0.5 ml coming through the column
34. collect the next 1 ml of protein
35. prepare appropriate aliquots of protein and flash-freeze them in liquid nitrogen
36. store in liquid nitrogen

6.2 Expression and purification of TA2 F_1F_o

I used C43 strain transformed with vector pET-3: cysteine-free mutant with added

- CYS after the second amino acid of the α subunit
- CYS after the second amino acid of the c subunit
- 6 HIS after the first amino acid of the β subunit

Protocol

1. prepare 50 ml of LB with ampicillin (200 μg/ml)
2. inoculate the medium with bacteria
3. incubate at 37 °C with shaking (200 rpm) overnight

   NEXT DAY
4. prepare two flasks of LB with ampicillin (200 μg/ml), 1 l each
5. add 10 ml of the culture to each of the two flasks
6. incubate at 37 °C with shaking (120 rpm) until A_{600} reaches 0.35-0.4
7. induce with 1 mM β - D - thiogalactopyranoside (IPTG)
8. incubate at 37 °C with shaking (120 rpm) for **5 hours**
9. centrifuge the solution at 4,000 g for 20 min at 4 °C
10. remove the supernatant and store the pellet at -80 °C
    (the day before extraction remove from freezer and keep on ice in the fridge overnight)

ON ICE

11. resuspend the pellets in 25 ml of buffer A (20 mM sodium phosphate, pH 8, 2 mM $MgCl_2$)
12. homogenise the solution in a glass homogeniser
13. add ϵ-aminocaproic acid (40 mM)
14. add DNase I (from bovine pancreas)
15. disrupt the cells by three passages through a French press cell
16. centrifuge at 8,000 g for 20 min at 4 °C
17. centrifuge the supernatant at 180,000 g for 1 hour at 4 °C
18. discard the supernatant and resuspend the pellets in 50 ml of extraction buffer (20 mM sodium phosphate, pH 8, 2 % dodecyl maltoside (DDM), 500 mM NaCl, 10 % glycerol, 40 mM imidazole, 2 mM $MgCl_2$)
19. homogenise the solution in a glass homogeniser
20. incubate at room temperature with gentle stirring for 1 hour
21. centrifuge the solution at 180,000 g for 1 hour at 4 °C

IN FRIDGE

22. assemble a gravity-flow chromatography column and fill it with milliQ water
23. add 750 μl of Ni-NTA
24. add another 750 μl of Ni-NTA
25. let the water through, wash with milliQ water
26. add 2 ml of 0.5 M imidazole
27. wash with milliQ water

28. wash with IMAC buffer (20 mM sodium phosphate, pH 8, 0.05 % dodecyl maltoside (DDM), 100 mM NaCl, 10 % glycerol, 40 mM imidazole, 2 mM $MgCl_2$)
29. run supernatant through the Ni-NTA column
30. wash with IMAC buffer
31. incubate with 100 mM 2-mercaptoethanol (BME) for 5 min
32. wash twice with IMAC buffer
33. incubate with 60 μM biotin for 5 min
34. wash with IMAC buffer
35. add 2 ml of elution buffer: IMAC buffer with 150 mM imidazole (and keep some of the elution buffer for BCA protein concentration assay)
36. discard the first 0.5 ml coming through the column
37. collect the next 1 ml of protein
38. prepare appropriate aliquots of protein and flash-freeze them in liquid nitrogen
39. store in liquid nitrogen

6.3 Protein concentration assay

Protocol was adapted from the Pierce Rapid Gold BCA Protein Assay Kit. I measured the intensity from two samples of the same protein, and the protein concentration was calculated from an average of the two measurements.

1. in a Falcon tube, mix 10 ml of Reagent A (containing a proprietary copper chelator) and 0.2 ml Reagent B (containing cupric sulfate)

	mixture of reagents	2 mg/ml BSA	protein sample	elution buffer
sample 1	1 ml	0 μl	0 μl	20 μl
sample 2	1 ml	5 μl	0 μl	20 μl
sample 3	1 ml	10 μl	0 μl	20 μl
sample 4	1 ml	15 μl	0 μl	20 μl
sample 5	1 ml	20 μl	0 μl	20 μl
sample 6	1 ml	25 μl	0 μl	20 μl
sample 7	1 ml	0 μl	20 μl	0 μl
sample 8	1 ml	0 μl	20 μl	0 μl

Table 6.1: BCA protein concentration assay

2. prepare 8 samples by mixing the prepared solution with 2 mg/ml bovine serum albumin (BSA) from the kit, the protein sample, and the elution buffer used for extracting the given protein, according to Table 6.1 - the sample needs to be in cuvettes appropriate for measuring the absorption of light

3. place sample 1 into the spectrophotometer and record the zero standard of absorption at nm

4. measure the absorption of samples 2-8 at 480 nm

5. plot absorption values of samples 1-6 against their BSA concentrations, fit the data points with a line

6. average the two absorption values measured for sample 6 and sample 8, and, using the equation of the fitting line, find the corresponding protein concentration

7. estimate the confidence interval by converting the difference in absorptions of sample 7 and sample 8 into a concentration difference using the equation of the fitting line

6.4 Protein gel

We used the SYPRO Ruby gel stain and the corresponding protocol provided by Thermo Fisher Scientific.

1. prepare 40 ml of loading buffer: 1.5 g of Tris, 4 g of SDS, 20 ml of glycerol, 10 mg of bromophenol blue, and milliQ water, adjust pH with HCl to pH 6.8
2. mix 250 μl of BME with 1 ml of loading buffer
3. assemble the mini gel holder and with Mini - PROTEAN TGX Precast Gel, $4-20\%$, use Tris-Glycine-SDS Buffer (Sigma-Aldrich) diluted $10\times$
4. dilute protein sample with milliQ water to a final concentration of 4 μg
5. mix 12 μl of diluted protein sample with 4 μl of loading buffer with BME
6. load samples, 5 μl of fluorescent ladder diluted with 11 μl of milliQ water for tracking the sample progress through gel during the experiment, and two columns of 5 μl of bench-mark protein ladder diluted with 11 μl of milliQ water, one in the middle of the gel, and one on the side, for determining the size of the protein subunits
7. run the gel at 120 V (approximately 1 hour)
8. place the gel in to a clean container with 100 ml of fix solution (50 % of methanol, 7 % of acetic acid, and milliQ water), and agitate on an orbital shaker for 30 minutes, protected from light by an aluminium foil
9. repeat the previous step with fresh fix solution
10. remove the fix solution, pour 60 ml of SYPRO Ruby gel stain, and agitate on an orbital shaker overnight, protected from light by an aluminium foil
11. transfer the gel to a clean container, pour 100 ml of wash solution (10 % of methanol, 7 % of acetic acid, and milliQ water), and place on an orbital shaker for 30 minutes, protected from light by an aluminium foil
12. remove the wash solution, pour 100 ml of milliQ water, and place on an orbital shaker for 5 minutes, protected from light by an aluminium foil
13. repeat the previous step with fresh milliQ water

14. image the gel and analyse the results.

6.5 Phenol red activity assay

- prepare reaction medium (10 mM of ATP, 100 mM of KCl, 4 mM of $MgCl_2$ and 60 μM of phenol red in milliQ water, pH 8)
- measure light absorbance of empty UV-Vis cuvette at 557 nm and record the zero value
- add 1 ml of the reaction medium to the UV-Vis cuvette and check absorbance kinetics - when stable, add 20.4 μg (30 μl of 0.68 mg/ml sample) of protein
- absorbance will decrease if the protein is active, and when it reaches a plateau, add 5 μl of 100 mM HCl
- calculate the rate of hydrolysis by comparing the absorbance decrease with the decreased caused by adding 0.5 μmol of HCl

6.6 Site-directed mutagenesis

I used the QuickChange Lightning Site-directed mutagenesis kit, and the following protocol is based on their Instruction manual, with several adjustments made during the troubleshooting process.

ON ICE, in a thin wall tube, mix

- 5 μl of 10 $\times$ reaction buffer from the kit
- 0.5 μl (109 ng) of DNA template, TA2.A1 F_1F_o in pET-3 vector - concentration verified by Nanodrop and diluted with molecular biology grade water
- 1.1 μl of forward primer (c or α subunit), diluted in molecular biology grade water

- 1.1 μl of reverse complement (c or α subunit), diluted in molecular biology grade water
- 1 μl of dNTP mix from the kit
- 1.5 μl of Quick Solution reagent from the kit
- 39.8 μl of molecular biology grade water

Than add

- 1 μl of QuickChange Lightning Enzyme at room temperature

PCR

1. preheat the lid of the PCR machine to 107 °C
2. place the sample into the PCR machine
3. run the first segment once: 95 °C for 2 minutes
4. run the second segment 18 times:
   95 °C for 20 seconds
   55 °C for 20 seconds
   68 °C for 11.5 minutes
5. run the third segment once: 68 °C for 5 minutes
6. store at 4 °C until ready for the next step
7. add 2 μl of Dpn I restriction enzyme and mix well with the pipette
8. incubate at 37 °C for 2 hours
9. store at -20 °C

Heat-shock transformation

ON ICE

1. thaw 45 μl of chemically competent cells C2984 (or XL-10 Gold cells with 2 μl of BME) in pre-chilled 14 ml round bottom Falcon tube for 15 minutes - cells are extremely temperature-sensitive and cannot be lifted from the ice before step 7 of this protocol
2. add 10 μl of PCR product and mix with a pipette
3. incubate on ice for 30 minutes
4. heat-pulse the tube at 42 °C for 1 minute
5. incubate on ice for 2 minutes
6. add 500 μl of Super Optimal broth (S.O.C. medium) cooled at 4 °C
7. incubate at 37 °C for 1 hour with shaking at 250 rpm
8. centrifuge for 5 minutes at 5000 rpm
9. resuspend the pellet in 100 μl of supernatant
10. spread the sample on LB-ampicillin agar plate (ampicillin concentration 100 μg/ml) using glass beads
11. incubate at 37 °C for at least 16 hours
12. visually inspect for bacterial colonies
    (positive control plate is helpful to check whether there is a problem in any stage of the protocol)

6.7 Preparation of calcium competent cells

THE DAY BEFORE:

- inoculate 5 ml of LB with competent cells (we used DH5$_\alpha$ cells - courtesy of Dr El Sayyed and C43 cells - courtesy of Dr Ishmukhametov)
- place the sample in a shaking incubator at 37 °C and 250 rpm overnight

Protocol

1. add 1 ml of overnight culture to 99 ml of freshly prepared LB
2. incubate at 37 °C with shaking at 250 rpm until the OD of the sample reaches 0.4

   ON ICE:

3. separate the sample into multiple Falcon tubes suitable for centrifuging
4. incubate on ice for 20 minutes
5. centrifuge at 1 °C and 4,000 rpm for 10 minutes
6. discard the supernatant
7. resuspend the pellet in 100 ml of filtered 0.1 M solution of $CaCl_2$
8. incubate on ice for 30 minutes
9. centrifuge at 1 °C and 4,000 rpm for 10 minutes
10. discard the supernatant
11. resuspend the pellet in 50 ml of filtered 0.1 M solution of $CaCl_2$
12. incubate on ice for 30 minutes

13. centrifuge at 1 °C and 4,000 rpm for 10 minutes
14. discard the supernatant
15. resuspend the pellet in 1 ml of filtered 0.1 M solution of $CaCl_2$ with 15 %(v/v) of glycerol
16. prepare 50 μl aliquots and freeze them in liquid nitrogen
17. store at -80 °C

Plasmid DNA purification

Overnight culture

NEAR FIRE

1. add 5 ml of autoclaved LB medium with 100 μg/ml of ampicillin into a round-bottom Falcon tube
2. scratch a bacterial colony from the agar plate with a toothpick and immerse the toothpick in the medium (inoculation)
3. incubate at 37 °C with shaking at 250 rpm overnight

Thermo Scientific GeneJET Plasmid Miniprep Kit

1. harvest bacteria by centrifugation at room temperature at 8,000 rpm for 2 minutes
2. decant the supernatant
3. resuspend the pellet in 250 μl of resuspension solution from the kit by pipetting until no cell clumps remain, and transfer the solution into an Eppendorf tube
4. add 250 μl of lysis solution from the kit and mix by inverting the tube 4-6 times

5. add 350 μl of neutralisation solution and mix by inverting the tube 4-6 times - the solution will become cloudy
6. centrifuge at room temperature at 13,000 rpm for 5 minutes
7. transfer the supernatant to the GeneJET spin column from the kit - do not disturb the white precipitant
8. apply vacuum to draw the sample through the column
9. add 500 μl of the wash solution from the kit and draw through
10. add another 500 μl of the wash solution from the kit and draw through
11. transfer the column to the collection tube and centrifuge at room temperature at 13,000 rpm for 1 minute to remove the residual solution
12. transfer the column to a fresh Eppendorf tube
13. add 50 μl of elution buffer from the kit - do not touch the membrane
14. incubate for 2 minutes at room temperature
15. centrifuge at room temperature at 13,000 rpm for 2 minutes
16. measure the concentration and purity by nanodrop
17. store at -20 °C

6.8 Preparation of agarose-streptavidin

1. dissolve 1 mg of low melting temperature agarose in 1.5 ml anhydrous DMSO while stirring continuously to avoid clustering of agarose
2. heat the mixture with constant stirring using a water bath at 70 °C
3. prepare 1 mg/ml CDI solution in anhydrous DMSO

4. add 0.5 ml of the CDI solution to the agarose solution
5. add drop-wise 0.5 ml of 1 mg/ml CDI in anhydrous DMSO with constant stirring
6. allow the solution to activate for 1 hour
7. dissolve 1 mg of streptavidin in 1 ml of 0.2 M Sodium Carbonate buffer, pH 10.3 (this ratio gives roughly 2.5 streptavidin molecules per average agarose molecule)
8. mix the streptavidin solution with the activated agarose solution dropwise and allow to react for 24 hours with constant mixing (it will eventually become jellified)
9. dialyse the agarose gel using Slide-A-Lyzer MINI Dialysis Device, 0.5 ml, 3.5 kDa molecular weight cut-off membrane in 50 ml of milliQ water for 24 hours with 3 changes of milliQ water - after 2, 3 and 18 hours
10. dry the agarose in a vacuum dryer and store the powder at room temperature

6.9 Agarose-streptavidin control experiment

Experiment with fluorescent dye

1. prepare fusion (low salt) buffer: 10 mM KCl, 1 mM $MgCl_2$ and 1 mM MOPS in milliQ water at pH 7.35, adjusted with 0.6 mM NaOH
2. prepare 1 : 10^6 dilution of fluorescein-biotin dye aliquot (450 ng/ml in DMSO) in milliQ water
3. mix low melting temperature agarose powder with agarose-streptavidin powder prepared according to Protocol 6.8 in a ratio 500 : 1 by weight
4. dissolve 10 mg of agarose mixture in 1 ml of fusion buffer

5. for negative control, dissolve 10 mg of low melting temperature agarose powder in 1 ml of fusion buffer
6. melt both samples in a shaking incubator at 70 °C and 800 rpm for 20 minutes

Sample preparation for both experiments

7. wipe a glass slide with a tissue soaked in ethanol, sonicate a cover slip in ethanol for 6 minutes
8. spread a thin layer of gel on the glass slide and let it dry
9. make a channel using double-sided tape and the cover slip
10. fill the channel with 100 μl of fusion buffer
11. observe the fluorescence of the gel under the microscope
12. flush the channel with 100 μl of fluorescein-biotin solution
13. observe the fluorescence of the gel under the microscope
14. flush the channel with 100 μl of fusion buffer
15. observe the fluorescence of the gel under the microscope
16. flush the channel with another 500 μl of fusion buffer
17. observe the fluorescence of the gel under the microscope

Experiment with fluorescent beads

18. prepare $1 : 10^4$ dilution of 200 nm yellow-green fluorobeads in fusion buffer

19. prepare channels in the same way in the same way than in the experiment with fluorescent dye
20. fill the channel with 100 μl of fusion buffer
21. flush the channel with 30 μl of beads solution
22. wait for 5 minutes
23. flush the channel with 100 μl of fusion buffer
24. flush the channel with another 500 μl of fusion buffer
25. observe the fluorescence of the gel under the microscope

6.10 Cleaning of glass vials

Glass vials can be washed in bulk and stored in a closed container for several months.

Protocol

1. Flush the vials three times with a 2 % milliQ water solution of Hellmanex
2. Sonicate with 2 % milliQ water solution of Hellmanex for 6 minutes
3. Flush three times with milliQ water
4. Sonicate with milliQ water for 6 minutes
5. Flush three times with ethanol
6. Sonicate with ethanol for 6 minutes
7. Flush three times with milliQ water
8. Sonicate with milliQ water for 6 minutes
9. Flush with milliQ water
10. Dry in nitrogen flow, close and seal with parafilm

6.11 Cleaning of cover slips

Cover slips can be washed in bulk and stored fully submerged in milliQ water for several months.

Protocol

1. Sonicate the cover slips with 2 % milliQ water solution of Hellmanex for 5 minutes
2. Flush five times with milliQ water
3. Sonicate with milliQ water for 5 minutes
4. Flush five times with milliQ water
5. Sonicate with ethanol for 5 minutes
6. Flush five times with milliQ water
7. Store submerged in milliQ water, seal the container with parafilm

6.12 Preparation of lipid mixture

1. transfer 1.25 mM of $POPA^-$ chloroform solution and 3.75 mM of DPhPC chloroform solution into a glass vial cleaned according to protocol 6.10.
2. slowly evaporate the chloroform in a fume hood under nitrogen flow, leaving a thin, even lipid film on the walls of the vial
3. place the glass vial with the lipid film under the vacuum for 2 hours, or overnight, to remove residual chloroform
4. add 0.25 ml of filtered hexadecane and 0.25 ml of filtered silicone oil
5. place the sample in a shaking incubator at 37 °C and 700 rpm for 1.5 hours

6. store at room temperature

6.13 Spin-coating

1. dry cover slips cleaned in advance following the protocol 6.11 in nitrogen flow
2. prepare 1 % of low melting temperature agarose milliQ water solution (or agarose and agarose-streptavidin in weight ratio 1:5000)
3. melt the agarose in a shaking incubator at 70 °C and 800 rpm for 15 minutes
4. activate the surface of the cover slips in plasma cleaner for 7 minutes at 95 W with 0.5 bar oxygen stream
5. within a few minutes after the plasma treatment, place each cover slip into a spin coater, place 140 μl of melted agarose solution on the top, and spin-coat at 3,000 rpm
6. label the corner of the clean side of the cover slip with a small piece of tape (the sides would otherwise be indistinguishable)
7. store in a clean glass container sealed with parafilm for several months

6.14 Assembling the chip

1. place a cover slip spin-coated with agarose following protocol 6.13 on the bottom of the chip, with the labelled (not coated) side facing outwards
2. secure the cover slip with a thin strip of tape around the circuit of the cover slip
3. prepare 2 % solution of low melting temperature agarose in the buffer of choice (same as the buffer used for the droplet)

4. melt the agarose in a shaking incubator at 70 °C and 800 rpm for 15 minutes

5. cut off a tip of a pipette tip 3 mm from the opening to make the opening larger, so the agarose can flow through more easily

6. using the pipette tip with the enlarged opening, inject approximately 100 μl of the melted agarose slowly into the chip through the single opening until it overflows through the two openings on the other side of the chip, while pressing the chip firmly against the cover slip

7. after a minute, the gelification of the agarose is completed and firm holding of the chips is no longer needed - turn the chip around and check that the wells of the chip were not flooded with the agarose, which is noticeable on the image of the light reflected from the cover slip

8. leave the chip for 15 minutes to ensure proper hydration of the agarose layer

9. fill the wells of the chip with lipid mixture prepared according to protocol 6.12, leave for 30 minutes to allow monolayer formation, before the droplet transfer

6.15 Preparing the droplets

1. fill the separated incubation compartment of the chip used for droplet preparation with the oil and lipid mixture prepared according to protocol 6.12

2. using a 2.5 μl syringe, inject eight 200 nl droplets of buffer of choice into the oil and lipid mixture - keep the droplets away from each other, so they don't fuse

3. leave the droplets for 30 minutes to allow forming of lipid monolayer on the surface of the droplets

4. transfer the droplets with a small amount of surrounding oil and lipid mixture into individual wells of the chip using a pipette, avoid contact with air

5. the droplets will sink to the bottom of the well, thus creating lipid bilayer below the droplet - transfer the chip to the microscope and start your experiment

6.16 Preparation of liposomes with two fluorescent labels

1. transfer 5 mg of 1,2-dioleoyl-sn-glycero-3-ethylphosphocholine (E-PC) in chloroform solution and 5 mg of 1,2-dioleoyl-sn-glycero-3-phosphocholine (DOPC) in chloroform solution into a glass vial cleaned according to the protocol 6.10

2. slowly evaporate the chloroform in a fume hood under nitrogen flow, leaving a thin, even lipid film on the walls of the vial

3. place the glass vial with the lipid film under the vacuum overnight, to remove residual chloroform

4. prepare fusion buffer (50 mM Tricine-NaOH solution in milliQ water, pH 8.11) and add 1 mM of pyranine

5. add 1 ml of buffer with dye into the glass vial with lipid film and leave for 30 minutes

6. vortex for 1 minute

7. extrude the liposomes through a 200 nm filter 21 times

8. run the liposomes through Sephadex G50 gravity-flow chromatography column equilibrated with fusion buffer to remove excess dye

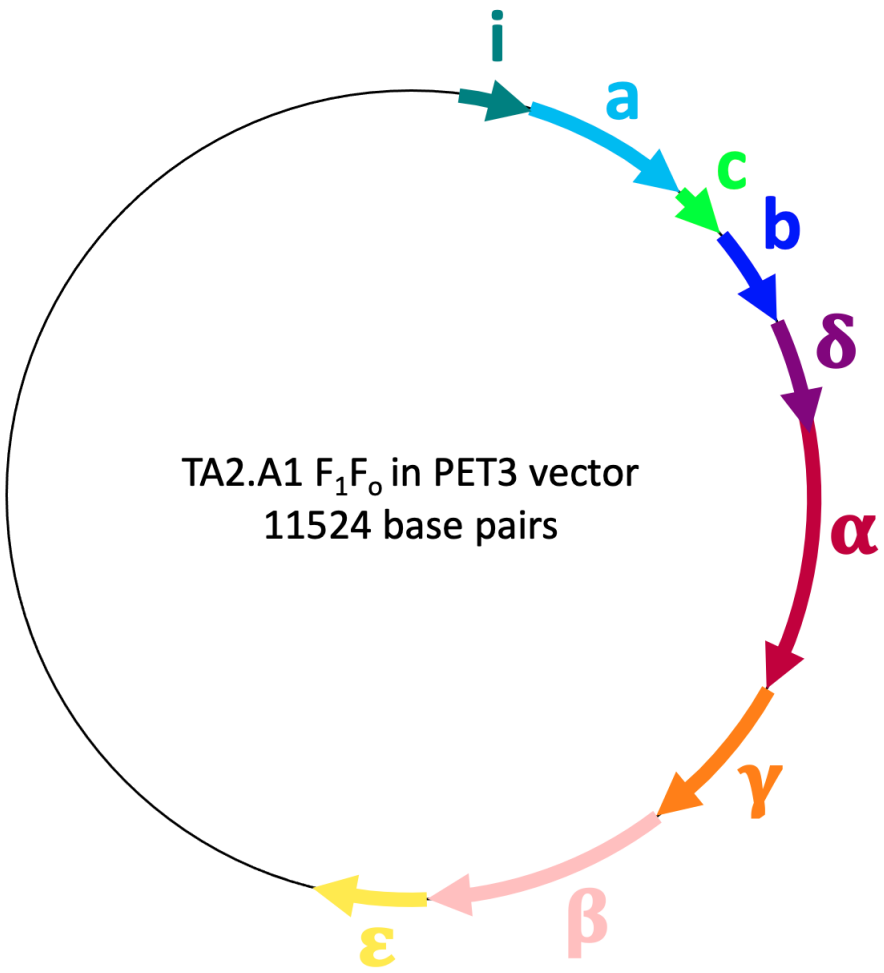
9. mix 150 μl of liposomes with 112 μl (approximately 100 μg) of mCherry-proteorhodopsin, 16.5 μl of 20 % cholate and 51.5 μl of the fusion buffer

10. place on roller shaker at 4 °C for 15 minutes

11. run the liposomes through Sephadex G50 gravity-flow chromatography column equilibrated with fusion buffer to remove excess dye and detergent

Appendix A

TA2.A1 F_1F_o operon



A.1 DNA sequence of the TA2.A1 F_1F_o operon inserted into PET3a

taatacgactcactatagggagaccacaacggtttccctctagaaataattttgtttaactttaagaaggagatatacat ATGCTGGAAGATTT
GACAGGACGTATCACGCGTTTAACCCGCTTTTTCTTTTTTACCCTGGCCGTCATAGTCCTGG
GCTGGGGATTTGGCGGCGCCCCTCCTTTCTTGGCTGGAATGGCATTGGGACTCGCCATCGGT
TATATCGGTGTCGTGCACCTGGCCAAGCGTGTCCATCGTTTTGTTCAAGCTGTGGCACAAGG
TGACAGACTGCCCAGTTTGGGGACCTTTACCCGGCTGGCATTGGTTGCGCTTGCTACCGTGA
CGGTTATGACCTACCCCCAGCATTTCGAATACACCGGCCTGGTGTTGGGCCTGGTTCTGCCG
ACAGTATTCGCCATAGGCGATGCTATATATACTCAACTGAAACAAGGGAAGTAG GGGAAA
GGGGTGAATACTGGTTGAAATATAAAGATCCGACATTTACCTTTTTAGGCCTGGAGTTTAGT
ATGACGGTTGTCCTCATGGTGACCATCACTGCCGCGTTAACCTTTGCCATTGCTTATGCAGG
TGCCCGGCAGGCCCAGACAGGCAAACCGTCAGGCATGCAAAACTTTATGGAATGGATGGT
GGAATTTATCCGCGGTCTTATGGCCAGCACCATGCATGTTCACCAGCGTAACAACCAGTTG
GTGATGCTGGCTTTGGCGTTTATCATGTTTATTTTCATTGGTAACTTCCTCAGCATACCGTTC
AAGATCACCACAACCAATGATTACATTCTATGGAAAGCGCCAACTTCCGACGCGCATGTCA
CTTTGACACTGGCGACCGCGGTCATTGTTCTGTCCAATATATTGGGCATCCGCATGCTAGGA
TTTAAAGATTACTTCCTCCATTATTTTAAGCCACAGGGTTGGCAATTTCCGTTACATATAAT
TGAGGAGTTCGCCAAGACATTGACCCTGGGCTTGCGACTGTTTGGTAATATTTTTGCCAAAG
AAACATTGGCCGGGATGCTGGCCGGAGCAGGAGTGGCCAGTGCGGTCGCCGTCGTTATCTT
TGCTTTGCCAATGATTGTGTGGCAAGCTTTCGGTATCTTTATGGGTGGGATTCAGGCCTTCG
TTTTTACCATCTTAATGCTAGTGTATATTGCACAGAAAGTGGAGCCTGATCATTAA ACGGAT
GCCGTGTGGCCAGAGTGCACAGTTTATCTTTTTCTGTCTGTCTTTCCAAATATGGGAGTGTG
TACAGTTGTGTGACCTCATCTCAACTTTTCTTGAGGTTGACTATATATTTGCTTGCATCAAGT
TGTCGATTATGTGAAAGGAGGAATTATA ATGGGA**TGC**GTCTTAGCTGCAGCCATTGCTGTGGGT
TTAGCCGCTCTCGGCGCCAGCTTTGGTGTATCTAACATTGTAAGCCGCACAATAGAAGGGA
TTGCACGCCAGCCAGAATCACGCGGCGTGCTGCAAACCACCATGTTCATTGGTATCGGTCT
GGTTGAGGCTATACCGATTATGGCGGTTGTGATTGCCTTTATTGCCTTAGGACAATAA AGCA
ACAGCACAGGCAAGTTGGGCGGGGCCGGCCAACGGCCTTCGCCTTTCCTTTGCAATGTGAA
CCTAAGGCTTACGCCCGCACTCCAACTTGGCGCAAGCCAAGTTTTCTTTTTAGGGTAAAAG
GT ATGGTAATAGATGTGAAGGGAGTGAACAAGATGTTGGAGTTGGGTTCCGTCCGCTGGGG
CGATATGCTGTTTTCTTTGCTCATGTTCATCATTCTTTTTCTTTTGCTCCGCAAATACGCTTTT
GGCCCGTTGATGAATGTTATGGAAAAACGGGCCAATCAAATTGAAAAAGATTTGGAAGAG
GCCAAGCGCAACCGGGCCGAAGCGGAAAAGTTGCTGGCCGAACAACGCGCCAACCTGGAG
CAAGCGAAAAAAGATGCCAAAACCATATTGGAAAATGCACGTAACACCAGCGAGAAACAG

GCTGAGGAGATCATCCGTGCAGCCAAAGCTGAAGTGGATCAGTATAAAAGTGTGGCCCGC
AAGGAAATTGAGCGTGAGAAAGAAAAAGCGGTTGAGGCTTTGCGAAAGGAAATGGGACA
GCTTTCGGTTCTTTTAGCCAGTAAAGTGATTGAAAAGGAACTGGATCCAAAGCAACAGCAG
CAATTGATTGATGATTTCCTGAAAGAGGTAGGGACCAAAAA ATGGGTGCAGTAG CCAAAC
GGTATGCCAAAGCTTTGTTTGAAGTGGCCAAAGAGCGGGAGGAACTGGATAAAATTGAGC
AAGATTTGCAATATACAGATCAGGTGCTCCGGGAACATCCAGACCTGGTCAGGTTCCTCAC
CCATCCATTGGTGAAAAAGGAAACCAAGAAAGAGCTTATCGGCACGGTGTTTGCGGAGCA
GCTGTCCCCAACCACCCTCTCCCTGTTGCGGTTGTTGGTGGACCGTGAACGTGAAAATGAA
CTGAGCGGGATTGCCACCTATTTTGTCAGACTGGCCAATGAAGTGCGAGGTCTGGTTGATG
TGGTGGTGACTACAGCTACCCCGCTGTTACCGGAAAAGCAGGAGGTCTTGCGCCAACAATT
AGCCCGCATGACAGGCAAAAAAGTCCGTTTGCATTTTGTTGTGGACGAGGGTGTGCTGGGC
GGTATCACCGTCAAAATCGGGGATCTAATCTACGATGGAACTGTCCGCGGCAAACTCTCCC
GCTTTGAACGTTTAATCGCAACAACCAAAAGCTAG AGGATTGGGGTGAACGAG ATGAGC**TG**
CATCAGACCTGAAGAAATCAGTGCGCTAATCAAAAAGCAGATTGAGAACTATGAAGCAGATC
TTGAAGTGGTGGAAGTGGGCACCGTTATCCAGGTTGGTGACGGCATTGCCCGCGTGCATGG
CCTGGAAAAGGTTATGGCCGGGGAACTTTTAGAATTTGAGAACGGGGTCATGGGGATGGCC
CAAAACTTGGAAGAAGACAACGTGGGTGTCGTCATTCTCGGGCCTTACACGGAAATCCGGG
AAGGCACGCAAGTGAAGCGTACAGGACGCATTATGGAGGTGCCTGTAGGCGAAGCCTTGC
TTGGCCGCGTAGTCAATCCCCTTGGTCAGCCCCTTGACGGACGTGGCCCGATTGAAACGGC
CGAGTACCGTCCCATTGAATCACCTGCACCCGGCGTCATGGATCGTAAATCAGTCCATGAG
CCGCTCCAAACCGGGATTAAAGCCATTGACTCCATGATTCCGATTGGGCGCGGTCAGCGTG
AGCTGATCATCGGTGACCGCCAGACCGGTAAAACCACCATTGCCATTGACACCATCATTAA
TCAAAAGGGACAAGACGTCATTGCCATTTACGTTGCCATCGGCCAGAAGCAATCCACAGTC
GCCGGTGTCGTGGAAACACTGCGCCAGCACGACGCACTGGATTACACTATTGTGGTGACAG
CTTCTGCTTCTGAACCCGCACCGCTGCTTTATCTGGCGCCTTATGCGGGTGCCGCCATGGGC
GAATACTTTATGTATAAAGGCAAGCATGCCCTTGTGGTTTACGATGACTTGTCCAAGCAGG
CGGCAGCATACCGTGAGCTGTCCTTGCTGTTAAGACGTCCGCCTGGACGGGAAGCTTACCC
TGGCGATGTATTCTATTTACACTCCCGCCTTTTAGAGCGTGCGGCTAAACTGAGCGATGAAA
AAGGCGGCGGTTCTTTGACAGCCCTGCCCTTTATCGAAACCCAGGCCGGCGACGTCTCTGC
CTACATTCCAACCAACGTGATCTCTATTACGGACGGGCAAATCTTCCTGGAGTCCGATCTGT
TCTACTCCGGTGTGCGTCCGGCTGTTAACGTCGGTATCTCTGTTTCCCGTGTAGGAGGTGCC
GCCCAAATTAAAGCGATGAAAAAAGTGGCCGGTACCTTGCGTTTGGACCTGGCCCAGTACC
GTGAACTGCAGGCTTTTGCCCAGTTTGGCTCAGACCTGGACAAAGCCACCCAGGCCAAATT
AAACCGTGGTGAGCGCACCGTCGAAATCCTTAAGCAAGATGAACACAAACCGATGCCGGT
TGAAGAACAAGTGATCAGCATCTATGCGGTTACCAACGGATTTATGGATGACATTCCGGTG

GAGGATGTACGCCGTTTTGAAGAAGAACTGTTAAGCTTTATGCGGGCGAATAAAGATTCCT
TGCTCGACCATATCCGCCAGACAGGCGAACTGCCGGACACCAAAGAACTGGATGCAGCTA
TTGAGGAATTTAAGAAAGGCTTTACCCCGTCTGCCTAA GCCCCTTGTTAATCAGAGGAAAA
AGGTGGTGAATGCGTC ATGCAAGGAATGAGAGAGATTAAACGGCGTATCCGCTCGGTAAA
AAATACACGCCAAATCACCAAAGCGATGAAGATGGTGGCTGCAGCCAAACTGCGCCGTGC
GCAGGAAACGGCTGAGAATGCCCGTCCCTACGCGGATAAAATTAAAGAAGTGATCTCCAG
CATTGCTGCAGGCACCAAAGATTTTAGCCATCCCATGCTGGAAGCCCGTCCGGTGAAGAAG
ACGGGCTACATGGTGATCACCTCAGACCGGGGATTGGCTGGACCGTATAACGCCAATATTT
TACGCCTGGTGTCCAAAACGATCGAGGAGCGCCATCAGTCCAAAGACGAGTATGTGATCTT
TGCCGTTGGACGCAAAGGGCGGGATTTCTTTAAGAAGCGGGGCTATCCGGTTGTGGAAGAG
GTGACGGGCATTTCGGACACCCCGTCTTTGACAGAGATTCAGGACATAGCCCAGAGCGCCA
TTGGCATGTTCGCCGATGAAACATTTGACAAGCTGACCATCTTTTATAATGAATTTGTCAGC
CCGATCGTGCAGCGCCCCGTGGAGAAGCAACTGCTTCCCCTGACCTCTGAAGAGGTGCTCG
ATGGGCCGGTCAGCGCCTATGAATACGAACCGGACAGTGAATCGGTCTTGGAAGTGTTGCT
GCCCAAGTATGCTGAAACGCTGATTTACAGCGCCCTTTTAGATGCCAAAGCAAGTGAGTTT
GGCGCACGGATGACCGCGATGGGCAATGCAACCGACAACGCCACGGAAATGCTTGAAACC
TTGACCCTGCAATTTAACCGTGCCCGCCAGGCTGCCATTACGCAAGAGATCGCCGAAATTG
TCGCAGGAGCCAATGCTTTAAGATAG GTAAAGCGAGGAGGGAAAACGC ATG**CACCACCAC**
CACCACCACAATAAAGGACGTATCATCCAAGTTATGGGTCCTGTTGTTGACATCCAATTTG
AAAGTGGACAACTGCCCGATATTTACAATGCGATTACCATCGAGCGGCCGCAAGGTGGCAC
TTTAACCGTTGAAGCTGCCGTCCATCTTGGAGATAACGTTGTCCGTGCCGTGGCCATGGCTT
CCACGGATGGACTGGTTCGCGGATTGGAAGCGGTAGATACCGGTGCCCCCATTTCTGTGCC
GGTCGGCAAAGCCACCTTGGGGCGTGTGTTTAACGTGTTGGGTGAACCGATTGATGAGCAA
GGAGAGGTCAATGCAGAGGAGAGACACCCGATCCACCGTCCTGCTCCAGAATTTGAAGAG
CTCTCCACGGCCGATGAAATTTTGGAAACAGGGATTAAAGTGATTGACCTTTTGGCTCCAT
ATGCCAAAGGGGGTAAGATCGGCCTGTTCGGCGGTGCCGGTGTCGGCAAAACGGTTTTGAT
CCAAGAGCTGATCAATAACGTGGCCCAAGAACACGGCGGCTTGTCCGTATTCGCCGGTGTC
GGTGAGCGTACCCGTGAGGGTAACGACCTGTATCACGAGATGAAAGACAGCGGCGTTATCT
CCAAAACATCCATGGTGTTCGGCCAGATGAACGAGCCGCCGGGAGCCCGTCTGCGCGTGGC
TTTGACCGGCTTGACCATGGCTGAGTATTTCCGTGACAGAGAAGGCCAGGATGTTTTGCTCT
TTATTGATAACATTTTCCGCTTTACCCAGGCCGGTTCAGAGGTATCTGCCTTGCTGGGACGC
ATGCCCTCTGCGGTAGGTTACCAGCCCACGCTGGCCACTGAGATGGGTCAATTGCAAGAGC
GGATCACATCCACCAAGAAAGGGTCCATCACTTCCATCCAGGCCATCTATGTTCCGGCTGA
CGACTATACAGACCCTGCTCCGGCCACCACGTTTGCGCACCTGGACGCTACAACCAACCTG
GAGCGTAAACTGGCCGAGATGGGGATCTATCCTGCTGTGGATCCGCTGGCTTCCACATCCC

GGATTCTCTCTCCTGCCGTCGTAGGCGAGGAACATTACCGGGTAGCTCGCGGTGTACAGCA
AGTGTTGCAGCGCTATAACGATTTGCAAGACATTATTGCCATCTTAGGTATGGATGAATTA
AGCGACGAGGACAAGCTGATCGTCGCCCGTGCCCGCAAAATCCAGCGTTTCCTCTCTCAAC
CGTTCCACGTGGCCGAACAGTTTACCGGTATGCCCGGTAAATATGTACCGGTAAAAGAAAC
GGTCCGCGGCTTTAAAGAGATCCTGGAAGGTAAACATGACAATTTGCCTGAAGAGGCCTTC
TACATGGTGGGTACCATTGACGAAGCGGTTGAGAAAGCAAAGAAACTGTAA TTCCCTGAG
ATAGGGGAGGATAAACA ATGGCAACTGTTCAAGTTGATATCGTCACACCTGAACGGAAAG
TGTTTCAAGGAGAGGCGGATATCGTCATTGCCCGCGGTGTGGAGGGTGAACTGGGGGTTAT
GGCTGGCCATATCCCCCTTGTGACTCCGCTCAAAACGGCACCTGTCCGCATTAAGCAAGGG
GATAAAGAAACGCTGATTGCCGTAAGCGGCGGGTTTTTGGAAGTGCGTCCCGATAAGGTTA
ACATCTTGGCCGATACAGCCGAATTGCCGGAAGAAATCGATGTCGAGCGCGCCAAAAAGG
CAAAGGCGCGCCATGAAACCATTTTGAAGCGTTTGGACAAGACAGATAAAGATTACCTGCG
GCACAAGCGTGCCCTGGAACGGGCCGAAGTTCGCCTGCAGGTGGCAAACAGCAAATCATA
A gctgagcaataactagcataacccctttggggcctctaaacgggtcttgaggggttttttgctgaaaggaggaactatatccggatatccacaggacgg
gtgtggtcgccatgatcgcgtagtcgatagtggctccaagtagcgaagcgagcaggactgggcggcggccaaagcggtcggacagtgctccgaga
acgggtgcgcatagaaattgcatcaacgcatatagcgctagcagcacgccatagtgactggcgatgctgtcggaatggacgatatcccgcaagaggc
ccggcagtaccggcataaccaagcctatgcctacagcatccagggtgacggtgccgaggatgacgatgagcgcattgttagatttcatacacggtgcc
tgactgcgttagcaatttaactgtgataaactaccgcattaaagcttatcgatgataagctgtcaaacatgagaattcttgaagacgaaagggcctcgtgat
acgcctatttttataggttaatgtcatgataataatggtttcttagacgtcaggtggcacttttcggggaaatgtgcgcggaacccctatttgtttatttttctaaa
tacattcaaatatgtatccgctcatgagacaataaccctgataaatgcttcaataatattgaaaaaggaagagt atgagtattcaacatttccgtgtcgcccttt
attccctttttgcggcattttgccttcctgtttttgctcacccagaaacgctggtgaaagtaaaagatgctgaagatcagttgggtgcacgagtgggttacat
cgaactggatctcaacagcggtaagatccttgagagttttcgccccgaagaacgttttccaatgatgagcacttttaaagttctgctatgtggcgcggtatt
atcccgtgttgacgccgggcaagagcaactcggtcgccgcatacactattctcagaatgacttggttgagtactcaccagtcacagaaaagcatcttac
ggatggcatgacagtaagagaattatgcagtgctgccataaccatgagtgataacactgcggccaacttacttctgacaacgatcggaggaccgaagg
agctaaccgcttttttgcacaacatgggggatcatgtaactcgccttgatcgttgggaaccggagctgaatgaagccataccaaacgacgagcgtgaca
ccacgatgcctgcagcaatggcaacaacgttgcgcaaactattaactggcgaactacttactctagcttcccggcaacaattaatagactggatggagg
cggataaagttgcaggaccacttctgcgctcggcccttccggctggctggtttattgctgataaatctggagccggtgagcgtgggtctcgcggtatcatt
gcagcactggggccagatggtaagccctcccgtatcgtagttatctacacgacggggagtcaggcaactatggatgaacgaaatagacagatcgctg
agataggtgcctcactgattaagcattggtaa ctgtcagaccaagtttactcatatatactttagattgatttaaaacttcatttttaatttaaaaggatctaggt
gaagatccttttttgataatctcatgaccaaaatcccttaacgtgagttttcgttccactgagcgtcagaccccgtagaaaagatcaaaggatcttcttgagat
ccttttttctgcgcgtaatctgctgcttgcaaacaaaaaaaccaccgctaccagcggtggtttgtttgccggatcaagagctaccaactctttttccgaagg
taactggcttcagcagagcgcagataccaaatactgtccttctagtgtagccgtagttaggccaccacttcaagaactctgtagcaccgcctacatacctc
gctctgctaatcctgttaccagtggctgctgccagtggcgataagtcgtgtcttaccgggttggactcaagacgatagttaccggataaggcgcagcggt
cgggctgaacgggggttcgtgcacacagcccagcttggagcgaacgacctacaccgaactgagatacctacagcgtgagctatgagaaagcgcc
acgcttcccgaagggagaaaggcggacaggtatccggtaagcggcagggtcggaacaggagagcgcacgagggagcttccagggggaaacgc

ctggtatctttatagtcctgtcgggtttcgccacctctgacttgagcgtcgatttttgtgatgctcgtcaggggggcggagcctatggaaaaacgccagca
acgcggccttttacggttcctggccttttgctggccttttgctcacatgttctttcctgcgttatcccctgattctgtggataaccgtattaccgcctttgagtga
gctgataccgctcgccgcagccgaacgaccgagcgcagcgagtcagtgagcgaggaagcggaagagcgcctgatgcggtattttctccttacgcat
ctgtgcggtatttcacaccgcatatatggtgcactctcagtacaatctgctctgatgccgcatagttaagccagtatacactccgctatcgctacgtgactg
ggtcatggctgcgccccgacacccgccaacacccgctgacgcgccctgacgggcttgtctgctcccggcatccgcttacagacaagctgtgaccgtc
tccgggagctgcatgtgtcagaggttttcaccgtcatcaccgaaacgcgcgaggcagctgcggtaaagctcatcagcgtggtcgtgaagcgattcaca
gatgtctgcctgttcatccgcgtccagctcgttgagtttctccagaagcgttaatgtctggcttctgataaagcgggccatgttaagggcggttttttcctgtt
tggtcactgatgcctccgtgtaagggggatttctgttcatgggggtaatgataccgatgaaacgagagaggatgctcacgatacgggttactgatgatga
acatgcccggttactggaacgttgtgagggtaaacaactggcggtatggatgcggcgggaccagagaaaaatcactcagggtcaatgccagcgcttc
gttaatacagatgtaggtgttccacagggtagccagcagcatcctgcgatgcagatccggaacataatggtgcagggcgctgacttccgcgtttccaga
ctttacgaaacacggaaaccgaagaccattcatgttgttgctcaggtcgcagacgttttgcagcagcagtcgcttcacgttcgctcgcgtatcggtgattc
attctgctaaccagtaaggcaaccccgccagcctagccgggtcctcaacgacaggagcacgatcatgcgcacccgtggccaggacccaacgctgcc
cgagatgcgccgcgtgcggctgctggagatggcggacgcgatggatatgttctgccaagggttggtttgcgcattcacagttctccgcaagaattgatt
ggctccaattcttggagtggtgaatccgttagcgaggtgccgccggcttccattcaggtcgaggtggcccggctccatgcaccgcgacgcaacgcgg
ggaggcagacaaggtatagggcggcgcctacaatccatgccaacccgttccatgtgctcgccgaggcggcataaatcgccgtgacgatcagcggtc
cagtgatcgaagttaggctggtaagagccgcgagcgatccttgaagctgtccctgatggtcgtcatctacctgcctggacagcatggcctgcaacgcg
ggcatcccgatgccgccggaagcgagaagaatcataatggggaaggccatccagcctcgcgtcgcgaacgccagcaagacgtagcccagcgcgt
cggccgccatgccggcgataatggcctgcttctcgccgaaacgtttggtggcgggaccagtgacgaaggcttgagcgagggcgtgcaagattccga
ataccgcaagcgacaggccgatcatcgtcgcgctccagcgaaagcggtcctcgccgaaaatgacccagagcgctgccggcacctgtcctacgagtt
gcatgataaagaagacagtcataagtgcggcgacgatagtcatgccccgcgcccaccggaaggagctgactgggttgaaggctctcaagggcatcg
gtcgacgctctcccttatgcgactcctgcattaggaagcagcccagtagtaggttgaggccgttgagcaccgccgccgcaaggaatggtgcatgcaa
ggagatggcgcccaacagtcccccggccacggggcctgccaccatacccacgccgaaacaagcgctcatgagcccgaagtggcgagcccgatct
tccccatcggtgatgtcggcgatataggcgccagcaaccgcacctgtggcgccggtgatgccggccacgatgcgtccggcgtagaggatcgagatc
tcgatcccgcgaaat

NOTE

The regions encoding the individual subunits are highlighted in colour, consistently with the scheme above. The overlapping region of the δ and the α subunit is emphasized by a purple frame. The grey region is encoding beta-lactamase. TGT codon encoding the cysteine added after the second amino acid of the α subunit and after the second amino acid of the c subunit, and six CAC codons encoding six histidine residues after the fourth amino acid of the β subunit, are underlined in the sequence.

Bibliography

[Abrahams et al., 1994] Abrahams, J. P., Leslie, A. G., Lutter, R., and Walker, J. E. (1994). Structure at 2.8 Angstrom resolution of F_1-ATPase from bovine heart mitochondria. *Nature*, 370:621–628.

[Bayley et al., 2008] Bayley, H., Cronin, B., Heron, A., Holden, M. A., Hwang, W., Syeda, R., Thompson, J., and Wallace, M. (2008). Droplet interface bilayers. *Molecular BioSystems*, page 1191â€“1208.

[Borch and Hamann, 2009] Borch, J. and Hamann, T. (2009). The nanodisc: a novel tool for membrane protein studies. *Biological Chemistry*, 390:805–814.

[Bublitz, 2015] Bublitz, M. (2015). *P-type ATPases. Methods and protocols*, chapter 11, pages 105–109. Humana Press.

[Carton et al., 1996] Carton, I., Brisson, A. R., and Richter, R. P. (1996). Label-free detection of clustering of membrane-bound proteins. *Analytical Chemistry*, 274:9275–9281.

[Cherepanov et al., 1999] Cherepanov, D. A., Mulkidjanian, A. Y., and Junge, W. (1999). Transient accumulation of elastic energy in proton translocating ATP synthase.

[Cook et al., 2003] Cook, G. M., Keis, S., Morgan, H. W., Ballmoos, C. V., Matthey, U., Kaim, G., and Dimroth, P. (2003). Purification and biochemical characterization of the F_1Fo-ATP synthase from thermoalkaliphilic Bacillus sp. strain TA2.A1. *Journal of Bacteriology*, 185:4442–4449.

[Duncan and Börsch, 2013] Duncan, T. M. and Börsch, M. (2013). Spotlighting motors and controls of single F_oF_1-ATP synthase.

[Duncan et al., 1995] Duncan, T. M., Bulygin, V. V., Zhou, Y., Hutcheon, M. L., and Cross, R. L. (1995). Rotation of subunits during catalysis by Escherichia coli F_1-ATPase. *Proceedings of the National Academy of Sciences of the United States of America*, 92:10964.

[Düsser et al., 2009] Düsser, M. G., Zarrabi, N., Cipriano, D. J., Ernst, S., Glick, G. D., Dunn, S. D., and Börsch, M. (2009). 36 degree step size of proton-driven c-ring rotation in F_oF_1-ATP synthase. *The EMBO Journal*, 28:2689.

[Fan et al., 2019] Fan, X., Wang, J., Zhang, X., Yang, Z., Zhang, J. C., Zhao, L., Peng, H. L., Lei, J., and Wang, H. W. (2019). Single particle cryo-EM reconstruction of 52 kDa streptavidin at 3.2 Angstrom resolution. *Nature Communications 2019 10:1*, 10:1–11.

[Gressers et al., 1982] Gressers, M. J., Myers, J. A., and Boyer, P. D. (1982). Catalytic site cooperativity of beef heart mitochondrial F_1 adenosine triphosphatase. Correlations of initial velocity, bound intermediate, and oxygen exchange measurements with an alternating three-site model. 257:12030–12038.

[Gross et al., 2011] Gross, L. C., Heron, A. J., Baca, S. C., and Wallace, M. I. (2011). Determining membrane capacitance by dynamic control of droplet interface bilayer area. *Langmuir*, 27:14335–14342.

[Ho, 2010] Ho, W.-M. (2010). *Single Molecule Characterisation of ATP Synthase*. PhD thesis, University of Oxford.

[Horner et al., 2009] Horner, A., Antonenko, Y. N., and Pohl, P. (2009). Coupled diffusion of peripherally bound peptides along the outer and inner membrane leaflets. *Biophysical Journal*, 96:2689–2695.

[Ishmukhametov et al., 2010] Ishmukhametov, R., Hornung, T., Spetzler, D., and Frasch, W. D. (2010). Direct observation of stepped proteolipid ring rotation in E. coli FoF_1-ATP synthase. *EMBO Journal*, 29:3911–3923.

[Ishmukhametov et al., 2005] Ishmukhametov, R. R., Galkin, M. A., and Vik, S. B. (2005). Ultrafast purification and reconstitution of His-tagged cysteine-less Escherichia coli F_1F_o ATP synthase. *Biochimica et Biophysica Acta - Bioenergetics*, 1706:110–116.

[Jagendorf and Uribe, 1966] Jagendorf, A. T. and Uribe, E. (1966). ATP formation caused by acid-base transition of spinach chloroplasts. *Proceedings of the National Academy of Sciences of the United States of America*, 55:170.

[Kayalar et al., 1977] Kayalar, C., Rosing, J., and Boyer, P. D. (1977). An alternating site sequence for oxidative phosphorylation suggested by measurement of substrate binding patterns and exchange reaction inhibitions. *Journal of Biological Chemistry*, 252:2486–2491.

[Kirat et al., 2009] Kirat, K. E., Morandat, S., and Dufrêne, Y. F. (2009). Nanoscale analysis of supported lipid bilayers using atomic force microscopy.

[Kunkel, 1985] Kunkel, T. A. (1985). Rapid and efficient site-specific mutagenesis without phenotypic selection. *Genetics*, 82:488–492.

[Lee et al., 2000] Lee, W.-K., Bani-Jaber, A., Mcguire, J., Daeschel, M. A., and Jung, I.-H. (2000). Interfacial tension kinetics of nisin and β-casein at an oil-water interface. *KoreanJ. Chem. Eng*, 17:179–183.

[Lee et al., 2018] Lee, Y., Park, S.-J., Lee, K. A., Kim, S.-H., Kim, H., Meroz, Y., Mahadevan, L., Jung, K.-H., Ahn, T. K., Parker, K. K., and Shin, K. (2018). Photosynthetic artificial organelles sustain and control ATP-dependent reactions in a protocellular system. *Nature Biotechnology*.

[Leptihn et al., 2013] Leptihn, S., Castell, O. K., Cronin, B., Lee, E. H., Gross, L. C., Marshall, D. P., Thompson, J. R., Holden, M., and Wallace, M. I. (2013). Construct-

ing droplet interface bilayers from the contact of aqueous droplets in oil. *Nature Protocols*, 8:1048–1057.

[Loose and Schwille, 2009] Loose, M. and Schwille, P. (2009). Biomimetic membrane systems to study cellular organization. *Journal of Structural Biology*, 168:143–151.

[Matzke et al., 2021] Matzke, N. J., Lin, A., Stone, M., and Baker, M. A. (2021). Flagellar export apparatus and ATP synthetase: Homology evidenced by synteny predating the last universal common ancestor. *BioEssays*, 43:2100004.

[McMillan et al., 2007] McMillan, D. G., Keis, S., Dimroth, P., and Cook, G. M. (2007). A specific adaptation in the a subunit of thermoalkaliphilic F_1F_O-ATP synthase enables ATP synthesis at high pH but not at neutral pH values. *The Journal of biological chemistry*, 282:17395–17404.

[Mitchell, 1961] Mitchell, P. (1961). Coupling of phosphorylation to electron and hydrogen transfer by a chemi-osmotic type of mechanism. *Nature 1961 191:4784*, 191:144–148.

[Mueller et al., 1962] Mueller, P., Rudin, D. O., Tien, H. T., and Wescott, W. C. (1962). Reconstitution of cell membrane structure in vitro and its transformation into an excitable system. *Nature*, 194:979–980.

[Murphy et al., 2019] Murphy, B. J., Klusch, N., Langer, J., Mills, D. J., Yildiz, Özkan., and Kühlbrandt, W. (2019). Rotary substates of mitochondrial ATP synthase reveal the basis of flexible F_1-F_o coupling. *Science*, 364.

[Nilsson et al., 2016] Nilsson, T., Lundin, C. R., Nordlund, G., Adelroth, P., Ballmoos, C. V., and Brzezinski, P. (2016). Lipid-mediated protein-protein interactions modulate respiration-driven ATP synthesis. *Scientific Reports*.

[Nirody et al., 2020] Nirody, J. A., Budin, I., and Rangamani, P. (2020). ATP synthase: Evolution, energetics, and membrane interactions. *The Journal of general physiology*, 152.

[Noji et al., 1997] Noji, H., Yasuda, R., Yoshida, M., and Kinosita, K. (1997). Direct observation of the rotation of F_1-ATPase. *Nature 1997 386:6622*, 386:299–302.

[Nord, 2013] Nord, A. (2013). *Stepping Dynamics of the Bacterial Flagellar Motor and F_1-ATPase*. PhD thesis, University of Oxford.

[Onoue et al., 2009] Onoue, Y., Suzuki, T., Davidson, M., Karlsson, M., Orwar, O., Yoshida, M., and Kinosita, K. (2009). A giant liposome for single-molecule observation of conformational changes in membrane proteins. *Biochimica et Biophysica Acta (BBA) - Biomembranes*, 1788:1332–1340.

[Panke and Rumberg, 1999] Panke, O. and Rumberg, B. (1999). Kinetic modeling of rotary CF_oF_1-ATP synthase: storage of elastic energy during energy transduction. *Biochimica et Biophysica Acta (BBA) - Bioenergetics*, 1412:118–128.

[Patel et al., 2020] Patel, B. A., D'Amico, T. L., and Blagg, B. S. (2020). Natural products and other inhibitors of F_1F_O ATP synthase. *European Journal of Medicinal Chemistry*, 207.

[Perez et al., 2023] Perez, I., Heitkamp, T., and Börsch, M. (2023). Mechanism of ADP-inhibited ATP hydrolysis in single proton-pumping F_oF_1-ATP synthase trapped in solution.

[Pullman et al., 1960] Pullman, M. E., Penefsky, H. S., Datta, A., and Racker, E. (1960). Partial resolution of the enzymes catalyzing oxidative phosphorylation. I. Purification and properties of soluble, dinitrophenol-stimulated adenosine triphosphatase. *The Journal of Biological Chemistry*, 235.

[Rebaud et al., 2014] Rebaud, S., Maniti, O., and Girard-Egrot, A. P. (2014). Tethered bilayer lipid membranes (tBLMs): Interest and applications for biological membrane investigations. *Biochimie*, 107:135–142.

[Rhee, 1977] Rhee, S. K. (1977). Surface energies of silicate glasses calculated from their wettability data. *Journal of Materials Science*, 12:823–824.

[Rieu et al., 2022] Rieu, M., Krutyholowa, R., Taylor, N. M., and Berry, R. M. (2022). A new class of biological ion-driven rotary molecular motors with 5:2 symmetry. *Frontiers in Microbiology*, 13:2791.

[Rolo et al., 2002] Rolo, L. I., Caço, A. I., Queimada, A., Marrucho, I. M., and Coutinho, J. A. P. (2002). Surface tension of heptane, decane, hexadecane, eicosane, and some of their binary mixtures.

[Sabbert et al., 1996] Sabbert, D., Engelbrecht, S., and Junge, W. (1996). Intersubunit rotation in active F-ATPase. *Nature 1996 381:6583*, 381:623–625.

[Sackmann, 1996] Sackmann, E. (1996). Supported membranes: Scientific and practical applications. *New Series*, 271:43–48.

[Sambongi et al., 1999] Sambongi, Y., Iko, Y., and Tanabe, M. (1999). Mechanical rotation of the c subunit oligomer in ATP synthase (F_oF_1): Direct observation. *Science*, 286:1722–1724.

[Sbeih et al., 2021] Sbeih, S., Steffen, W., and Kappl, M. (2021). Anti-wettability of chemically and physically modified glass surfaces. *Advanced Materials Proceedings*, 6.

[Schmidt and Gräber, 1985] Schmidt, G. and Gräber, P. (1985). The rate of ATP synthesis by reconstituted CF_oF_1 liposomes. *Biochimica et Biophysica Acta*, 808:46–51.

[Schwamborn, 2017] Schwamborn, M. (2017). *Establishment of a fluorescence assay for characterization of protein-mediated vesicle fusion and acidification*. PhD thesis, Georg-August-Universität Göttingen.

[Sobti et al., 2016] Sobti, M., Smits, C., Wong, A. S., Ishmukhametov, R., Stock, D., Sandin, S., and Stewart, A. G. (2016). Cryo-EM structures of the autoinhibited E. coli ATP synthase in three rotational states. *eLife*, 5.

[Sobti et al., 2020] Sobti, M., Walshe, J. L., Wu, D., Ishmukhametov, R., Zeng, Y. C., Robinson, C. V., Berry, R. M., and Stewart, A. G. (2020). Cryo-EM structures pro-

vide insight into how E. coli F_1F_o ATP synthase accommodates symmetry mismatch. *Nature Communications*, 11.

[Sone et al., 1977] Sone, N., Yoshida, M., Hirata, H., and Kagawa, Y. (1977). Adenosine triphosphate synthesis by electrochemical proton gradient in vesicles reconstituted from purified adenosine triphosphatase and phospholipids of thermophilic bacterium. *Journal of Biological Chemistry*, 252:2956–2960.

[Sternweis, 1978] Sternweis, P. C. (1978). The epsilon subunit of Escherichia coli coupling factor 1 is required for its binding to the cytoplasmic membrane. *Journal of Biological Chemistry*, 253:3123–3128.

[Stewart et al., 2012] Stewart, A. G., Lee, L. K., Donohoe, M., Chaston, J. J., and Stock, D. (2012). The dynamic stator stalk of rotary ATPases.

[Su et al., 2020] Su, Z., Juhaniewicz-Debinska, J., Sek, S., and Lipkowski, J. (2020). Water structure in the submembrane region of a floating lipid bilayer: The effect of an ion channel formation and the channel blocker. *Langmuir*, 36:409–418.

[Tachezy and Smid, 2007] Tachezy, J. and Smid, O. (2007). *Hydrogenosomes and mitosomes: Mitochondria of anaerobic eukaryotes*.

[Tamm and Mcconnell, 1985] Tamm, L. K. and Mcconnell, H. M. (1985). Supported phospholipid bilayers. *Biophysical Journal*, 47:105–113.

[Taylor et al., 2015] Taylor, G. J., Venkatesan, G. A., Collier, C. P., and Sarles, S. A. (2015). Direct in situ measurement of specific capacitance, monolayer tension, and bilayer tension in a droplet interface bilayer. *Cite this: Soft Matter*, 11:7592.

[Veshaguri et al., 2016] Veshaguri, S., Christensen, S. M., Kemmer, G. C., Ghale, G., Møller, M. P., Lohr, C., Christensen, A. L., Justesen, B. H., Jørgensen, I. L., Schiller, J., Hatzakis, N. S., Grabe, M., Pomorski, T. G., and Stamou, D. (2016). Direct observation of proton pumping by a eukaryotic P-type ATPase. *Science*, 351:1469–1473.

[Watanabe et al., 2018] Watanabe, R., Komatsu, T., Sakamoto, S., Urano, Y., and Noji, H. (2018). Lab on a chip high-throughput single-molecule bioassay using micro-reactor arrays with a concentration gradient of target molecules. 18:2849.

[Watanabe et al., 2014a] Watanabe, R., Soga, N., Fujita, D., Tabata, K. V., Yamauchi, L., Kim, S. H., Asanuma, D., Kamiya, M., Urano, Y., Suga, H., and Noji, H. (2014a). Arrayed lipid bilayer chambers allow single-molecule analysis of membrane transporter activity. *Nature Communications*.

[Watanabe et al., 2014b] Watanabe, R., Soga, N., Yamanaka, T., and Noji, H. (2014b). High-throughput formation of lipid bilayer membrane arrays with an asymmetric lipid composition. *Scientific Reports*.

[Watanabe et al., 2013] Watanabe, R., Tabata, K. V., Iino, R., Ueno, H., Iwamoto, M., Oiki, S., and Noji, H. (2013). Biased Brownian stepping rotation of F_1-ATP synthase driven by proton motive force. *Nature Communications*, 4:1631 – 1637.

[Wauer et al., 2013] Wauer, T., Gerlach, H., Mantri, S., Hill, J., Bayley, H., and Sapra, K. T. (2013). Construction and manipulation of functional three-dimensional droplet networks. *ACS Nano*.

[Yasuda et al., 2001] Yasuda, R., Noji, H., Yoshida, M., Jr, K. K., and Itoh, H. (2001). Resolution of distinct rotational substeps by submillisecond kinetic analysis of F_1-ATPase. *Nature*, 410:898 – 904.

[Zimmermann et al., 2005] Zimmermann, B., Diez, M., Zarrabi, N., Gräber, P., and Börsch, M. (2005). Movements of the epsilon-subunit during catalysis and activation in single membrane-bound H^+-ATP synthase. *EMBO Journal*, 24:2053–2063.